Boundary Value Problems in Electrophoresis, with Applications to Separations and Colloid Science

by

Joseph A. Erker

A Dissertation Submitted to the Faculty of the

Graduate Interdisciplinary Program
in Applied Mathematics

In Partial Fulfillment of the Requirements
For the Degree of

Doctor of Philosophy

In the Graduate College

The University of Arizona

2002

THE UNIVERSITY OF ARIZONA ®
GRADUATE COLLEGE

As members of the Final Examination Committee, we certify that we have read the dissertation prepared by Joseph A. Erker entitled Boundary Value Problems in Electrophoresis, with Applications to Separations and Colloid Science and recommend that it be accepted as fulfilling the dissertation requirement for the Degree of Doctor of Philosophy

James C. Baygents	24 October 2002
Bruce J. Bayly	24 October 2002
Wilfred M. Greenlee	10/24/02
Juan M. Restrepo	10/24/02

Date

Final approval and acceptance of this dissertation is contingent upon the candidate's submission of the final copy of the dissertation to the Graduate College.

I hereby certify that I have read this dissertation prepared under my direction and recommend that it be accepted as fulfilling the dissertation requirement.

James C. Baygents — Dissertation Director — 2 Dec 2002 — Date

Statement by Author

This dissertation has been submitted in partial fulfillment of requirements for an advanced degree at The University of Arizona and is deposited in the University Library to be made available to borrowers under rules of the Library.

Brief quotations from this dissertation are allowable without special permission, provided that accurate acknowledgment of source is made. Requests for permission for extended quotation from or reproduction of this manuscript in whole or in part may be granted by the copyright holder.

Signed: 

Acknowledgements

I have had the good fortune to know many people who have helped me on personal, scientific, and professional levels, and I regret that in the list that follows, I will inadvertently omit a name or two, but thanks are in order to the following:

My family back home in New York who have provided moral support and put up with my infrequent visiting. Most especially, my parents, who in addition to providing love, showed me the importance and joy of learning, thus giving me an outlook that has shaped my life and work immeasurably.

My thesis committee: Jim Baygents, for friendship and also ingraining in me as a scientist the importance of knowing the physics behind a mathematical model, scale analysis, and knowledge of the literature. Because of this, I feel that in addition to being a mathematician who knows a few tricks, I am a reasonably competent research scientist. Bruce Bayly and Wilfred Greenlee, for insights when I was beginning this research project, and support throughout. Juan Restrepo, who appeared in the department in the later years of this work, and has provided his own insight, not to mention encouragement toward the end. Lee White, for agreeing at the eleventh hour to review this thesis.

The various staff members in the department: Bob Condon, for being a great friend and boss. The folks downstairs: Carole, Jerrie, *et al.* ; and on the fourth floor: Lois, Kathleen, Stacey and Linda for putting up with my neverending confusion over administrative matters. And in the grad college, Dorian, who could somehow unearth my financial paperwork from someone else's mess.

My Tucson family: Nita, Alain, Francisco, Craig, and Cecilia. I cannot sufficiently express what your friendship means to me, so I won't try.

My classmates: Wayne, Mario, Martin, Karl, Kevin, Brandon, Anu, and the rest. Wayne, thanks for the late-night mutual research updates at Waffle House and IHOP, and for the many amusing times.

My office mates: Jack, Brett, Nick, Monica, Tom, Jamie, and honorary office mate Jen. Jack, you are like a younger brother to me even though you look older.

M.K., Erin, Sarah, and the GB's gang. It's been a blast.

Dedication

This work is dedicated in loving memory to my mother

Elaine Theresa Erker

1935-2000

Table of Contents

List of Figures 8

List of Tables 10

Abstract 11

1. Introduction 12

2. The Electrokinetic Model of a Fluid Drop 16
   - 2.1. Background 16
   - 2.2. The Conservation Laws 18
   - 2.3. Expansion of the Model 22
     - 2.3.1. $O(1)$ Equations — Equilibrium Electrostatics 23
     - 2.3.2. $O(\beta)$ Equations — The Mobility Problem 24

3. Equilibrium Electrostatics of a Fluid Drop 32
   - 3.1. Introduction 32
   - 3.2. The Poisson-Boltzmann Equation 33
   - 3.3. Small Interfacial Potentials 35
   - 3.4. Thin Double-Layer Analysis 36
   - 3.5. Comparison with Numerical Solution 46
   - 3.6. Additional Work 47

4. Electrophoretic Mobility of a Fluid Drop 51
   - 4.1. Integral Formulation of the Electrokinetics 51
   - 4.2. Mobility Formula for Small Interfacial Potentials 58
   - 4.3. Results and Discussion 63
     - 4.3.1. Comparison with Numerical Solution 64
     - 4.3.2. Comparison with Experimental Observations 65
   - 4.4. Conclusions 72

5. Radial Temperature Variations in Cylindrical Electrophoresis Columns 76
   - 5.1. Background 76
   - 5.2. Problem Formulation 79
   - 5.3. Perturbation Scheme 81
   - 5.4. Acceleration of Convergence 85
   - 5.5. Comparison with Numerical Solution 87
   - 5.6. Discussion 90

TABLE OF CONTENTS—*Continued*

5.7. Determining the Wall Temperature in Capillary Electrophoresis 98
5.7.1. Heat Flux at the Inner Wall 99
5.7.2. Evaluating the Wall Temperature 101
5.7.3. Results 102

6. FUTURE STUDY 108
6.1. Drop Electrophoresis 108
6.2. Heating in Capillary Electrophoresis 110

A. TEMPERATURE VARIATIONS: THE $O(S^4)$ AND $O(S^5)$-SOLUTIONS 111

B. CORRELATIONS FOR THERMAL AND ELECTRICAL CONDUCTIVITY . . . 114

C. NOMENCLATURE 116

D. THE EQUILIBRIUM ELECTRIC POTENTIAL AND SURFACE CHARGE DENSITY OF SPHERICAL EMULSION DROPS WITH THIN DOUBLE LAYERS . . 120

REFERENCES 134

List of Figures

FIGURE 2.1. Definition sketch. 30

FIGURE 3.1. Plausible equilibrium potential profiles for the drop interior and exterior. 49

FIGURE 3.2. Comparison of boundary layer equilibrium potential estimates to numerical solution, various orders. 49

FIGURE 3.3. Comparison of boundary layer equilibrium potential estimates to numerical solution, third-order. 50

FIGURE 4.1. Comparison of linear analytic approximations of electrophoretic mobility of a fluid drop to a numerically-derived mobility, for several values of surface excesses Γ_G 73

FIGURE 4.2. Comparison of linear analytic approximations of dimensionless electrophoretic mobility of a fluid drop with numerically-derived values, interior scaled radius $a\bar{\kappa} = 10$ 74

FIGURE 4.3. Comparison of linear analytic approximations of dimensionless electrophoretic mobility of a fluid drop with numerically-derived values, interior scaled radius $a\bar{\kappa} = 100$ 74

FIGURE 4.4. Comparison of mobility formula with experimental data of Mooney 75

FIGURE 4.5. Comparison of numerically-derived electrophoretic mobility with experimental data 75

FIGURE 5.1. Dimensionless temperature profiles, $\Theta(\rho)/S$, for $T_w = 298$ K, as given by analytic approximations and the numerical solution. 92

FIGURE 5.2. Variation of dimensionless centerline temperature $\Theta_{\mathfrak{C}}/S$ with S, as given by analytic approximations and the numerical solution, for $T_w = 298$ K. 92

FIGURE 5.3. Relative error in analytic approximations of the centerline temperature $\Theta_{\mathfrak{C}}$, as a function of S, in log-log form. $T_w = 298$ K. 93

FIGURE 5.4. Variation of the dimensionless gradient at the inner capillary wall with S, as given by analytic approximations and the numerical solution for $T_w = 298$ K. 93

FIGURE 5.5. Relative error in analytic approximations of dimensionless temperature gradient at the inner capillary wall, $(\partial_\rho \Theta)_w$, as a function of S. 94

FIGURE 5.6. Radial variations of dimensionless electrical conductivity as given by analytic approximations and the numerical solution. 95

FIGURE 5.7. Wall temperature, T_w and dimensionless power input, S, plotted against applied electric field, with Peltier thermostating. 105

LIST OF FIGURES—*Continued*

FIGURE 5.8. Wall temperature, T_w and dimensionless power input, S, plotted against applied electric field, with forced air cooling. 106
FIGURE 5.9. Wall temperature, T_w, and dimensionless power generation, S, plotted agains applied electric field, with the reference and wall conductivies, σ_{ref} and σ_w fixed at 0.1 S/m. 107

List of Tables

Table 2.1. Characteristic scales. 30
Table 2.2. Dimensionless Constants 31

Table 4.1. Fitting Parameters for comparison of mobility formula with experimental data. 67
Table 4.2. Fitting Parameters for comparison of numerically-derived electrophoretic mobility with experimental data. 68

Table 5.1. Comparison of asymptotic expansions, $\Theta_{\mathfrak{C}}^{(n)}/S$, of the dimensionless centerline temperature with numerically-computed values. 96
Table 5.2. Comparison of asymptotic expansions of dimensionless temperature gradient at the capillary wall with numerically-computed values. . . 97

Abstract

The topic of this thesis is investigation of models applied to different aspects of separations and colloid science. Many tools are used for solving the models, which are manifested as boundary value problems. The problems are to determine the equilibrium electrostatics of a fluid droplet, the electrokinetics of such, the (nonuniform) temperature profile of an electrophoresis capillary due to Joule heating, and the temperature at the wall of the capillary. In the fluid drop model, special attention given to a drop that, in addition to the surrounding fluid, supports electrolytes. Matched asymptotic expansions based on thin double layers are applied to the equilibrium electrostatics problem. Attention is given to how conditions on the interface of the drop, such as discontinuity of equilibrium potential and the presence of surface excesses of solutes, affect the electrokinetics. A perturbation scheme is used to formulate a problem for the electrophoretic mobility of a droplet. An approximate solution for the the mobility of a drop is derived, based on small interfacial potentials. The formula encompasses those of several past theoretical studies. A regular perturbation is used to determine heating effects in capillary electrophoresis, based on a small power input to the system. The resulting expression for temperature in the capillary is then used implicitly to determine the temperature at the wall of the capillary. Some of the results are compared with experimental data. For the drop electrophoresis problem, the electrophoretic mobility formula is compared with measured mobility of oil drops and drops in aqueous two-phase systems. In the study of heating in capillary electrophoresis, the implicit expression is used to make reasonable estimates of the wall temperature based on published operating conditions. Accuracy of all analytic estimates of the problems are tested against numerical solutions, taken to be exact. In all cases, the analytic approximations are satisfactorily accurate under appropriate conditions.

1. Introduction

When new or casual acquaintances ask me about my research, I have come to first use the word "electrohydrodynamics." To those not scared off by that phrase but who nonetheless don't know what it means, I simply break down the phrase, and say I study the movement of water-based solutions and other fluids when an electric field is applied. Then, if they are still interested, I point out that electrical interactions have a profound influence on the movement of water or other fluids — and the particles in them — over very small distances. This often leads to the question of why one would be interested in studying the small-scale behaviour of fluids. Current events of the past few years make that question easily answerable to the layperson. For example, it seems that most everyone has by now heard of DNA analysis in forensics, even though most may not understand how it works. No matter, such analysis is often electrically-driven, and obviously the molecules in question are quite small. Moreover, it helps to make a contrast with more familiar examples of the (large-scale) flow of water as in an ocean, river, or pipes, where electricity plays no significant role.

Indeed, the length scales of the research presented herein are microscopic, and over such distances, one cannot ignore the effects of electrical conductivity, especially when the fluid contains electrolytes, as does water. In addition, in the mathematical models considered here, not only must electricity be included, it provides the nonlinearities that make the models so difficult - and interesting - to investigate. Charge distribution, and electrical and thermal conductivities are the sources of nonlinearities that are contended with herein.

In the interest of providing cohesion to the voluminous work that follows, I state that mathematically, all the work here comes down to non-linear boundary-value problems, with approximate solutions based on asymptotic analysis compared to (exact) numerical solutions. As for applications, the work falls under the category of

electrophoresis. Herein are examined the problem of electrophoresis of a microscopic fluid drop, as well as the heating effects in a capillary electrophoresis buffer. In the case of electrostatics and electrophoretic mobility of fluid drops, the goal is to seek a better understanding of a liquid-liquid interface, under the general condition that both liquids contain electrolytes. In particular, aqueous two-phase systems are used in partitioning of biological material [7, 52, 56]. And of course, capillary electrophoresis is widely used in separating proteins and other molecules according to size and valence [28].

The first topic is the electrokinetic model of a fluid drop, with a weak applied electric field. By weak is meant small compared to the field that typically appears at the drop interface. The model is concerned with microscopic drops, whose electrical properties are of greater influence on the dynamics than with larger-scale drops. Understanding the dynamics of a droplet suspended in a different fluid — particularly in response to an applied field — helps in determining the structure of the interface of two fluids surrounding fluid. This is important, for example, in understanding aqueous two-phase systems such as those used in bioseparations. The scales considered also enable generalize well-established theory of small scale particles and droplets with less interesting electrical properties. The model is a simple yet profound generalization of that of Baygents and Saville [2], and is treated as a perturbation problem with the scaled field as the perturbation parameter, and a correction is made to the equilibrium case of no applied field. The model is presented in Chapter 2 in dimensionless form, with the scale factors given. The breakdown of the model according to the perturbation scheme is subsequently presented. The equilibrium, or leading-order case is non-linear - as is typical in asymptotic analysis - and is itself approached with matched asymptotics. This is the subject of Chapter 3 as well as the manuscript of Appendix D. More detail of the derivation of the matched asymptotic formulas is presented in Chapter 3 than in the manuscript.

In Chapter 4 is examined the first correction to the equilibrium problem, where

a solution is given for the electrophoretic mobility of a fluid drop. Because of the complicated nature of the boundary conditions, it is found that an integral equation representation of the equations facilitates both analytic approximations and a numerically-derived solution. The integral equations resemble those of Ohshima, Healy, and White [40, 41], who formulated approximations for the electrophoretic mobilities of a non-conducting spherical particle and for a mercury drop, respectively. In both of these situations, interior electrostatics are not considered. By considering the interior electrostatics, the model becomes considerably more complicated than in these two cases. An approximate solution is formulated based on the limiting case that the interfacial potentials are limited to a few millivolts. This enables one to linearize the equations in these interfacial potentials. Baygents and Saville [2] have demonstrated in limited cases of the model the plausibility of such a linearization, by plotting a numerically-derived solution that is seen to be nearly linear through values of these potentials up to 50 millivolts. There is presented the small interfacial potential approximation to the electrophoretic mobility and a numerical solution, to which the formula is compared.

The subject matter changes from here, and in Chapter 5 is examined another problem related to electrophoresis, but a different problem nonetheless. The problem considered is to determine the amount of heating that takes place in a cylindrical capillary electrophoresis tube due to the imposition of an electrical current. As in the problems considered previously, the concern here is with an electrolytic solution, which in this case is the buffer used in electrophoresis. The applied voltage that drives the electrophoresis generates current due to the electrolytes in the water, and heat is generated. The radial temperature profile is nonuniform, and the governing equation is nonlinear, in the sense that the thermal and electrical conductivities are nonlinear functions of the temperature, which is the dependent variable. Because of axial symmetry, the problem is a nonlinear ordinary differential equation over the radial variable, and a solution is presented as a regular perturbation expansion about the

case for which no heating (uniform temperature) occurs. This problem and solution are presented in great detail in Chapter 5. A derivative result to this work appears at the end of that chapter. In particular, the derived temperature profile depends on the temperature at the wall of the capillary, which is not an easily-measured quantity. It is shown how one can use the approximate solution implicitly to estimate the capillary wall temperature - and thus the entire radial temperature profile - if one knows the experimentally controllable parameters, such as applied voltage and conductivity at room temperature.

In some cases comparisons are made against experimental observations in order to test the validity of the models. The formula for electrophoretic mobility of a fluid droplet was compared with mobility measurements on oil drops, and also drops in aqueous two-phase systems. Results from the implicit formula for the temperature at the inner wall of an electrophoresis capillary are compared to estimates of the temperature based on experimental data regarding electrical input and current for different mechanisms for cooling the capillary.

The various approximate solutions derived herein are compared against numerical solutions in order to test their accuracy of solutions to the models. A wide variety of numerical methods for solving differential equations are used, each appropriate for nonlinear problems, including the shooting method and orthogonal collocation on finite elements.

In the last chapter, some ideas for future research based on the present study are briefly discussed. With the results and the ideas presented, it is hoped that the problems considered here are timely and the results satisfactory and provocative.

2. The Electrokinetic Model of a Fluid Drop

2.1. Background

A powerful tool in the analysis of the interface between two media is to observe the electrokinetic behaviour of particles or drops of one of the two media suspended in the other. Water-based media are particularly intriguing, due to the effect of electrolytes. Well-established theories exist for electrophoresis of solid particles suspended in water and for liquids whose electrostatics are simple or trivial compared to those of water, such as mercury or paraffin oil. When both media are fluids that support electrolytes, the behaviour is understandably more complicated, due to the non-trivial electrostatics within as well as without the drop interior.

Indeed, some very interesting experimental observations have been made regarding electrophoresis of drops in an aqueous two-phase system. For example, Brooks *et al.* [8] prepared a dispersion of drops and noticed that (i) electrophoretic mobility appears to be linearly-dependent on the size of the drop, for drops up to about 15 microns in diameter, (ii) when the phases are reversed, that is when the drop phase in one experiment is made to be the bulk phase in another, the sign of the mobility is reversed, and (iii) the sign of the mobility is opposite the sign of the interphase potential difference. These observations have also been made elsewhere [43]. Observation (i) is in contrast to observed behaviour of solid particles, for which mobility increases with size only for drops of diameter less than one micron before leveling off. Observation (ii) suggests the possibility of a electrostatic dipolar interface, perhaps due to the adsorption of adsorbed dipolar molecules on the interface. Therefore, unlike a dispersed phase for which the interior electrostatics are trivial, there is an interior surface potential and potential profile, generally distinct from the exterior one. Observation (iii) suggests that if indeed there is a dipole moment at the interface, that

the interphase potential difference may not have much influence on the mobility.

Much theoretical study has been done, mostly concentrating on the effects of surface, or zeta potential, of the dispersed phase, and ionic strength of the solute, the latter of which is manifested by an electrical double-layer, on the electrophoretic mobility of a particle or drop. For example, Henry [20] derived an expression for the mobility of a non-conducting spherical particle, valid for small values of the ζ-potential. Ohshima, Healy, and White [41] also derived a mobility expression for the solid particle, but for a thin double-layer. There have been several studies on mobility of a conducting drop such as mercury. Frumkin and Levich [29] derived an expression that is valid for thin double-layers but does not consistent with established results for a solid particle as the viscosity of the drop becomes large. Ohshima, Healy, and White [42] did numerical and thin double-layer and small ζ-potential analyses for a mercury drop, with the assumption that the drop suspended in water is ideally-polarizable. Booth [5] formulated a mobility for a drop whose interior as well as exterior supports an electrolyte. The analysis is based in part on the premise that the drop and continuous phases are ohmic conductors and that dipoles may exist at the interface, causing a jump in equilibrium potential. In addition, that analysis is limited to small zeta potentials. All these results reduce to the well-known Smoluchowksi formula [48] for the electrophoretic mobility of a solid particle in the limits of small ζ-potential, and thin double-layer. In this case, the mobility is independent of particle size. Levine [30] too employed surface dipoles in his analysis, in which unlike the Booth model, the interface is completely polarizable. This yielded an heuristic result that shows drop mobility increasing with the drop size, but failed to account for interfacial current. This analysis was based on small zeta potentials and thin double-layers. Baygents and Saville [2] offered numerically-derived results to a model that accounts for current across the drop surface, but considered only the case that the equilibrium potential is continuous at the interface. The double-layer and electrokinetic theory, and some of the important results can be found in various

texts [1, 23, 37, 45].

The model used here is very similar to that of Baygents and Saville [2], differing in that surface dipoles are accounted for. The analysis is based on small interfacial potentials and small interphase potential difference, with no restriction on the size of the electrical double-layer. It distinguishes itself from other past treatments in several ways. As opposed to Booth's treatment, the drops are taken to be ionic as opposed to ohmic conductors. Also, surface excesses of solute ions are included in the model. This consideration is borne out of classical thermodynamics [1], and was included in the model of Baygents and Saville but not included in the generation of their numerical results. Unlike the model of Levine, it is allowed that current - in the form of the ionic species - can pass through as well as within the interface.

Although the analysis is based on small surface potentials — that is, only a few millivolts — it will be seen that the results are accurate (when compared to a numerically-derived solution of the model) for potentials of moderate values, and account for a wide variety of behaviour. For example, it will be seen that the mobility changes sign when the parameters for the two phases are interchanged, and that the sign of the mobility is less effected by the interphase potential difference than the orientation of the interfacial dipole. In addition, in the case of a non-conducting drop the results show size dependence on mobility through larger sizes than for a solid particle, with mobility eventually leveling off as the drops become larger. The algebraic form also reduces to results of aforementioned studies [5, 20] for different limiting cases of the physical parameters.

2.2. The Conservation Laws

Here is followed the electrokinetic model of Baygents and Saville [2], which is a more generalized version of some previously published models. A contrast is made with the model for a mercury drop [42], since the mercury/water interface has been treated

as 'ideally polarizable', and so does not allow electric current to cross the phase boundary.

The model is described as follows: The drop phase (interior) and the host phase (exterior) are each electrolytic. The two phases may differ in viscosity and electric permittivity, each of which is taken to be constant within each phase. It is not assumed that the conductivity of each medium is constant. See FIG 2.1 for some detail. The physical parameters relevant to the analysis are in that figure, will be defined as needed, and also appear in Appendix C. Corresponding parameters exist for the interior of a drop will be denoted with overbars. At equilibrium, the drop is spherical. Surface charge (and/or dipoles) induce a charge cloud adjacent to the exterior and interior surface (double-layer) and the ions in each phase have a Boltzmann distribution, with the densities settling to their bulk values. In the bulk, the phases are electrically neutral. Inside the drop, the ions do not necessarily attain their bulk densities. If the interior fluid attained its bulk properties - and in general those bulk properties are different than those of the exterior - the potential would settle to the interphase potential difference, $\Delta\Psi$. The model allows for electric current both across and within the interface.

A uniform externally-applied electric field E_∞ will cause migration of the drop with velocity U_e, as well as circulation of fluid surrounding and within the drop. For the drop sizes considered here, the Reynolds number will be sufficiently low that the fluid motion is treated as Stokes flow.

Here is given the model in dimensionless form. A conversion to the dimensional form can be made via TABLE 2.1, which will also be referred to in the evaluation of the mobility results for experimental parameters. In addition, one can observe in TABLE 2.2 a list of dimensionless groups that aid in the analysis. A description of the model in dimensional form appears in [2].

In each of the two phases, the conservation of momentum, mass, and current are

accounted for, *viz.*

$$-\nabla p = \nabla^2\Phi\nabla\Phi - \nabla\times\nabla\times\mathbf{u}, \tag{2.1}$$

$$\nabla\cdot\mathbf{u} = 0, \tag{2.2}$$

and

$$\nabla\cdot\left(\mathrm{Pe}\,\mathbf{u}n^k - \omega^k\nabla n^k - \omega^k z^k\nabla\Phi\right) = 0; \qquad k = 1,2,\ldots,N, \tag{2.3}$$

where $\mathbf{u}, \Phi$, and p are the fluid velocity, electric potential, and pressure, respectively. n^k denotes the number density, and ω^k is the ionic mobility of the kth ion type of the system. The kth ion type has a valence of z^k, and there are N types of ions in the solution. Pe is a Peclet number. In the ion conservation equation can be seen the mechanisms for ionic transport, namely convection and electrochemical gradients, the latter encompassing Brownian motion and electromigration.

The Poisson equation for charge regulation is also included,

$$\nabla^2\Phi = -(a\kappa)^2\sum_{k=1}^{N} z^k n^k. \tag{2.4}$$

Analogous equations exist for the interior. For clarity, the corresponding variables will be expressed with overbars. The radius of the drop is denoted by a, and κ is the inverse of the Debye length, which is the characteristic length scale of the exterior electrical double-layer around the interface. See TABLE 2.2 for its definition.

At the interface, there is also the conservation of current, *viz.*

$$\begin{aligned}&\frac{1}{a\kappa}\nabla_{\mathrm{S}}\cdot\left(\mathrm{Pe}\,\mathbf{u}\,\Gamma^k - \omega_{\mathrm{S}}^k\Gamma^k - z^k\omega_{\mathrm{S}}^k\Gamma^k\nabla_{\mathrm{S}}\Phi\right)\\ &+\Big[\,\mathrm{Pe}\,\mathbf{u}\,n^k - \omega^k\nabla n^k - z^k\omega^k n^k\nabla\Phi\\ &\quad -\left(\mathrm{Pe}\,\mathbf{u}\,\bar{n}^k - \bar{\omega}^k\nabla\bar{n}^k - z^k\bar{\omega}^k\bar{n}^k\nabla\bar{\Phi}\right)\Big]\cdot\mathbf{n} = 0, \qquad k = 1,2,\ldots,N,\end{aligned} \tag{2.5}$$

where Γ^k denotes the surface density of the kth ion type, and ω_S^k is the surface mobility of that type. $\mathbf{n}$ represents the unit normal vector outward from the interface. The first line of (2.5) accounts for the current within the interface, and the remaining part for the current through it. The subscript S on the differential operator indicates a surface gradient, and accordingly on variables and parameters indicates their surface values.

The charge regulation at the interface is

$$-\nabla\Phi\cdot\mathbf{n}+\frac{\bar{\epsilon}}{\epsilon}\nabla\bar{\Phi}\cdot\mathbf{n}=a\kappa\sum_{k=1}^{N}z^k\Gamma^k, \tag{2.6}$$

where ϵ and $\bar{\epsilon}$ are the relative permittivities of the exterior and interior media, respectively.

Interfacial density Γ^k of bulk solutes are taken to be linearly related to volume density n^k at the interface, *viz.*

$$\Gamma^k=K^k n_S^k=\bar{K}^k\bar{n}_S^k,\qquad k=1,2,\ldots,N, \tag{2.7}$$

where K^k and $\bar{K}^k$ are the adsorption coefficients.

Continuity of velocity is also taken into account, *viz.*

$$\mathbf{u}=\bar{\mathbf{u}}, \tag{2.8}$$

as well as an interfacial stress balance

$$(\mathbf{S}_N+\mathbf{S}_M)\cdot\mathbf{n}-(\bar{\mathbf{S}}_N+\bar{\mathbf{S}}_M)\cdot\mathbf{n}+\gamma(\nabla_S\cdot\mathbf{n})\mathbf{n}+\nabla_S\gamma=\mathbf{0}, \tag{2.9}$$

where $\mathbf{S}_N$ and $\mathbf{S}_M$ represent the Newtonian and Maxwell stress tensors. γ is the interfacial tension, scaled on the (constant) equilibrium surface tension, γ_0, and is given by

$$\nabla_S\gamma=-a\kappa\sum_{k=1}^{N}K^k\nabla_S n_S^k. \tag{2.10}$$

Conditions in the far field ($r \to \infty$) are

$$-\nabla\Phi \to \mathbf{i}_z \tag{2.11}$$

$$\mathbf{u} \to -\mu_e \mathbf{i}_z \tag{2.12}$$

$$\nabla p \to 0 \tag{2.13}$$

$$n^k \to n^k_\infty; \qquad k = 1, 2, \ldots, N, \tag{2.14}$$

where μ_e is the *scaled electrophoretic mobility* of the drop. $\mathbf{i}_z$ is the unit vector in the direction of the applied field. The negative sign in the far-field velocity reflects that the frame of reference is the center of the drop.

Finally, since the phases are electrically neutral in the bulk,

$$\sum_{k=1}^{N} z^k n^k_\infty = 0; \qquad \sum_{k=1}^{N} z^k \bar{n}^k_\infty = 0 \tag{2.15}$$

2.3. Expansion of the Model

As is common in applications, it is held in this model that the characteristic field in the electrical double-layer is considerably larger than the applied field. With the potential in the double-layer characterized by $k_B T/e$ at equilibrium, the scaled applied field $\beta = aeE_\infty/k_B T$ is introduced, with a representing the drop radius, e the charge of a proton, E_∞ the strength of the applied field, k_B the Boltzmann constant, and T the (constant, room) temperature. This parameter is then considerably smaller than unity, which is to say that the imposition of the applied field brings but a small perturbation of the equilibrium electrostatics. This allows for the expression of the dependent variables as expansions based on orders of β, *viz.*

$$\Phi = \Phi_0 + \beta\Phi_1 + \ldots, \tag{2.16}$$

$$n^k = n^k_\infty + n^k_0 + \beta n^k_1 + \ldots; \qquad k = 1, 2, \ldots, N, \tag{2.17}$$

$$\mathbf{u} = \beta \mathbf{u}_1 + \ldots, \tag{2.18}$$

$$\Gamma = \Gamma_0 + \beta \Gamma_1 + \ldots \tag{2.19}$$

and similarly for the interior variables. Φ_0 and other variables with the zero subscript are the values at equilibrium, that is in the absence of an applied field. The velocity of course, is zero at equilibrium, and so its leading term is of $O(\beta)$. The ion densities n^k_0 here denote the disturbance from the bulk values n^k_∞ due to the existence of an electrical double-layer at equilibrium.

This expansion is useful in finding approximate solutions based on a small interfacial potentials, as well as those based on an expansion for thin double-layers.

For the analysis, the pressure, p, need not be considered, as it appears only in the normal stress balance. Because the system is inertialess, the drop will retain its spherical shape through $O(\beta)$, making the normal stress balance superfluous [51].

2.3.1. $O(1)$ Equations — Equilibrium Electrostatics

The relevant balance laws in leading order are those of charge regulation,

$$\nabla^2 \Phi_0 = -(a\kappa)^2 \sum_{k=1}^{N} (n^k_\infty + n^k_0), \tag{2.20}$$

and ion balances,

$$\omega^k \nabla \cdot \left[\nabla (n^k_\infty + n^k_0) + z^k (n^k_\infty + n^k_0) \nabla \Phi_0 \right] = 0, \qquad k = 1, 2, \ldots, N, \tag{2.21}$$

with an analogous representation for the interior of the drop. In the far-field, the variables tend to their bulk values, thus as the distance r from the center of the drop goes to infinity,

$$\begin{aligned} &\Phi_0 \to 0 \\ &n^k_0 \to 0, \qquad k = 1, 2, \ldots N. \end{aligned} \tag{2.22}$$

At the drop center ($r = 0$), continuity dictates that

$$\begin{aligned} \frac{d\Phi_0}{dr} &= 0 \\ \frac{dn_0^k}{dr} &= 0, \qquad k = 1, 2, \ldots N. \end{aligned} \tag{2.23}$$

At the interface ($r = 1$), charge regulation reads

$$\frac{d\Phi_0}{dr} + \frac{\bar{\epsilon}}{\epsilon}\frac{d\bar{\Phi}_0}{dr} = (a\kappa)\sum_{k=1}^{N}\Gamma_0^k, \tag{2.24}$$

where Γ_0^k relates to the volume densities of solutes as in (2.7).

In solving the leading-order system, the interfacial potentials $\tilde{\zeta}_{\mathrm{E}}$ and $\tilde{\zeta}_{\mathrm{I}}$ will be treated as prescribed parameters. These potentials are dimensionless, scaled as indicated in TABLE 2.1. These potentials are taken to be at the interface proper, as opposed to the zeta potential in the Gouy-Chapman model of a double-layer, which has a zeta potential distinct from the surface, or Stern potential [1, 23]. With the zeta potentials prescribed, surface charge density would then be determined via (2.24). One can alternatively prescribe the surface charge density and the jump in the potential at the interface. Interfacial potentials would then be recovered from (2.24). In fact, this approach is used in Chapter 4 when comparing the drop mobility formula to experimental measurements.

The leading-order equations will reduce to the charge regulation equation (2.20) with Φ_0 as the only dependent variable, and is further simplified by spherical symmetry. However, the problem remains quite challenging due to the nonlinearity of (2.20). In the next chapter, an approximate solution to the equilibrium model is shown for small interfacial potentials, and another, based on thin double-layer analysis.

2.3.2. $O(\beta)$ Equations — The Mobility Problem

The applied electric field disturbs the equilibrium ion distributions, and fluid motion is generated. As has been pointed out [51], at $O(\beta)$ the drop migrates but its spherical

shape remains intact. It is thus at this order that the electrophoretic mobility of the drop is solved.

The governing laws are, for charge regulation

$$\nabla^2\Phi_1 = -(a\kappa)^2 \sum_{k=1}^{N} z^k n_1^k, \tag{2.25}$$

ion balances

$$\begin{aligned} \mathrm{Pe}\, \mathbf{u}_1 \cdot \nabla(n_\infty^k + n_0^k) - \omega^k \nabla^2 n_1^k - z^k \omega^k \nabla \cdot \left[(n_\infty^k + n_0^k)\nabla\Phi_1 + n_1^k \nabla\Phi_0\right] = 0; \\ k = 1, 2, \ldots, N, \end{aligned} \tag{2.26}$$

momentum balance

$$\mathbf{0} = -\nabla p_1 + (\nabla^2\Phi_0)\nabla\Phi_1 + (\nabla^2\Phi_0)\nabla\Phi_1 + (\nabla^2\Phi_1)\nabla\Phi_0 - \nabla \times \nabla \times \mathbf{u}_1, \tag{2.27}$$

and continuity

$$\nabla \cdot \mathbf{u}_1 = 0, \tag{2.28}$$

with analogous equations for the interior of the drop.

Because of axisymmetry (with respect to the direction of the applied field), the model can be expressed in terms of the radial variable, r and θ, the angle between the position $\mathbf{r}$ and the z-axis. Accordingly, the velocity $\mathbf{u}$ is resolved into radial component u and angular component v.

The interfacial boundary conditions thus read, for tangential stress balance

$$\begin{aligned} &\frac{1}{r}\frac{\partial u_1}{\partial\theta} + r\frac{\partial}{\partial r}\left(\frac{v_1}{r}\right) + \frac{1}{r}\frac{d\Phi_0}{dr}\frac{\partial\Phi_1}{\partial\theta} - \frac{\bar{\mu}}{\mu}\left[\frac{1}{r}\frac{\partial\bar{u}_1}{\partial\theta} + r\frac{\partial}{\partial r}\left(\frac{\bar{v}_1}{r}\right)\right] \\ &- \frac{1}{r}\frac{\bar{\epsilon}}{\epsilon}\frac{d\bar{\Phi}_0}{dr}\frac{\partial\bar{\Phi}_1}{\partial\theta} - \frac{(a\kappa)}{r}\sum_{k=1}^{N} K^k \frac{\partial n_1^k}{\partial\theta}(1,\theta) = 0, \end{aligned} \tag{2.29}$$

continuous velocity

$$\begin{aligned} u_1(1,\theta) = \bar{u}_1(1,\theta) = 0 \\ v_1(1,\theta) = \bar{v}_1(1,\theta), \end{aligned} \tag{2.30}$$

charge regulation

$$-\frac{d\Phi_1}{dr}+\frac{\bar{\epsilon}}{\epsilon}\frac{d\bar{\Phi}_1}{dr}=a\kappa\sum_{k=1}^{N}z^kK^kn_1^k(1,\theta), \tag{2.31}$$

continuity of electric field

$$\frac{\partial\Phi_1}{\partial\theta}(1,\theta)=\frac{\partial\bar{\Phi}_1}{\partial\theta}(1,\theta), \tag{2.32}$$

and interfacial ion balance

$$\begin{aligned}&\omega^k\left\{\frac{\partial n_1^k}{\partial r}+z^k\left[n_1^k\frac{d\Phi_0}{dr}+(n_\infty^k+n_0^k)\frac{\partial\Phi_1}{\partial r}\right]\right\}\\&\quad-\bar{\omega}^k\left\{\frac{\partial\bar{n}^k}{\partial r}+z^k\left[\bar{n}_1^k\frac{d\bar{\Phi}_0}{dr}+(\bar{n}_\infty^k+\bar{n}_0^k)\frac{\partial\bar{\Phi}_1}{\partial r}\right]\right\}\\&=\frac{1}{(a\kappa)r\sin\theta}\frac{\partial}{\partial\theta}\left\{\sin\theta\left[\mathrm{Pe}\,v_1\Gamma_0^k-\frac{\omega_S^k}{r}\left(\frac{\partial\Gamma_1^k}{\partial\theta}+z^k\Gamma_0^k\frac{\partial\Phi_1}{\partial\theta}\right)\right]\right\}\\&\qquad\qquad k=1,2,\ldots,N.\end{aligned} \tag{2.33}$$

The far-field ($r\to\infty$) conditions are

$$\begin{aligned}&\Phi_1\to-r\cos\theta,\\&u_1\to-\mu_e\cos\theta,\\&v_1\to-\mu_e\sin\theta,\\&n_1^k\to0;\qquad k=1,2,\ldots,N.\end{aligned} \tag{2.34}$$

The first of these conditions is simply that the electric field is purely the applied field far from the drop. The second is that the velocity of the fluid (relative to the center of the drop) is the velocity of the drop, which in the scaled system is the mobility. The last is that the concentration of each ion species far from the drop is that of the bulk value n_∞^k, and so the disturbance from the equilibrium value goes to zero.

At the center of the drop ($r = 0$)

$$\begin{aligned} \bar{\Phi}_1 &= 0, \\ r\bar{\mathbf{u}}_1 &= 0, \\ \bar{n}_1^k &= 0; \qquad k = 1, 2, \ldots, N. \end{aligned} \tag{2.35}$$

Introducing the Ionic Potentials

It has been shown [38] that combining the dependent variables of concentration and mobility greatly simplifies the electrokinetics problem. The ionic potentials are defined as

$$n_1^k(r,\theta) = -z^k(n_\infty^k + n_0^k)\left[\Phi_1(r,\theta) + \Phi_1^k(r,\theta)\right]; \qquad k = 1, 2, \ldots, N, \tag{2.36}$$

and similarly for the interior.

The only dependent variables are now those of velocity and ionic potential. They are separated according to

$$\begin{aligned} u_1(r,\theta) &= -\frac{2}{r}h_1(r)\cos\theta, \\ v_1(r,\theta) &= \frac{1}{r}\frac{d}{dr}[rh_1(r)]\sin\theta, \\ \Phi_1^k(r,\theta) &= \phi^k(r)\cos\theta; \qquad k = 1, 2, \ldots, N. \end{aligned} \tag{2.37}$$

h_1 is the radial dependence of the stream function. ϕ_1^k will be referred to as the ionic potential for each ion species, k.

The electrokinetic problem is now reduced to a set of $N + 1$ ordinary differential equations in r

$$\frac{d^2\phi_1^k}{d^2r} + \frac{2}{r}\frac{d\phi_1^k}{dr} - \frac{2}{r^2}\phi_1^k - z^k\frac{d\Phi_0}{dr}\frac{d\phi_1^k}{dr} + 2\frac{\mathrm{Pe}}{\omega^k}\frac{d\Phi_0}{dr}\frac{h_1}{r} = 0; \qquad k = 1, 2, \ldots, N \tag{2.38}$$

for the ion balances, and

$$\frac{d^4h_1}{d^2r}+\frac{4}{r}\frac{d^3h_1}{d^2r}-\frac{4}{r^2}\frac{d^2h_1}{d^2r}+\frac{(a\kappa)^2}{r}\frac{d\Phi_0}{dr}\sum_{k=1}^{N}(z^k)^2(n_\infty^k+n_0^k)\phi_1^k=0 \tag{2.39}$$

for the momentum balance.

The interfacial conditions now read, for stress balance

$$\frac{d^2h_1}{d^2r}(1)-\frac{\bar{\mu}}{\mu}\frac{d^2\bar{h}_1}{d^2r}(1)-(a\kappa)\sum_{k=1}^{N}K^k(n_\infty^k+n_0^k)\phi_1^k(1)=0, \tag{2.40}$$

ion balances

$$\begin{aligned}&-z^k\omega^k(n_\infty^k+n_0^k)\frac{d\phi^k}{dr}(1)+z^k\bar{\omega}^k(\bar{n}_\infty^k+\bar{n}_0^k)\frac{d\bar{\phi}_1^k}{dr}(1)\\&=\frac{2}{a\kappa}\left[\mathrm{Pe}\,K^k(n_\infty^k+n_0^k)\frac{dh_1}{dr}(1)-z^k\omega_S K^k(n_\infty^k+n_0^k)\phi_1^k(1)\right];\\&\qquad\qquad k=1,2,\ldots,N,\end{aligned} \tag{2.41}$$

continuity of velocity

$$\begin{aligned}h_1(1)=\bar{h}_1(1)=0\\\frac{dh_1}{dr}(1)=\frac{d\bar{h}_1}{dr}(1),\end{aligned} \tag{2.42}$$

and continuity of electric field

$$\phi_1^k(1)=\bar{\phi}_1^k(1);\qquad k=1,2,\ldots,N. \tag{2.43}$$

In the far-field,

$$\begin{aligned}\phi_1^k\to r;\qquad k=1,2,\ldots,N,\\h_1\to\frac{1}{2}\mu_e r,\end{aligned} \tag{2.44}$$

and at the drop center

$$\begin{aligned}\bar{\phi}^k=0;\qquad k=1,2,\ldots,N\\\bar{h}_1=0\\\frac{d^2\bar{h}_1}{d^2r}=0.\end{aligned} \tag{2.45}$$

This is the system of equations that will be treated in Chapter 4. It is noted that the system (2.38) – (2.45) is linear. What makes it challenging to solve are the coupling of the exterior and interior electrokinetics via the interfacial ion balance (2.41), and that the electrokinetics are so heavily dependent on the equilibrium electrostatics. In many cases of interest, it is a highly nonlinear problem, and that is the subject of the next chapter.

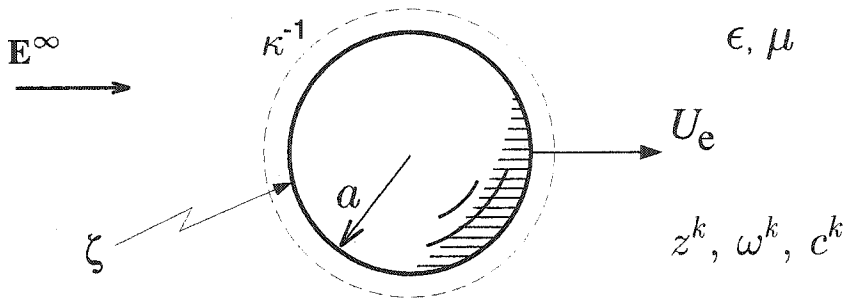

FIGURE 2.1. Definition sketch.

TABLE 2.1. Characteristic scales used in making the governing equations dimensionless

Name	Characteristic Scale
Radial distance	a
Electric potential	$\dfrac{k_B T}{e}$
Velocity	$\dfrac{\epsilon\epsilon_0 (k_B T)^2}{e^2 \mu a}$
Electrophoretic mobility	$\dfrac{\epsilon\epsilon_0 k_B T}{\mu e}$
Pressure	$\dfrac{\epsilon\epsilon_0 (k_B T)^2}{(ea)^2}$
Ion mobility	ω_0
Volumetric ion concentration	$\sum_{k=1}^{N} (z^k)^2 c_\infty^k$
Interfacial ion concentration	$\kappa^{-1} \sum_{k=1}^{N} (z^k)^2 c_\infty^k$
Surface charge density	$\dfrac{\kappa\epsilon_0\epsilon k_B T}{e}$
Surface tension	γ_0

TABLE 2.2. Dimensionless Constants

Name	Symbol	Expression
Reynolds number	Re	$\frac{\rho U a}{\mu}$
Scaled field	β	$\frac{aeE_\infty}{k_\mathrm{B}T}$
Capillary number	Ca	$\frac{\epsilon\epsilon_0(k_\mathrm{B}T)^2}{ae^2\gamma_0}$
Peclet number	Pe	$\frac{\epsilon\epsilon_0 k_\mathrm{B}T}{\mu\omega_0 e^2}$
Scaled radius	$a\kappa$	$a\sqrt{\frac{e^2\sum_{k=1}^{N}(z^k)^2 c_\infty^k}{\epsilon\epsilon_0 k_\mathrm{B}T}}$

3. Equilibrium Electrostatics of a Fluid Drop

3.1. Introduction

In the expansion of the electrokinetic system (2.16) – (2.19), it is noted that the only nonlinear problem is that of the equilibrium electrostatics. As such, this leading-order problem provides its own difficulty, and the success with which this difficulty is met has great bearing on one's ability to work successfully with the mobility, or $O(\beta)$ problem. Here, the leading-order problem — the Poisson-Boltzmann equation — is written and give two approximate solutions are derived. First are shown approximations for small interfacial potentials, known as the Debye-Hückel formulas. In addition, a thin double-layer analysis is applied to determine a matched asymptotic expansion. This method is an extension of a strained-coordinate method applied by Natarajan and Schecter [35] to the exterior problem, which is employed to third-order for both the interior and exterior potentials. The results are summarized in a paper by Erker and Baygents [17] which appears here in Appendix D. In that paper, there was also applied a rescaling technique used by Ohshima, Healy, and White [40] to determine estimates for the interior potential and for the interfacial charge density of the drop. Here is provided the derivation of estimates given by the strained coordinate method, in greater detail than in the article [17].

Recall that the possibility of a jump in interfacial potential is considered, with distinct interior and exterior surface potentials, denoted as $\Phi(1)$ and $\bar{\Phi}(1)$. In Fig 3.1, hypothetical potential profiles of the drop for the interior and exterior are shown. At equilibrium, the interior and exterior problems are decoupled, thus the problems may be solved independently. Following are the analytic estimates will be derived, based on small interfacial potentials and thin double-layers. In the latter case, the complete derivation for the interior problem will be shown, with an explanation of how one

derives the exterior approximations in an analogous way.

3.2. The Poisson-Boltzmann Equation

At equilibrium, or leading order, spherical symmetry reduces the governing equations to ordinary differential equations in the radial variable r. The ion balance is then integrated and the Boltzmann distribution of ions in the double-layer is seen, *viz.*

$$n_\infty^k + n_0^k = n_\infty^k \exp(-z^k \Phi_0), \qquad k = 1, 2, \ldots, N, \tag{3.1}$$

and

$$\bar{n}_\infty^k + \bar{n}_0^k = \bar{n}_\infty^k \exp[-z^k(\bar{\Phi}_0 - \Delta\Psi)], \qquad k = 1, 2, \ldots, N, \tag{3.2}$$

for the exterior and interior phases, respectively.

The charge regulation, or Poisson-Boltzmann equation, in spherical coordinates reads

$$\frac{\partial^2 \Phi_0}{\partial r} + \frac{2}{r}\frac{\partial \Phi_0}{\partial r} = -(a\kappa)^2 \sum_{k=1}^{N} z^k n_\infty^k \exp(-z^k \Phi_0), \tag{3.3}$$

with boundary conditions

$$\Phi_0(1) = \tilde{\zeta}_{\mathrm{E}}, \tag{3.4}$$

$$\lim_{r\to\infty} \Phi_0(r) = 0. \tag{3.5}$$

And for the interior,

$$\frac{\bar{\epsilon}}{\epsilon}\left(\frac{\partial^2 \bar{\Phi}_0}{\partial r} + \frac{2}{r}\frac{\partial \bar{\Phi}_0}{\partial r}\right) = -(a\kappa)^2 \sum_{k=1}^{N} z^k \bar{n}_\infty^k \exp[-z^k(\bar{\Phi}_0 - \Delta\Psi)]. \tag{3.6}$$

The potential $\tilde{\zeta}_{\mathrm{E}}$ is the scaled surface potential on the exterior side of the interface, that is

$$\tilde{\zeta}_{\mathrm{E}} = \frac{e\zeta}{k_{\mathrm{B}}T}. \tag{3.7}$$

Before writing the boundary conditions for the interior problem, the substitution

$$\Psi_0 = \bar{\Phi}_0 - \Delta\Psi. \tag{3.8}$$

is made. Thus (3.6) now reads

$$\frac{\bar{\epsilon}}{\epsilon}\left(\frac{\partial^2\Psi_0}{\partial r} + \frac{2}{r}\frac{\partial\Psi_0}{\partial r}\right) = -(a\kappa)^2 \sum_k z^k \bar{n}_\infty^k \exp(-z^k\Psi_0). \tag{3.9}$$

The boundary conditions for the interior are

$$\Psi_0(1) = \tilde{\zeta}_\mathrm{I}, \tag{3.10}$$

$$\Psi'(0) = 0. \tag{3.11}$$

$\tilde{\zeta}_\mathrm{I}$ is the (scaled) potential at the interior side of the interface, $\bar{\Phi}(1)$, minus the interfacial potential difference $\Delta\Psi$. That is

$$\tilde{\zeta}_\mathrm{I} = \frac{e}{k_\mathrm{B}T}(\bar{\Phi}_0(1) - \delta\psi) = \Phi_0(1) - \Delta\Psi. \tag{3.12}$$

The potentials $\delta\psi$ and $\Delta\Psi$ each represent the interphase potential difference, in dimensional and scaled form, respectively.

The charge regulation at the interface is

$$-\frac{d\Phi_0}{dr}(1) + \frac{\bar{\epsilon}}{\epsilon}\frac{d\bar{\Phi}_0}{dr}(1) = a\kappa \sum_{k=1}^{N} z^k \Gamma_0^k. \tag{3.13}$$

Because the interfacial potentials are specified as boundary conditions, the surface charge density must relate to these potentials and the specific and non-specific adsorption of ions to ensure that the charge regulation condition is satisfied. Recall the linear adsorption expression for surface densities of solutes (2.7), which at equilibrium reads

$$\Gamma_0^k = K^k(n_\infty^k + n_0^k) = \bar{K}^k(\bar{n}_\infty^k + \bar{n}_0^k); \qquad k = 1, 2, \ldots, N. \tag{3.14}$$

Now are introduced the surface, or Gibbs excesses, $\Gamma_{\rm G}^k$ of solutes

$$\begin{aligned}\Gamma_{\rm G}^k =&\Gamma_0^k + a\kappa \int_1^\infty r^2 \left[1 - e^{-z^k\Phi_0(r)}\right] dr \\ &+ a\kappa\frac{\bar{n}_\infty^k}{n_\infty^k}\int_0^1 r^2 \left[1 - e^{-z^k\Psi_0(r)}\right] dr\Bigg\} \qquad k = 1, 2, \ldots, N.\end{aligned} \tag{3.15}$$

The surface excesses account for the difference between the numbers of solutes specifically and non-specifically adsorbed to the interface and and what their actual populations in the system. Combining these last two expressions gives the adsorption coefficients, K^k

$$\begin{aligned}K^k = e^{z^k\tilde{\zeta}_{\rm E}}\Bigg\{&\frac{\Gamma_{\rm G}^k}{n_\infty^k} + a\kappa \int_1^\infty r^2 \left[1 - e^{-z^k\Phi_0(r)}\right] dr \\ &+ a\kappa\frac{\bar{n}_\infty^k}{n_\infty^k}\int_0^1 r^2 \left[1 - e^{-z^k\Psi_0(r)}\right] dr\Bigg\} \qquad k = 1, 2, \ldots, N\end{aligned} \tag{3.16}$$

The charge regulation (3.13) is now expressed as The charge regulation at the interface is

$$-\frac{d\Phi_0}{dr}(1) + \frac{\bar{\epsilon}}{\epsilon}\frac{d\bar{\Phi}_0}{dr}(1) = a\kappa\sum_{k=1}^N z^k K^k n_\infty^k \exp(-z^k\tilde{\zeta}_{\rm E}). \tag{3.17}$$

It is noted that

$$\sum_{k=1}^N z^k\Gamma_{\rm G}^k = 0, \tag{3.18}$$

which means that the net charge of surface excesses of solutes is zero. This is to say that the surface excesses contribute no net charge to the interface.

3.3. Small Interfacial Potentials

For small potentials $\tilde{\zeta}_{\rm E}$ and $\tilde{\zeta}_{\rm I}$, the Poisson-Boltzmann equations can be linearized, *viz.*

$$\frac{d^2\Phi_0}{dr} + \frac{2}{r}\frac{d\Phi_0}{dr} = (a\kappa)^2\Phi_0, \tag{3.19}$$

and

$$\frac{\bar{\epsilon}}{\epsilon}\left(\frac{\partial^2\Psi_0}{\partial r}+\frac{2}{r}\frac{\partial\Psi_0}{\partial r}\right)=(a\kappa)^2\sum_k z^k\bar{n}_\infty^k\Psi_0. \tag{3.20}$$

The equation for the interior simplifies to

$$\frac{\partial^2\Psi_0}{\partial r}+\frac{2}{r}\frac{\partial\Psi_0}{\partial r}=(a\bar{\kappa})^2\Psi_0, \tag{3.21}$$

where the $a\bar{\kappa}$ is the radius scaled by the *interior* Debye screening length, defined analogously to that of the interior (see TABLE 2.2).

The solutions to (3.19) and (3.21) are well-known and referred to as the Debye-Hückel approximations, *viz.*

$$\Phi_0(r)=\tilde{\zeta}_{\mathrm{E}}\left\{\frac{\exp[-a\kappa(r-1)]}{r}\right\} \tag{3.22}$$

and

$$\Psi_0(r)=\frac{A}{\sinh(a\bar{\kappa})}\frac{\sinh(a\bar{\kappa}r)}{r}. \tag{3.23}$$

The derivatives of the potential are easily computed, but they will be expressed here anyway, since they are important:

$$\frac{d\Phi_0}{dr}=-\Phi_0\left(a\kappa+\frac{1}{r}\right), \tag{3.24}$$

$$\frac{d\Psi_0}{dr}=\Psi_0\left[a\bar{\kappa}\coth(a\bar{\kappa}\ r)-\frac{1}{r}\right]. \tag{3.25}$$

3.4. Thin Double-Layer Analysis

There have been many treatments of the Poisson-Boltzmann equation for thin double-layers. The simple case of a flat surface bounding an electrolyte is well-known. For the electrostatic profile of an electrolyte surrounding a sphere, several analyses have

been done that provide analytic estimates to the nonlinear problem, including [40] and [35]. Like those, consideration is limited to a z-z electrolyte.

The Poisson-Boltzmann equations for a z-z electrolyte are

$$\frac{\partial^2 \Phi_0}{\partial r} + \frac{2}{r}\frac{\partial \Phi_0}{\partial r} = (a\kappa)^2 \frac{\sinh z\Phi_0}{z} \tag{3.26}$$

and

$$\frac{\partial^2 \Psi_0}{\partial r} + \frac{2}{r}\frac{\partial \Psi_0}{\partial r} = (a\bar{\kappa})^2 \frac{\sinh z\Psi_0}{z}. \tag{3.27}$$

Φ_0 and Ψ_0 are the equilibrium potentials for which will be solved, and z is the valence of the cation of the electrolyte.

Because the right hand side, which gives the volume charge density, is a nonlinear function of the dependent variable Φ_0 or Ψ_0, the differential equation is nonlinear, and an exact analytical solution is not hoped for. However, taking into account two limiting cases will be seen to give highly accurate estimates. First are examined the electrostatics far from the drop interface, where the electrolyte is essentially neutral. The electric potential is therefore small and the differential equation linear. In addition, for reasonably high dielectric constants of the fluid (water, for example), the characteristic length scale of the electric field is much smaller than the size of the drop. The electrostatics then closely resemble those near a flat interface. While in this case the governing equation remains nonlinear, the scaling according to the thinness of the double layer renders the problem tractable to analytic approximation methods. Thus, there will be two approximate solutions each for the exterior and interior: one away from the interface and one near it. The principles of matched asymptotics will be used to help determine those solutions.

In this section, the interior problem is treated, with the scaling given and the matched asymptotic solution derived. The method for the exterior problem is analogous and the results are stated thereafter.

Method of Strained Coordinates

To approximate the interior problem 3.27, 3.8, a method that was applied to the exterior problem 3.19, 3.5, is used. The method is described in the excellent book by Van Dyke [54], and is called the *strained coordinate* method. To describe it as it is applied here, it is noted that because the double-layer is thin, the interface appears flat from a perspective in the double-layer. Indeed, in the limit that the dimensionless parameter $a\bar{\kappa}$ goes to infinity, the interface is flat. In this case, the nonlinear problem has a closed-form solution. An approximate solution is made by adding to the flat-interface solution terms multiplied by successive powers of $1/a\bar{\kappa}$, or $a\kappa$ for the corresponding exterior problem.

The proper length scale for the interior problem in the double-layer is the Debye length, $\bar{\kappa}^{-1}$, which for a z-z electrolyte is given by

$$\bar{\kappa}^2 = \frac{2e^2 z^2 \bar{c}_\infty}{\bar{\epsilon}\epsilon_0 k_B T}, \tag{3.28}$$

where $\bar{c}_\infty$ is the bulk concentration of the anions and cations. By a thin double-layer, it is meant that the Debye length is small compared to the radius of the drop, *viz.*

$$\bar{\delta} = \frac{1}{a\bar{\kappa}} \ll 1.$$

In the dimensionless system, the dimensionless parameter $\bar{\delta}$ is the characteristic length scale of the double-layer. Far from the interface, the characteristic length scale is the drop radius, a, or in the dimensionless system, unity. The disparate length scales of the problem indicate that matched asymptotic expansions should be use to approximate solutions near to and far from the drop interface. Such an approximation will be generated via the strained coordinate method.

To start, the simpler problem for the electrostatics far from the interface is solved. This problem is called the "outer" problem in the parlance of matched asymptotics. It is pointed out that although when the region deep inside the drop is referred to, the

word outer is applicable in the sense that it is far from the boundary layer, or "inner" layer, which is the region (near the interface) where the solution varies rapidly. For the exterior problem, the outer region is indeed the region far outside the drop.

Far from the interface in the interior, the electrostatic potential should be very close to the interphase potential difference $\Delta\Psi$, and so the variable Ψ_0 is small enough to justify the linearization of the problem 3.9. The solution then reads

$$\Psi_{\text{out}}(r) = \frac{\bar{Y}}{\sinh(a\bar{\kappa})}\frac{\sinh(a\bar{\kappa}\, r)}{r}, \tag{3.29}$$

where $\bar{Y}$ is an as-of-yet undetermined constant of integration called the *reduced surface potential* for the interior. This solution is easily seen to satisfy the condition at the drop center, but the interfacial boundary condition ($\Psi_0(1) = A$) must not be used to determine $\bar{Y}$, since again this solution is not appropriate near the interface (unless, as noted earlier, A is itself small). To determine $\bar{Y}$ and thus complete the outer solution, an inner solution Ψ_{in}, must be generated, which will in turn be partly determined by matching it with the outer solution.

To begin generating the inner solution, first rescale the inner, or double-layer region

$$\bar{x} = \frac{1-r}{\bar{\delta}}. \tag{3.30}$$

The Poisson-Boltzmann equation for the interior now reads

$$\frac{d\Psi_{\text{in}}^2}{d\bar{x}} - \frac{2\bar{\delta}}{1-\bar{\delta}}\frac{d\Psi_{\text{in}}}{d\bar{x}} = \sinh\Psi_{\text{in}} \tag{3.31}$$

Note that when $\bar{\delta}$ is zero, that is when the double-layer is infinitely thin, the problem is considerably simpler, and is in fact integrable, with solution

$$z\Psi_{\text{in}} = 4\tanh^1(\bar{p}e^{-s}), \qquad \bar{p} = \tanh(\tilde{\zeta}_{\text{I}}/4). \tag{3.32}$$

In general, the parameter $\bar{\delta}$ is not zero, and for a small value of it, this "flat-interface" solution can be adjusted by making an expansion of the coordinate $\bar{x}$, *viz.*

$$\bar{x} = s + \bar{\delta}\bar{\alpha}_1(s) + \bar{\delta}^2\bar{\alpha}_2(s) + \bar{\delta}^3\bar{\alpha}_3(s) + \ldots,. \tag{3.33}$$

This is unlike conventional perturbation schemes in the sense that the *independent* variable is expanded with respect to the perturbation parameter. The new variable s is called the strained coordinate. (Overbars will not be used in this variable, even though it is distinct from the corresponding exterior strained coordinate. The reason for this is simply to avoid a mess.) The functions $\bar{\alpha}_i(s)$ are called *straining functions.*

With the change in variable (3.33), the Poisson-Boltzmann is changed according to the changes in derivatives, *viz.*

$$\frac{d\Psi_0}{d\bar{x}} = \frac{d\Psi_0}{ds}\frac{ds}{d\bar{x}},$$

$$\frac{d^2\Psi_0}{d^2\bar{x}} = \frac{d\Psi_0}{ds}\frac{d^2s}{d^2\bar{x}} + \frac{d^2\Psi_0}{d^2\bar{x}}\left(\frac{ds}{d\bar{x}}\right)^2,$$

where

$$\frac{ds}{d\bar{x}} = 1 - \bar{\delta}\bar{\alpha}_1' + \bar{\delta}^2\left[(\bar{\alpha}_1')^2 - \bar{\alpha}_2'\right] + \bar{\delta}^3\left[2\bar{\alpha}_1'\bar{\alpha}_2' - (\bar{\alpha}_1')^3 - \bar{\alpha}_3'\right], \tag{3.34}$$

$$\frac{d^2s}{d^2\bar{x}} = -\bar{\delta}\bar{\alpha}_1'' + \bar{\delta}^2(3\bar{\alpha}_1'\bar{\alpha}_1'' - \bar{\alpha}_2'') + \bar{\delta}^3\left[-6(\bar{\alpha}_1')^2\bar{\alpha}_1'' + 3\bar{\alpha}_1''\alpha_2' + 3\bar{\alpha}_1'\bar{\alpha}_2'' - \bar{\alpha}_3''\right], \tag{3.35}$$

and

$$\left(\frac{ds}{d\bar{x}}\right)^2 = 1 - 2\bar{\delta}\bar{\alpha}_1' + \bar{\delta}^2\left[3(\bar{\alpha}_1')^2 - 2\bar{\alpha}_2'\right] + \bar{\delta}^3\left[-4(\bar{\alpha}_1')^3 + 6\bar{\alpha}_1'\bar{\alpha}_2' - 2\bar{\alpha}_3'\right]. \tag{3.36}$$

Substituting these derivatives into (3.21) and grouping terms according to orders in $\bar{\delta}$, generates a hierarchy of differential equations. The leading-order equation is, as it should be, the flat-plate equation

$$\frac{d\Psi_{\text{in}}^2}{ds} = \frac{\sinh z\Psi_{\text{in}}}{z}, \tag{3.37}$$

with solution

$$z\Psi_{\text{in}} = 4\tanh^1(\bar{p}e^{-\bar{x}}), \qquad \bar{p} = \tanh(\tilde{\zeta}_{\text{I}}/4). \tag{3.38}$$

With the nonlinearity occurring at leading-order, the higher-order equations are all linear, which is quite common in perturbation solutions to nonlinear differential equations. At orders $i = 1$, 2, and 3, the equations read

$$\bar{\alpha}_i''(s) - 2q(s)\bar{\alpha}_i'(s) = \bar{r}_i(s), \tag{3.39}$$

where

$$\bar{r}_1(s) = -2, \tag{3.40}$$

$$\bar{r}_2(s) = \frac{3}{2}\bar{\alpha}_1'\bar{\alpha}_1'' - \bar{\alpha}_1' - 2s, \tag{3.41}$$

and

$$\bar{r}_3(s) = \bar{\alpha}_1'^2\left(\frac{\bar{\alpha}_1''}{2} - 1\right) - 2\bar{\alpha}_1 - 4\bar{\alpha}_1's - 2s^2 + \bar{\alpha}_2'(3\bar{\alpha}_1'' + 2). \tag{3.42}$$

The expressions for $\bar{r}_i$ will become explicit as the solution at each order is worked out.

Solving the differential equation (3.39) is straightforward, but becomes increasingly tedious as one goes further along in the hierarchy.

To solve, first is found the integration factor

$$\mu(s) = \exp\left[-2\int_s q(s)ds\right] = \frac{\bar{p}^2e^{-2s}}{(1-\bar{p}^2e^{-2s})^2} \tag{3.43}$$

Thus,

$$[\mu(s)\bar{\alpha}_i'(s)]' = \mu(s)\bar{r}_i(s), \tag{3.44}$$

$$\bar{\alpha}_i'(s) = \frac{1}{\mu(s)}\int_s \mu(\xi)\bar{r}_i(\xi)d\xi + \frac{c_1}{\mu(s)}, \tag{3.45}$$

and

$$\bar{\alpha}_i(s) = \int_s \frac{1}{\mu(\xi)} \int_\xi \mu(\eta)\bar{r}_i(\eta)d\eta \; d\xi + c_1 \int_s \frac{1}{\mu(\xi)} d\xi + c_2 \tag{3.46}$$

The constants c_1 and c_2 will be chosen so as to satisfy the condition that $\bar{\alpha}_i(0) = 0$ and to ensure that no terms in $\bar{\alpha}_i$ grow exponentially with s, which would render the inner solution Ψ_{in} unmatchable to the outer solution Ψ_{out}.

With

$$\bar{r}_1(s) = -2, \tag{3.47}$$

the solution to the first correction to the flat-plate potential is

$$\bar{\alpha}_1'(s) = 1 - \bar{p}^2 e^{-2s}, \tag{3.48}$$

and

$$\bar{\alpha}_1(s) = s - \frac{\bar{p}^2}{2}(1 - \bar{p}^2 e^{-2s}). \tag{3.49}$$

Plugging this solution into (3.41) gives

$$\bar{r}_2(s) = \; -(1 - 3\bar{p}^2 e^{-2s})(1 - \bar{p}^2 e^{-2s}) - 2s, \tag{3.50}$$

with solutions

$$\begin{aligned} \bar{\alpha}_2'(s) =& \frac{1}{2}(1 - \bar{p}^2 e^{-2s}) \\ & \times \left[3(1 - \bar{p}^2 e^{-2s}) - \frac{\ln(1 - \bar{p}^2 e^{-2s})}{\bar{p}^2 e^{-2s}} - \ln(1 - \bar{p}^2 e^{-2s}) + 2s \right], \end{aligned} \tag{3.51}$$

and

$$\begin{aligned} \bar{\alpha}_2(s) =& \frac{s^2}{2} + s + \frac{s\bar{p}^2 e^{-2s}}{2} - 2\bar{p}^2(1 - \bar{p}^2 e^{-2s}) + \frac{3}{8}\bar{p}^4(1 - e^{-4s}) \\ & - \frac{1 - \bar{p}^4}{4\bar{p}^4} \ln(1 - \bar{p}^2) + \frac{e^{2s}}{4\bar{p}^2} \ln(1 - \bar{p}^2 e^{-2s}) - \frac{\bar{p}^2 e^{-2s}}{4} \ln(1 - \bar{p}^2 e^{-2s}) \\ & - \frac{1}{2} \int_{\bar{p}^2 e^{-2s}}^{\bar{p}^2} \frac{\ln(1 - t)}{t} dt. \end{aligned} \tag{3.52}$$

Now, while it is regrettable that the integral that appears in (3.52) has no closed form solution, to compute it numerically is much simpler than computing the exact solution of the Poisson-Boltzmann equation.

Plugging the first and second order solutions and their derivatives into (3.42) gives

$$\begin{aligned}\bar{r}_3(s) = &-(1-\bar{p}^2e^{-2s})^3 - 2s - 2s^2 + \bar{p}^2(1-\bar{p}^2e^{-2s}) - 4s(1-\bar{p}^2e^{-2s}) \\ &+ 3\left[3(1-\bar{p}^2e^{-2s})^2 + \frac{(1-\bar{p}^2e^{-2s})^2}{\bar{p}^2e^{-2s}}\ln(1-\bar{p}^2e^{-2s}) + 2s(1-\bar{p}^2e^{-2s})\right] \\ &\times (1+3\bar{p}^2e^{-2s})\end{aligned} \tag{3.53}$$

$$\begin{aligned}\bar{\alpha}_3'(s) = &+ s\Bigg[\, 3\bar{p}^4e^{-4s} - 8\bar{p}^2e^{-2s} + \bar{p}^2e^{-2s}\ln\left(1-\bar{p}^2e^{-2s}\right) + \frac{\ln\left(1-\bar{p}^2e^{-2s}\right)}{\bar{p}^2e^{-2s}} \\ &\quad - \frac{\bar{p}^4e^{-4s}}{1-\bar{p}^2e^{-2s}} + \frac{1}{1-\bar{p}^2e^{-2s}} + 3\Bigg] \\ &+ s^2\left(1-\bar{p}^2e^{-2s}\right) + \frac{\bar{p}^4e^{-2s}}{2} - \frac{5\bar{p}^6e^{-6s}}{2} - 2\left(\frac{9}{4} + \ln\bar{p}\right)\ln\left(1-\bar{p}^2e^{-2s}\right) \\ &+ 7\bar{p}^4e^{-4s} + \frac{5}{2} - \frac{\bar{p}^2}{2} - 7\bar{p}^2e^{-2s} - \frac{\bar{p}^2e^{-2s}\ln\left(1-\bar{p}^2e^{-2s}\right)}{2} \\ &+ \frac{\ln\left(1-\bar{p}^2e^{-2s}\right)}{2\bar{p}^2e^{-2s}} + \frac{1}{4}\left(4 + 17\bar{p}^2e^{-2s} - 3\bar{p}^4e^{-4s}\right)\ln\left(1-\bar{p}^2e^{-2s}\right) \\ &+ \frac{\left(1-\bar{p}^2e^{-2s}\right)\left(4 + 17\bar{p}^2e^{-2s} - 3\bar{p}^4e^{-4s}\right)\ln\left(1-\bar{p}^2e^{-2s}\right)}{4\bar{p}^2e^{-2s}}\end{aligned} \tag{3.54}$$

and

$$\begin{aligned}\bar{\alpha}_3(s) =& \frac{s^3}{3} + \frac{s^2}{2}\left(3+\bar{p}^2e^{-2s}\right) \\ & s\Bigg[\frac{3}{2} - \frac{\bar{p}^2}{2} + \frac{9}{2}\bar{p}^2e^{-2s} - \frac{3}{4}\bar{p}^4e^{-4s} - \frac{\bar{p}^2e^{-2s}}{2}\ln\left(1-\bar{p}^2e^{-2s}\right) \\ & \quad \frac{\ln\left(1-\bar{p}^2e^{-2s}\right)}{2\bar{p}^2e^{-2s}}\Bigg] \\ & -\frac{63}{8}\bar{p}^2\left(1-e^{-2s}\right) + \frac{19}{4}\bar{p}^4 - \frac{\bar{p}^4e^{-4s}}{4} - \frac{5}{12}\bar{p}^6(1-e^{-6s}) \\ & + \frac{\left(1-\bar{p}^2e^{-2s}\right)\left(4+17\bar{p}^2e^{-2s}-3\bar{p}^4e^{-4s}\right)\ln\left(1-\bar{p}^2e^{-2s}\right)}{8\bar{p}^2e^{-2s}} \\ & - \frac{(1-\bar{p}^2)(1+17\bar{p}^2-3\bar{p}^4)\ln(1-\bar{p}^2)}{8\bar{p}^2} \\ & - \frac{17}{8}\bar{p}^4e^{-4s} - \left(\frac{9}{4}+\ln\bar{p}\right)\left[\int_1^s \frac{t}{1-t}dt - \int_{\bar{p}^2e^{-2s}}^1 \frac{t}{1-t}dt\right] \\ & + \frac{1}{2}\int_{\bar{p}^2e^{-2s}}^{\bar{p}^2} \frac{\ln t\ln(1-t)}{t}dt\end{aligned} \tag{3.55}$$

Now, having the straining functions $\bar{\alpha}_i$ for $i = 1, 2, 3$, it is now necessary to transform the solution back into the scaled radial variable $\bar{x}$. If x is expanded as in (3.33), then it can be said that s can be expanded in x, *viz.*

$$s = \bar{x} + \bar{\delta}\bar{\beta}_1(\bar{x}) + \bar{\delta}^2\bar{\beta}_2(\bar{x}) + \bar{\delta}^3\bar{\beta}_3(\bar{x}) + \ldots,. \tag{3.56}$$

Substituting (3.56) into (3.33) yields

$$\begin{aligned}x =& x + \bar{\delta}\bar{\beta}_1(x) + \bar{\delta}^2\bar{\beta}(x) + \bar{\delta}^3\bar{\beta}(x) \\ & + \bar{\delta}\bar{\alpha}_1(x+\bar{\delta}\bar{\beta}_1 + \bar{\delta}^2\bar{\beta}_2) \\ & + \bar{\delta}^2\bar{\alpha}_2(x+\bar{\delta}\bar{\beta}_1) + \bar{\delta}^3\bar{\alpha}_3(x)\end{aligned} \tag{3.57}$$

Now, the functions $\bar{\alpha}_i$ can be expanded as Taylor series. For example,

$$\begin{aligned}&\bar{\alpha}_1\left(x+\bar{\delta}\bar{\beta}_1(x)+\bar{\delta}^2\bar{\beta}_2(x)\right)\\&=\bar{\alpha}_1(x)+\bar{\alpha}_1'(x)(\bar{\delta}\bar{\beta}_1+\bar{\delta}^2\bar{\beta}_2)+\frac{\bar{\alpha}_1''(x)}{2}(\bar{\delta}\bar{\beta}_1+\bar{\delta}^2\bar{\beta}_2)^2.\end{aligned}\tag{3.58}$$

The straining functions $\bar{\alpha}_2$ and $\bar{\alpha}_2$ are expanded accordingly. The expansions are all made in (3.57), and after multiplying out, terms in like powers of $\bar{\delta}$ are collected up to order 3, and thus

$$\begin{aligned}\bar{\beta}_1(x)&=-\bar{\alpha}_1(x),\\\bar{\beta}_2(x)&=-\bar{\alpha}_1'(x)\bar{\beta}_1(x)-\bar{\alpha}_2(x),\\\bar{\beta}_3(x)&=-\bar{\alpha}_1'(x)\bar{\beta}_2(x)-\bar{\alpha}_2'(x)\bar{\beta}_1(x)-\frac{1}{2}\bar{\alpha}_1''(x)\bar{\beta}_1^2(x)-\bar{\alpha}_3(x).\end{aligned}\tag{3.59}$$

The solution for the potential is The inverse straining functions $\bar{\beta}_i$, $i=1,2,3$, is (3.32), with (3.56) and (3.59).

The Solution in the Exterior

As mentioned, the solution to the Poisson-Boltzmann equation for the exterior equilibrium problem has been computed with the same method by Natarajan and Schecter [35], through $O(\delta^2)$. The solution is derived in the same manner as for the interior, with

$$x=\frac{r-1}{\delta},\tag{3.60}$$

where δ is the dimensionless Debye length, or $1/a\kappa$. The strained coordinate s is defined in analogous fashion, and thus is derived a solution of the form

$$\Phi_0=\frac{4\tanh^{-1}(pe^{-s})}{z},\qquad p=\tanh(\tilde{\zeta}_{\mathrm{E}}/4),\tag{3.61}$$

and the hierarchy of differential equations is

$$\alpha_i''(s)-2q(s;p)\alpha_i'(s)=(-1)^i\bar{r}_1(s),\qquad i=1,2,3,\ldots\ .\tag{3.62}$$

Thus,

$$\alpha_i(s;p) = (-1)^i \bar{\alpha}_i(s;p), \tag{3.63}$$

and

$$\beta_i(s;p) = (-1)^i \bar{\beta}_i(s;p), \tag{3.64}$$

3.5. Comparison with Numerical Solution

The large-$a\kappa$ analytic approximations are compared to numerically-derived solutions, which are taken to be exact. To solve the Poisson-Boltzmann equation numerically, a collocation method was used [46]. Note that in the accompanying paper in Appendix D, a shooting method [25] was used in conjunction with a Runge-Kutta method. For the values of $a\kappa$ considered in that paper, this was adequate. For $a\kappa$ values of up to 100 — which are quite realistic — a collocation method was favorable, though not ideal. The numerical results will be used for solving the electrokinetic, or $O(\beta)$ problem.

For the exterior problem, the far-field boundary condition needs to be modified because the boundary is at infinity. Equation (3.19) is linearized due to to the smallness of the potential far from the interface. The far-field solution should then obey the relationship given by (3.24). Denoting a far-field point as b, the following boundary condition is used:

$$\frac{d\Phi_0}{dr}(b) + \left(a\kappa + \frac{1}{b}\right)\Phi_0(b) = 0. \tag{3.65}$$

Experience shows that $b = 1 + 20/a\kappa$, or 20 double-layers from the interface, is sufficiently far from the interface to satisfy the condition.

The numerically-derived exterior electrostatics agree with the well-known results of Loeb, Overbeek, and Wiersema [31] for the exterior potential.

A comparison is made of the numerical solution and the four solutions that come from the strained coordinate approximation — that is, the leading order (flat interface), and the solutions with the three corrections added successively. In FIG 3.2 is shown the error in the boundary layer, or inner solution from leading order through $O(\delta^3)$, for interior and exterior scaled radii $a\kappa$ and $a\bar{\kappa}$ of 10 and scaled interfacial potentials of 10. Note that while the relative error of the inner solution is quite large, the potentials beyond the layers (interior and exterior) are so small that perhaps the absolute error is a more appropriate measure of accuracy. The smallness of this error even beyond the inner regions indicates that for the electrokinetics equations, these estimates of the equilibrium potential may be quite useful. This is more strongly demonstrated in FIG 3.3, where the error in the third-order inner solution is shown for scaled radii $a\kappa$ and $a\bar{\kappa}$ of 100, and interfacial potentials of 8. The maximum error is seen to be of the order of δ^4, which is as small as 10^{-8}.

3.6. Additional Work

Other analyses based on large $a\kappa$ and $a\bar{\kappa}$ were made by the author. They are summarized in [17], and appear in Appendix D. The asymptotic expansions for the potentials Φ_0 and Ψ_0 were used for determining the surface charge density according to (3.13). As will be done in the next chapter, when applying the equilibrium electrostatics to the mobility problem, the surface charge density will be taken as a free parameter. Thus the charge regulation will determine the interfacial potentials $\tilde{\zeta}_{\mathrm{E}}$ and $\tilde{\zeta}_{\mathrm{I}}$.

In addition, another approach was used for determining a thin double-layer estimate of potential and surface charge density. In particular, the Poisson-Boltzmann equation was rescaled according to the functional form of the leading-order potential, or flat-plate potential. This has the effect of transforming the boundary-layer problem into a regular perturbation problem, *i.e.*, an asymptotic expansion in this rescaled coordinate is valid over all space, and so no matching is required. Such a method

was used by Ohshima, Healy, and White [40] for the equilibrium potential outside a sphere. As shown in Appendix D, the same method was applied to the interior. The exterior and interior results were used to determine an estimate for the surface charge density. In this analysis, the benefit of a uniformly valid expansion was offset by the complicated form of the solution. Because of this, only one correction to the flat-plate potential was generated, and so the approximations are not as accurate as those generated via the strained coordinate method.

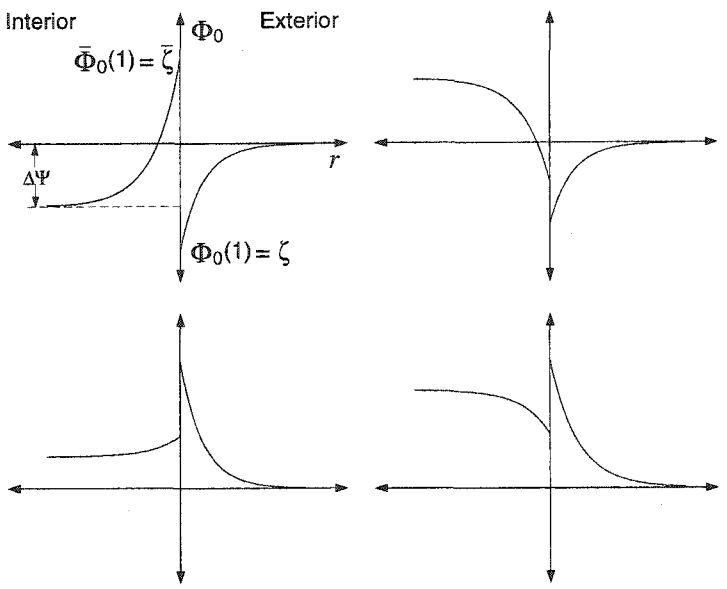

FIGURE 3.1. Plausible equilibrium potential profiles for the drop interior and exterior. The horizontal axis represents the radial coordinate r, with the interfacial value of one at the origin. In general, the potentials are discontinuous at the interface.

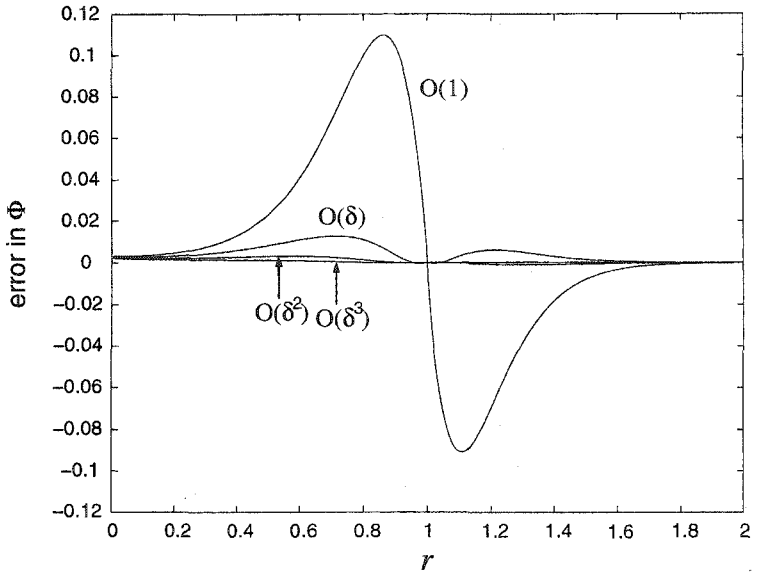

FIGURE 3.2. Comparison of boundary layer equilibrium potential estimates to numerical solution, various orders. Scaled radii $a\kappa = a\bar{\kappa} = 10$; Interfacial potentials $\tilde{\zeta}_E = \tilde{\zeta}_I = 8, \Delta\Psi = 0$.

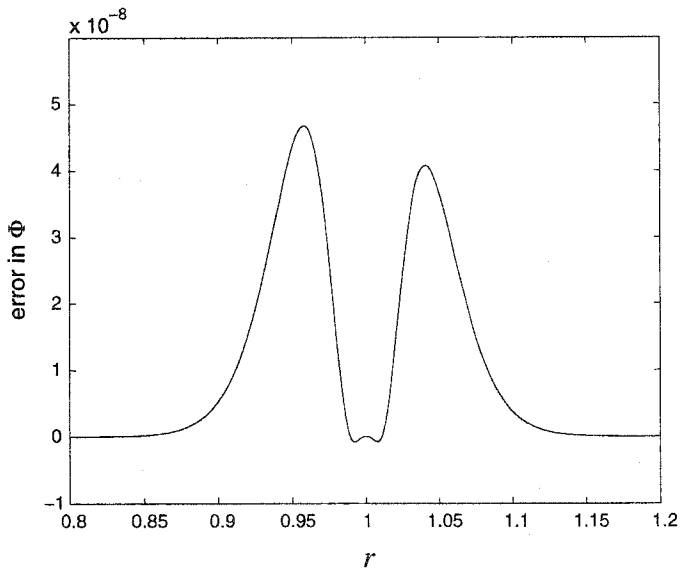

FIGURE 3.3. Comparison of boundary layer equilibrium potential estimates to numerical solution, third-order. Scaled radii $a\kappa = a\bar{\kappa} = 100$; $\tilde{\zeta}_{\mathrm{E}} = \tilde{\zeta}_{\mathrm{I}} = 8, \Delta\Psi = 0$.

4. Electrophoretic Mobility of a Fluid Drop

4.1. Integral Formulation of the Electrokinetics

Here is derived an integral form of the solution to the electrokinetic equations. They will prove useful in solving the problem numerically, as well as making analytic estimates. They are generalizations of equations derived by Ohshima, Healy, and White [41, 42].

At order β, the governing equations are those at the end of Chapter 2, namely (2.38) and (2.45), for the velocity and ionic potentials, *viz.*

$$L[L(h_1)] = -\frac{a\kappa}{r}\frac{d\Phi_0}{dr}\sum_{k=1}^{N}(z^k)^2(n_\infty^k + n_0^k)\phi_1^k(r), \qquad r > 1, \tag{4.1}$$

and

$$L[L(\bar{h}_1)] = -\frac{\mu}{\bar{\mu}}\frac{a\kappa}{r}\frac{d\bar{\Phi}_0}{dr}\sum_{k=1}^{N}(z^k)^2(\bar{n}_\infty^k + \bar{n}_0^k)\bar{\phi}_1^k(r), \qquad r < 1, \tag{4.2}$$

where

$$L < \cdot >= \frac{d}{dr}\left[\frac{1}{r^2}\frac{d}{dr}(r^2 < \cdot >)\right]. \tag{4.3}$$

The equations for ion concentration are

$$L(\phi_1^k) = z^k\frac{d\Phi_0}{dr}\left(\frac{d\phi_1^k}{dr} - 2\frac{\mathrm{Pe}}{z^k\omega^k}\frac{h_1}{r}\right); \qquad k = 1, 2, \ldots, N, \qquad r > 1, \tag{4.4}$$

and

$$L(\bar{\phi}_1^k) = z^k\frac{d\bar{\Phi}_0}{dr}\left(\frac{d\bar{\phi}_1^k}{dr} - 2\frac{\mathrm{Pe}}{z^k\bar{\omega}^k}\frac{\bar{h}_1}{r}\right); \qquad k = 1, 2, \ldots, N, \qquad r < 1. \tag{4.5}$$

For easy reference, the boundary conditions are now repeated as well. For the far field:

$$\phi_1^k(r) \to r; \qquad k = 1, 2, \ldots, N, \tag{4.6a}$$

$$h_1(r) \to \frac{1}{2}\mu_e r \tag{4.6b}$$

as $r \to \infty$. At the drop center:

$$\bar{\phi}_1^k(0) = 0; \qquad , k = 1, 2, \ldots, N, \tag{4.7a}$$

$$\bar{h}_1(0) = 0, \tag{4.7b}$$

$$\frac{d^2\bar{h}_1}{dr^2}(0) = 0, \tag{4.7c}$$

and at the interface:

$$h_1(1) = \bar{h}_1(1) = 0, \tag{4.8a}$$

$$\frac{dh_1}{dr}(1) = \frac{d\bar{h}_1}{dr}(1), \tag{4.8b}$$

$$\frac{d^2h_1}{dr^2}(1) - \frac{\bar{\mu}}{\mu}\frac{d^2\bar{h}_1}{dr^2}(1) - (a\kappa)\sum z^k K^k (n_\infty^k + n_0^k)\phi_1^k(1) = 0, \tag{4.8c}$$

$$\phi_1^k(1) = \bar{\phi}_1^k(1), \qquad k = 1, 2, \ldots, N, \tag{4.8d}$$

$$\begin{aligned} &- z^k\omega^k(n_\infty^k + n_0^k)\frac{d\phi_1^k}{dr}(1) + z^k\bar{\omega}^k(\bar{n}_\infty^k + \bar{n}_0^k)\frac{d\bar{\phi}_1^k}{dr}(1) \\ &= \frac{2}{a\kappa}\left[\mathrm{Pe}\,\frac{dh_1}{dr}(1)K^k(n_\infty^k + n_0^k) - z^k\omega_S K^k(n_\infty^k + n_0^k)\phi_1^k(1)\right], \quad k = 1, 2, \ldots, N, \end{aligned} \tag{4.8e}$$

where K^k, the adsorption coefficients for each ion, are

$$\begin{aligned} K^k = -a\kappa\, e^{z^k\tilde{\zeta}_E}\Bigg(&\frac{\bar{n}_\infty}{n_\infty}\int_0^1 \left\{\exp\left[-z^k\left(\bar{\Phi}_0 - \Delta\Psi\right)\right] - 1\right\} r^2\, dr \\ &+ \int_1^\infty r^2\left[e^{-z^k\Phi_0(r)} - 1\right] dr\Bigg), \qquad k = 1, 2, \ldots, N. \end{aligned} \tag{4.9}$$

Integrating the differential equations above, gives the following set of integral equations:

$$\phi_1^k(r) = r + \frac{B^k}{r^2} - \frac{z^k}{3}\int_1^\infty \left(r - \frac{\xi^3}{r^2}\right) G^k(\xi)\, d\xi + \frac{z^k}{3}\int_1^r \left(r - \frac{\xi^3}{r^2}\right) G^k(\xi)\, d\xi \tag{4.10}$$

$$\begin{aligned} h_1(r) =& \frac{\mu^e}{2}\left(r - \frac{1}{r^2}\right) + \frac{(a\kappa)^2}{r^2}\int_1^\infty \left(-\frac{\xi^2}{6} + \frac{\xi}{6} - \frac{1}{30\xi}\right) F(\xi)\, d\xi \\ & - (a\kappa)^2 \int_1^\infty \left(-\frac{\xi^2}{6} + \frac{r\xi}{6} - \frac{r^3}{30\xi}\right) F(\xi)\, d\xi \\ & + (a\kappa)^2 \int_1^r \left(\frac{\xi^4}{30r^2} - \frac{\xi^2}{6} + \frac{r\xi}{6} - \frac{r^3}{30\xi}\right) F(\xi)\, d\xi \end{aligned} \tag{4.11}$$

$$\bar{\phi}_1^k(r) = \bar{A}^k r + \frac{z^k}{3}\int_0^1 \left(r - \frac{\xi^3}{r^2}\right) \bar{G}^k(\xi)\, d\xi - \frac{z^k}{3}\int_r^1 \left(r - \frac{\xi^3}{r^2}\right) \bar{G}^k(\xi)\, d\xi \tag{4.12}$$

$$\begin{aligned} \bar{h}_1(r) =& \bar{C}(r - r^3) - (a\kappa)^2 \frac{\mu}{\bar{\mu}} r^3 \int_0^1 \left(\frac{\xi^4}{30} - \frac{\xi^2}{6} + \frac{\xi}{6}\right) \bar{F}(\xi)\, d\xi \\ & + (a\kappa)^2 \frac{\mu}{\bar{\mu}} \int_0^1 \left(\frac{\xi^4}{30r^2} - \frac{\xi^2}{6} + \frac{r\xi}{6}\right) \bar{F}(\xi)\, d\xi \\ & - (a\kappa)^2 \frac{\mu}{\bar{\mu}} \int_r^1 \left(\frac{\xi^4}{30r^2} - \frac{\xi^2}{6} + \frac{r\xi}{6} - \frac{r^3}{30\xi}\right) \bar{F}(\xi)\, d\xi, \end{aligned} \tag{4.13}$$

where

$$G^k(\xi) = \frac{d\Phi_0}{d\xi}\left[\frac{d\phi_1^k}{d\xi} - \frac{2\mathrm{Pe}}{z^k\omega^k}\frac{h_1(\xi)}{\xi}\right], \tag{4.14}$$

$$\bar{G}^k(\xi) = \frac{d\bar{\Phi}_0}{d\xi}\left[\frac{d\bar{\phi}_1^k}{d\xi} - \frac{2\mathrm{Pe}}{z^k\bar{\omega}^k}\frac{\bar{h}_1(\xi)}{\xi}\right], \tag{4.15}$$

$$F(\xi) = \frac{d\Phi_0}{d\xi} \sum_{k=1}^{N} (z^k)^2 (n_\infty^k + n_0^k) \phi_1^k, \tag{4.16}$$

and

$$\bar{F}(\xi) = \frac{d\bar{\Phi}_0}{d\xi} \sum_{k=1}^{N} (z^k)^2 (\bar{n}_\infty^k + \bar{n}_0^k) \bar{\phi}_1^k. \tag{4.17}$$

Notice that solution (4.12) satisfies its drop center boundary condition (4.7a). In addition, equation (4.13) satisfies (4.7b) and that (4.11) and (4.13) satisfy (4.8a). Applying the continuity of surface tangential velocity (4.8b) and continuity of ionic potential (4.8d) allows us to eliminate two more constants, viz.

$$\begin{aligned} \bar{C} = -\frac{3}{4}\mu_e + \frac{(a\kappa)^2}{2} \Bigg[& \int_1^\infty \left(-\frac{\xi^2}{3} + \frac{\xi}{2} - \frac{1}{6\xi} \right) F(\xi)\, d\xi \\ & + \frac{\mu}{\bar{\mu}} \int_0^1 \left(-\frac{\xi^4}{6} + \frac{\xi^2}{2} - \frac{\xi}{3} \right) \bar{F}(\xi)\, d\xi \Bigg], \end{aligned} \tag{4.18}$$

and

$$\bar{A}^k = 1 + B^k - \frac{z^k}{3} \int_0^1 (1 - \xi^3) \bar{G}^k(\xi)\, d\xi - \frac{z^k}{3} \int_1^\infty (1 - \xi^3) G^k(\xi)\, d\xi. \tag{4.19}$$

Those constants are then eliminated to get

$$\begin{aligned} \bar{\phi}_1^k(r) = & r \left\{ 1 + B^k - \frac{z^k}{3} \int_1^\infty (1 - \xi^3) G^k(\xi)\, d\xi \right\} \\ & + \frac{z^k}{3} \left(r - \frac{1}{r^2} \right) \int_0^1 \xi^3 \bar{G}^k(\xi)\, d\xi - \frac{z^k}{3} \int_r^1 \left(r - \frac{\xi^3}{r^2} \right) \bar{G}^k(\xi)\, d\xi, \end{aligned} \tag{4.20}$$

and

$$\begin{aligned}\bar{h}_1(r) =&(r-r^3)\left[(a\kappa)^2\int_1^\infty\left(-\frac{\xi^2}{6}+\frac{\xi}{4}-\frac{1}{12\xi}\right)F(\xi)\,d\xi-\frac{3}{4}\mu_e\right]\\&+(a\kappa)^2\frac{\mu}{\bar{\mu}}\left(\frac{r^3}{20}-\frac{r}{12}+\frac{1}{30r^2}\right)\int_0^1\xi^4\bar{F}(\xi)\,d\xi\\&-(a\kappa)^2\frac{\mu}{\bar{\mu}}\left(\frac{r^3}{12}-\frac{r}{4}+\frac{1}{6}\right)\int_0^1\xi^2\bar{F}(\xi)\,d\xi\\&-(a\kappa)^2\frac{\mu}{\bar{\mu}}\int_r^1\left(\frac{\xi^4}{30r^2}-\frac{\xi^2}{6}+\frac{r\xi}{6}-\frac{r^3}{30\xi}\right)\bar{F}(\xi)\,d\xi,\end{aligned}\tag{4.21}$$

Now, the constants B^k and μ_e can be determined from the ion and stress balances. They can be substituted into the above system, leaving a set of integral equations from which one can in theory solve to get the $2N+2$ functions $\phi_1^k(r)$, $\bar{\phi}_1^k(r)$, $h_1(r)$, and $\bar{h}_1(r)$. However, this method is outrageously complicated. It turns out to be much simpler to apply the stress balance (4.8c), saving application of the ion balance to the very last. Application of the stress balance to the equations for h_1 and $\bar{h}_1$ gives

$$\begin{aligned}h_1(r) =&\frac{(a\kappa)^2}{6}\int_1^r\left(\frac{\xi^4}{5r^2}-\xi^2+r\xi-\frac{r^3}{5\xi}\right)F(\xi)\\&+\frac{(a\kappa)^2}{6}\int_1^\infty\left\{\left[\frac{r^3}{5}-\left(\frac{\bar{\mu}}{2\mu+3\bar{\mu}}\right)r+\left(\frac{2\bar{\mu}-2\mu}{2\mu+3\bar{\mu}}\right)\frac{1}{5r^2}\right]\frac{1}{\xi}\right.\\&\qquad\left.+\left[1-\left(\frac{2\mu+2\bar{\mu}}{2\mu+3\bar{\mu}}\right)r-\left(\frac{\bar{\mu}}{2\mu+3\bar{\mu}}\right)\frac{1}{r^2}\right]\xi^2\right\}F(\xi)\,d\xi\\&-\left(r-\frac{1}{r^2}\right)\frac{\mu}{2\mu+3\bar{\mu}}\left[\frac{(a\kappa)^2}{6}\int_0^1(\xi^4-\xi^2)\bar{F}(\xi)\,d\xi\right.\\&\qquad\left.+\frac{a\kappa}{3}\sum_{k=1}^N(z^k)^2K^k(n_\infty^k+n_0^k)\phi_1^k(1)\right]\end{aligned}$$

and

$$\bar{h}_1(r) =(r-r^3)\frac{\mu}{2\mu+3\bar{\mu}}\Bigg[\frac{(a\kappa)^2}{6}\int_1^\infty\left(\xi^2-\frac{1}{\xi}\right)F(\xi)\,d\xi + \frac{a\kappa}{2}\sum_{k=1}^{N}(z^k)^2K^k(n_\infty^k+n_0^k)\phi_1^k(1)\Bigg]$$
$$+(a\kappa)^2\int_0^1\Bigg(\xi^4\left\{\frac{r^3}{10}\left[\frac{\mu(\mu-\bar{\mu})}{\bar{\mu}(2\mu+3\bar{\mu})}\right]+\frac{\mu}{\bar{\mu}}\frac{1}{30r^2}-\frac{r}{6}\frac{\mu}{\bar{\mu}(2\mu+3\bar{\mu})}\right\}$$
$$-\xi^2\left[\frac{r^3}{6}\frac{\mu^2}{\bar{\mu}(2\mu+3\bar{\mu})}+\frac{1}{6}\frac{\mu}{\bar{\mu}}-\frac{r}{2}\frac{\mu(\mu+\bar{\mu})}{\bar{\mu}(2\mu+3\bar{\mu})}\right]\Bigg)\bar{F}(\xi)\,d\xi$$
$$-\frac{(a\kappa)^2}{6}\frac{\mu}{\bar{\mu}}\int_r^1\left(\frac{\xi^4}{5r^2}-\xi^2+r\xi-\frac{r^3}{5\xi}\right)\bar{F}(\xi)\,d\xi.$$

These last two equations can be simplified greatly, as

$$h_1(r) =\frac{(a\kappa)^2}{30}\int_1^r\left(\frac{\xi^4}{r^2}-5\xi^2+5r\xi-\frac{r^3}{\xi}\right)F(\xi)$$
$$+\frac{(a\kappa)^2}{6}\int_1^r\left[\left(\frac{r^3}{5}-\frac{r}{3}+\frac{2}{15r^2}\right)\frac{1}{\xi}+\left(-\frac{2r}{3}+1-\frac{1}{3r^2}\right)\xi^2\right]F(\xi)\;d\xi,$$
$$+\frac{a\kappa}{6}R_\mu\left(r-\frac{1}{r^2}\right)\left[a\kappa\left(\frac{2}{3}P-\bar{P}\right)-2S\right]$$

$$\bar{h}_1(r) =(r^3-r)\frac{a\kappa}{4}R_\mu\left[a\kappa\left(\frac{2}{3}P-\bar{P}\right)-2S\right]$$
$$-\frac{(a\kappa)^2}{30}\frac{\mu}{\bar{\mu}}\int_r^1\left(\frac{\xi^4}{r^2}-5\xi^2+5r\xi-\frac{r^3}{\xi}\right)\bar{F}(\xi)\,d\xi$$
$$+\frac{(a\kappa)^2}{6}\frac{\mu}{\bar{\mu}}\int_0^1\left[\left(\frac{3r^3}{10}-\frac{r}{2}+\frac{1}{5r^2}\right)\xi^4-\left(\frac{r^3}{2}-\frac{3r}{2}+1\right)\right]\bar{F}(\xi)\;d\xi,$$

where

$$P=\int_1^\infty\left(\frac{1}{\xi}-\xi^2\right)F(\xi)\,d\xi, \tag{4.22}$$

$$\bar{P} = \int_0^1 \left(\xi^4 - \xi^2\right) \bar{F}(\xi)\, d\xi, \tag{4.23}$$

$$S = \sum_k z^k n_\infty^k K^k e^{-z^k \tilde{\zeta}_E} \phi_1^k(1), \tag{4.24}$$

and

$$R_\mu = \frac{\mu}{2\mu + 3\bar{\mu}} \tag{4.25}$$

The integrals for h_1 and $\bar{h}_1$ can be expressed more simply by noting that

$$\frac{dh_1}{dr}(1) = (a\kappa)^2 \frac{R_\mu}{2}\left(\frac{2}{3}P - \bar{P}\right) - a\kappa R_\mu S \tag{4.26}$$

For brevity, this surface derivative will be denoted as H. The integrals are once more rewritten, this time as

$$\begin{aligned} h_1(r) =& \frac{1}{3}\left(r - \frac{1}{r^2}\right) H + \frac{(a\kappa)^2}{30}\int_1^r \left(\frac{\xi^4}{r^2} - 5\xi^2 + 5r\xi - \frac{r^3}{\xi}\right) F(\xi) \\ &+ \frac{(a\kappa)^2}{6}\int_1^\infty \left[\left(\frac{r^3}{5} - \frac{r}{3} + \frac{2}{15r^2}\right)\frac{1}{\xi} + \left(-\frac{2r}{3} + 1 - \frac{1}{3r^2}\right)\xi^2\right] F(\xi)\, d\xi, \end{aligned} \tag{4.27}$$

$$\begin{aligned} \bar{h}_1(r) =& \frac{1}{2}(r^3 - r)H - \frac{(a\kappa)^2}{30}\frac{\mu}{\bar{\mu}}\int_1^r \left(\frac{\xi^4}{r^2} - 5\xi^2 + 5r\xi - \frac{r^3}{\xi}\right) F(\xi)\, d\xi \\ &+ \frac{(a\kappa)^2}{6}\frac{\mu}{\bar{\mu}}\int_0^1 \left[\left(\frac{3r^3}{10} - \frac{r}{2} + \frac{1}{5r^2}\right)\xi^4 - \left(\frac{r^3}{2} - \frac{3r}{2} + 1\right)\xi^2\right] \bar{F}(\xi)\, d\xi \end{aligned} \tag{4.28}$$

The above form makes it easy to verify the surface tangential stress balance. Also, it is noted that this form is easily seen to reduce to the equivalent problem for a rigid spherical particle.

In integral form, the expression for the electrophoretic mobility is quite simple. In implementation, the expression will be complicated depending upon the conditions imposed as regards values of interfacial potentials, double-layer thicknesses, and

whether interior electrostatics play a role. Now, recall that the limit of the velocity in the dimensionless system relates to the mobility, as

$$h_1 \;\rightarrow \tfrac{1}{2}\mu_e r; \qquad r \rightarrow \infty.$$

taking the limit of h_1/r from (4.27) leads to

$$\frac{3}{2}\mu_e = H + \frac{3}{2}\mu_e^c, \tag{4.29}$$

where

$$\frac{3}{2}\mu_e^c = -\frac{(a\kappa)^2}{6}\int_1^\infty \left(2\xi^2 - 3\xi + \frac{1}{\xi}\right) F(\xi)\, d\xi. \tag{4.30}$$

μ_e^c in the above expression denotes the mobility of a rigid colloidal particle. In the case of a solid spherical particle, the mobility reduces to (4.30), from which one can easily recover Henry's formula [20] for small $\tilde{\zeta}_E$ (and Smoluchowski's equation in the limit of large-$a\kappa$) and also the thin double-layer (large-$a\kappa$) results of Ohshima, Healy, and White [40].

4.2. Mobility Formula for Small Interfacial Potentials

The integral equations (4.10), (4.20), (4.27), and (4.28) are a representation of the electrokinetics problem and are valid for all values of interfacial potentials and double layer thicknesses. They lend themselves well, however, to approximations based on small interfacial potentials. Here these equations are used to derive an expression for the electrophoretic mobility, which linear in the potentials. This derivation begins with computation of the interfacial ionic potentials. The constants B^k are eliminated from the integral equations (4.10) and (4.20), by evaluation of the integrals at $r = 1$, leaving $\phi_1^k(1)$ and $\bar{\phi}_1^k(1)$ as the constants whose solution is necessary. To this end, the interfacial ion balances at $O(\beta)$ are invoked:

$$
\begin{aligned}
&- z^k\omega^k(n_\infty^k + n_0^k)\frac{d\phi_1^k}{dr}(1) + z^k\bar{\omega}^k(\bar{n}_\infty^k + \bar{n}_0^k)\frac{d\bar{\phi}_1^k}{dr}(1) \\
&= \frac{2}{a\kappa}\left[\mathrm{Pe}\, K^k(n_\infty^k + n_0^k)H - z^k\omega_{\mathrm{S}}^k K^k(n_\infty^k + n_0^k)\phi_1^k(1)\right], \quad k = 1, 2, \ldots, N
\end{aligned}
\tag{4.31}
$$

The derivatives of the ionic potentials are eliminated by having them expressed in terms of $\phi_1^k(1)$, *viz.*

$$
\frac{d\phi_1^k}{dr}(1) = 3 - 2\phi_1^k(1) - z^k\int_1^\infty G^k(\xi)\, d\xi, \tag{4.32}
$$

$$
\frac{d\bar{\phi}_1^k}{dr}(1) = \phi_1^k(1) + z^k\int_0^1 \xi^3\bar{G}^k(\xi)\, d\xi; \qquad k = 1, 2, \ldots, N. \tag{4.33}
$$

Thus is obtained a linear system of equations that will be used to solve for $\phi_1^k(1)$ and $\bar{\phi}_1^k(1)$. The system reads

$$
f^k\phi_1^k(1) - \frac{2}{a\kappa}\frac{\mathrm{Pe}}{z^k\omega^k}K^k H = g^k; \qquad k = 1, ..., N, \tag{4.34}
$$

where

$$
\begin{aligned}
g^k = 3 - z^k\int_1^\infty G^k(\xi)\, d\xi - z^k\frac{\bar{\omega}^k}{\omega^k}\frac{\bar{n}_\infty^k}{n_\infty^k}\exp\left[z^k(\tilde{\zeta}_{\mathrm{E}} - \tilde{\zeta}_{\mathrm{I}})\right]\int_0^\infty \xi^3\bar{G}^k(\xi)\, d\xi; \\
k = 1, 2, \ldots, N,
\end{aligned}
\tag{4.35}
$$

and

$$
f^k = 2 + \frac{\bar{\omega}^k}{\omega^k}\frac{\bar{n}_\infty^k}{n_\infty^k}e^{z^k(\tilde{\zeta}_{\mathrm{E}} - \tilde{\zeta}_{\mathrm{I}})} + \frac{2}{a\kappa}\frac{\omega_{\mathrm{S}}^k}{\omega^k}K^k; \qquad k = 1, 2, \ldots, N. \tag{4.36}
$$

The equations (4.34) and (4.26) provide a linear system for the $N + 1$ constants $\phi_1^k(1)$ and the surface velocity H, in which the coupling of the velocity field and electric potential is obvious.

Now it is begun to solve this system in a way suitable to small potentials $\tilde{\zeta}_{\mathrm{E}}$ and $\tilde{\zeta}_{\mathrm{I}}$. Formally, this requires expanding the solutions as

$$
H = H_0 + \tilde{\zeta}_{\mathrm{E}} H_{\tilde{\zeta}_{\mathrm{E}}} + \tilde{\zeta}_{\mathrm{I}} H_{\tilde{\zeta}_{\mathrm{I}}} + O(\mathrm{Q}), \tag{4.37}
$$

and

$$\phi_1^k(1) = \phi_{1,0}^k(1) + \tilde{\zeta}_{\mathrm{E}}\,\phi_{1,\tilde{\zeta}_{\mathrm{E}}}^k(1) + \tilde{\zeta}_{\mathrm{I}}\,\phi_{1,\tilde{\zeta}_{\mathrm{I}}}^k(1) + O(\mathrm{Q}); \qquad k = 1, 2, \ldots, N. \tag{4.38}$$

The term Q represents quadratic terms in $\tilde{\zeta}_{\mathrm{E}}$ and $\tilde{\zeta}_{\mathrm{I}}$. (Note that all parameters in the system, namely K^k, f^k, and g^k, are expanded in the same manner as H and $\phi_1^k(1)$.)

Now, it is implied by the form of surface velocity H that there is fluid motion (and hence drop migration) even at zero interfacial potentials.

Note that at this point, the coefficient for the interior electrostatic potential has not yet been specified. Solving at $O(1)$ will work for all cases regarding the constituents of the interface.

The linear system at $O(1)$ reads

$$\begin{aligned} f_0^k \phi_{1,0}^k(1) - \frac{2}{a\kappa}\frac{\mathrm{Pe}}{z^k\omega^k} K_0^k H_0 &= 3, \qquad k = 1, ..., N, \\ H_0 + a\kappa R_\mu \sum_{k=1}^{N} z^k K_0^k \phi_{1,0}^k(1) &= 0. \end{aligned} \tag{4.39}$$

The solution to this system is

$$H_0 = -\frac{3a\kappa R_\mu \sum_k z^k \Gamma_{\mathrm{G}}^k / f_0^k}{D}, \tag{4.40}$$

$$\phi_{1,0}^k = \frac{1}{f_0^k}\left(3 + \frac{2}{a\kappa}\frac{\mathrm{Pe}}{z^k\omega^k}\frac{\Gamma_{\mathrm{G}}^k}{n_\infty^k} H_0\right); \qquad k = 1, 2, \ldots, N \tag{4.41}$$

where

$$g_0^k = 3; \qquad K_0^k = \frac{\Gamma_{\mathrm{G}}^k}{n_\infty^k}; \qquad f_0^k = 2 + \frac{\bar{\omega}^k}{\omega^k}\frac{\bar{n}_\infty^k}{n_\infty^k} + \frac{2}{a\kappa}\frac{\omega_{\mathrm{S}}^k}{\omega^k}\frac{\Gamma_{\mathrm{G}}^k}{n_\infty^k}; \qquad k = 1, 2, \ldots, N, i \tag{4.42}$$

and

$$D = 1 + 2\mathrm{Pe}\, R_\mu \sum_k (\Gamma_{\mathrm{G}}^k)^2 / (n_\infty^k f_0^k \omega^k). \tag{4.43}$$

In general, the expression for H_0 is not zero, which indicates that there is fluid motion at the interface, and hence drop migration even when the interfacial potentials are zero. In most cases of interest, however, H_0 does in fact, vanish. This is seen this by noting: (i) the ion mobility ratios $\bar{\omega}^k/\omega^k$ are identical for sufficiently low electrolyte concentrations (they are equal to the ratio $\mu/\bar{\mu}$ due to the Stokes-Einstein relations), with a similar relationship for the ratios of surface mobilities $\omega_{\mathrm{S}}^k/\omega^k$; (ii) for co-ion and counter-ion pairs the ratios of ion densities $\bar{n}_\infty^k/n_\infty^k$ for those ion pairs are equivalent, which is consistent which the electroneutrality condition; and (iii) the condition on Gibbs surface excess (3.18). All results presented herein are subject to conditions such that H_0 is zero.

In carrying out the expansion, first the linear terms for each function in $\tilde{\zeta}_{\mathrm{E}}$ and $\tilde{\zeta}_{\mathrm{I}}$ are combined, and denoted with a subscript of L. The resulting set of equations is

$$\begin{aligned} f_0^k \phi_{1,\mathrm{L}}^k(1) - \frac{2}{a\kappa}\frac{\mathrm{Pe}}{z^k\omega^k}\frac{\Gamma_{\mathrm{G}}^k}{n_\infty^k}H_{\mathrm{L}} &= R_{\mathrm{L}}^k; \qquad k = 1, ..., N, \\ H_{\mathrm{L}} + a\kappa R_\mu \sum_{k=1}^{N} z^k \Gamma_{\mathrm{G}}^k \phi_{1,\mathrm{L}}^k(1) &= H^{\mathrm{B}}, \end{aligned} \tag{4.44}$$

where

$$R_{\mathrm{L}}^k = g_{\mathrm{L}}^k - f_{\mathrm{L}}^k \phi_{1,0}^k(1) + \frac{2}{a\kappa}\frac{\mathrm{Pe}}{z^k\omega^k} K_{\mathrm{L}}^k H_0; \qquad k = 1, 2, \ldots, N, \tag{4.45}$$

and

$$H^{\mathrm{B}} = (a\kappa)^2 \frac{R_\mu}{2}\left(\frac{2}{3}P_{\mathrm{L}} - \bar{P}_{\mathrm{L}}\right) - a\kappa R_\mu \sum_k z^k n_\infty^k e^{-z^k\tilde{\zeta}_{\mathrm{E}}} K_{\mathrm{L}}^k \phi_{1,0}^k(1). \tag{4.46}$$

The superscript B denotes that this is the surface velocity derived by Booth [5] The linear system is easily solved, and

$$H_{\mathrm{L}} = \frac{1}{D}\left(H^{\mathrm{B}} - a\kappa R_\mu \sum_{k=1}^{N} z^k \Gamma_{\mathrm{G}}^k R_{\mathrm{L}}^k / f_0^k\right) \tag{4.47}$$

This is the fluid velocity at the interface for small interfacial potentials. Recall (4.29), which gives the drop mobility as the sum of this velocity and the mobility for a solid

particle, and now the expression for drop mobility reads

$$\frac{3}{2}\mu_{\mathrm{e}} = H_0 + \frac{1}{D}\left(H^{\mathrm{B}} - a\kappa R_\mu \sum_{k=1}^{N} \frac{z^k \Gamma_{\mathrm{G}}^k}{f_0^k} R_{\mathrm{L}}\right) + \frac{3}{2}\mu_{\mathrm{e}}^{\mathrm{C}}, \tag{4.48}$$

where the colloid mobility $\mu_{\mathrm{e}}^{\mathrm{C}}$ is computed from (4.30), and is

$$\frac{3}{2}\mu_{\mathrm{e}}^{\mathrm{C}} = \tilde{\zeta}_{\mathrm{E}}\left\{1 + \lambda\left[1 + 6e^{a\kappa}E_5(a\kappa) - 15e^{a\kappa}E_7(a\kappa)\right]\right\}, \tag{4.49}$$

with

$$\lambda = \sum_{k=1}^{N}(z^k)^2 n_\infty^k \phi_{1,0}^k(1) - 1, \tag{4.50}$$

It is noted that (4.49) is equivalent to the formula of Henry [20] with the exception that for the (dimensionless) value of λ is one-half in the case that the interior phase is non-conducting.

To implement this formula for the surface fluid velocity, it is necessary to give explicit expressions for H^{B} and R_{L}^k :

$$H^{\mathrm{B}} = R_\mu \tilde{\zeta}_{\mathrm{E}}\lambda\left[-6 + 30e^{a\kappa}E_7(a\kappa)\right] - 5R_\mu A\frac{\bar{\epsilon}}{\epsilon}(1+\bar{\lambda})\left[1 - 3\frac{\coth a\bar{\kappa}}{a\bar{\kappa}} + \frac{3}{(a\bar{\kappa})^2}\right], \tag{4.51}$$

where

$$\bar{\lambda} = \frac{\sum_k (z^k)^2 \bar{n}_\infty^k \phi_{1,0}^k(1)}{\sum_k (z^k)^2 \bar{n}_\infty^k} - 1. \tag{4.52}$$

It is noted that when the surface excesses Γ_{G}^k are zero, (4.48) reduces to

$$\frac{3}{2}\mu_{\mathrm{e}} = H^{\mathrm{B}} + \frac{3}{2}\mu_{\mathrm{e}}^{\mathrm{C}}, \tag{4.53}$$

which is identical to the formula derived by Booth [5], up to the differences in the constants λ and $\bar{\lambda}$. Booth defined λ as the dipole coefficient of the system, according to the assumption that both phases are ohmic conductors. In addition, it is noted that in the limit of a solid, non-conducting interior phase ($R_\mu = 0$, $\lambda = 1/2$), the result reduces to Henry's formula.

It remains to compute R_{L} from (4.45), in which must be included the linear terms (in $\tilde{\zeta}_{\mathrm{E}}$ and $\tilde{\zeta}_{\mathrm{I}}$) in (4.10), (4.35), and (4.36). The result is

$$\begin{aligned} R_{\mathrm{L}}^{k} =& 6z^{k}\tilde{\zeta}_{\mathrm{E}}\left[\phi_{1,0}^{k}(1)-1\right]e^{a\kappa}E_{5}(a\kappa)+3z^{k}\tilde{\zeta}_{\mathrm{I}}\frac{\bar{\omega}^{k}}{\omega^{k}}\frac{\bar{n}_{\infty}^{k}}{n_{\infty}^{k}}\phi_{1,0}^{k}(1)\left[\frac{\coth a\bar{\kappa}}{a\bar{\kappa}}-\frac{1}{(a\bar{\kappa})^{2}}\right] \\ &-\frac{2}{a\kappa}\frac{\omega_{\mathrm{S}}^{k}}{\omega^{k}}\left[z^{k}\tilde{\zeta}_{\mathrm{E}}\left(1+\frac{1}{a\kappa}\right)+z^{k}\tilde{\zeta}_{\mathrm{I}}\frac{\bar{n}_{\infty}^{k}}{n_{\infty}^{k}}\frac{a\kappa}{a\bar{\kappa}}\left(\coth a\bar{\kappa}-\frac{1}{a\bar{\kappa}}\right)\right]\phi_{1,0}^{k}(1) \\ &-2\frac{\mathrm{Pe}}{\omega^{k}}H_{0}\Bigg\{\tilde{\zeta}_{\mathrm{E}}\left[\frac{1}{a\kappa}\frac{\Gamma_{\mathrm{G}}^{k}}{n_{\infty}^{k}}+e^{a\kappa}E_{5}(a\kappa)\right] \\ &\qquad+\tilde{\zeta}_{\mathrm{I}}\frac{\bar{n}_{\infty}^{k}}{n_{\infty}^{k}}\left[\frac{\coth a\bar{\kappa}}{a\bar{\kappa}}-\frac{6}{(a\bar{\kappa})^{2}}+30\frac{\coth a\bar{\kappa}}{(a\bar{\kappa})^{3}}-\frac{30}{(a\bar{\kappa})^{4}}\right]\Bigg\}; \\ & \qquad\qquad k=1,2,\ldots,N. \end{aligned} \tag{4.54}$$

The main result is encapsulated by equations (4.48), (4.43), (4.40), (4.51), and (4.54). The mobility expression here is in its most general form, allowing for situations that would induce drop mobility even for the case of no surface potential (both sides of the interface) and no net surface charge.

Given the model, the solution here is quite general with the exception that only small interfacial potentials are considered. It may seem rather unwieldy considering it is a linear approximation. Nonetheless, the expression does cover a variety of previously derived results in limiting cases, and in the algebra is seen the effect of various physical parameters on the behaviour of the system.

4.3. Results and Discussion

An advantage of the analytic formula is that it enables one to examine behaviour for many hypothetical cases. While the form presented here is perhaps too cumbersome to be implemented on a calculator, it requires only a few lines of computer code - an

obvious advantage over a numerically-derived solution, which even today's computers take significantly more time to run. The ease of use of the analytic formula enables one to test the effects of a wide variety of physical cases, manifested as parameters.

First it will be shown that the analytic solution to be accurate as compared to the numerical solution, taken to be exact. With confidence in the accuracy of the formula, the model is then tested — via the formula — against experimental data that describes drop mobility as a function of drop size. In these cases, the unmeasured physical quantities are used as fitting parameters.

In all cases considered here, conditions will be such that there is no drop motion for zero zeta potentials and no net interfacial charge. Thus H_0 is zero, which simplifies the mobility expression somewhat.

4.3.1. Comparison with Numerical Solution

In all plots where comparisons are made, the numerical solution is that derived by Baygents and Saville [2]. The method used was orthogonal collocation on finite elements [11], and was used for the case of a continuous equilibrium potential at the interface. In these graphs, the electrolyte in each phase is KCl. In all cases considered here, the dielectric constants and viscosities of the phases were taken to be identical. The surface and interior ion mobilities are also taken to be identical to those of the exterior.

In FIG 4.1 the analytic and numerical solutions are compared. In this case the equilibrium potential is taken to be continuous at the interface, with a value of 25 mV, which is unity in the dimensionless system. The value of $a\bar{\kappa}$ was fixed while $a\kappa$ was allowed to vary. This is tantamount to varying the ionic strength on the exterior while holding constant that of the interior. Also, several values of surface excesses Γ_G^k were considered. The plots show good agreement, which is especially encouraging considering that the analysis is based on dimensionless values of $\tilde{\zeta}_E \ll 1$. Beyond

this value, the nonlinearity of the mobility in $\tilde{\zeta}_{\mathrm{E}}$ becomes more pronounced and the solution is less accurate. Nonetheless, for $\tilde{\zeta}_{\mathrm{E}}$ up to unity, agreement is close enough to render the analytic solution to be qualitatively trustworthy. One of those qualities is that a negative mobility is attained even for a positive $\tilde{\zeta}_{\mathrm{E}}$-potential and no interphase potential difference $\Delta\Psi$. Unlike for a solid particle [20, 40] or perfectly-conducting drop [42], this outcome should not be surprising. Indeed, circulation patterns of fluid inside a drop depend on many factors [51]. A profound influence of surface excess of solute on the mobility is also noted.

In FIGS 4.2 and 4.3, a comparison is made between the approximate mobility numerically-derived values for various interfacial potentials. The potential was taken to be continuous at the interface, with values from 0 to 50 mV, which is zero to 2 in dimensionless form. In each plot, the interior scaled radii $a\kappa$ and $a\bar{\kappa}$ were held constant, and there surfaces excesses Γ_{G}^{k} were held to zero. The error becomes substantial only for dimensionless potentials of unity, further validating the small-$\tilde{\zeta}_{\mathrm{E}}$ formula.

4.3.2. Comparison with Experimental Observations

The mobility formula derived here has been compared to published measurements of electrophoretic mobility of fluid drops of various sizes. In one case, the drop mobility varied with the drop size for relatively small drops (less than 10 microns in diameter), before leveling off for larger drops, while in another case the mobility varied linearly with drop size for drops up to 40 microns in diameter. The comparisons are summarized below.

Comparison with Experimental Observations: Oil Drops in Water

For the limiting case of non-conducting drops, as is the case with many oils, the mobility formula (4.48) simplifies greatly. as there are no electrostatics to consider

inside the drop. The resulting expression reads

$$\frac{3}{2}\mu_{\mathrm{e}} = \tilde{\zeta}_{\mathrm{E}}\frac{R_\mu}{D}\left[-3 + 15e^{a\kappa}E_7(a\kappa) - \frac{3}{2}a\kappa e^{a\kappa}E_5(a\kappa)\sum_{k=1}^{N}(z^k)^2\Gamma_{\mathrm{G}}^k\right] \tag{4.55}$$

$$+\,\tilde{\zeta}_{\mathrm{E}}\left\{1 + \lambda\left[1 + 6e^{a\kappa}E_5(a\kappa) - 15e^{a\kappa}E_7(a\kappa)\right]\right\}.$$

A comparison of this formula with experimental data of Mooney [34] has been made. In particular, it is desired to see how the result describes electrophoretic mobility as a function of drop size. To vary the drop size mathematically, a value was chosen for surface charge density ρ_{S} and then computed the $\tilde{\zeta}_{\mathrm{E}}$-potential from the interfacial charge regulation,

$$\tilde{\zeta}_{\mathrm{E}}\,(a\kappa + 1) = a\kappa\rho_S, \tag{4.56}$$

ρ_S, being an unmeasured quantity in the experiment, is a free parameter in this treatment. The other free parameters are surface excesses of solutes, Γ_{G}^k, and the surface mobilities of each ion, ω_{S}^k. To choose a value of ω_{S}^k, an average of the viscosities of the two phases was used, *viz.*

$$\frac{\omega_{\mathrm{S}}^k}{\omega^k} = \frac{1}{2}\left(1 + \frac{\mu}{\bar{\mu}}\right); \qquad k = 1, 2, \ldots, N.$$

Several studies on interfacial ion mobilities have been made [49], but these are based on models with finite thickness of the interface. To vary the drop size while holding the surface charge density constant, the value of $a\kappa$ was varied. The viscosity of the oil — a nujol-like oil named Stanolind — was estimated to be 85 times that of water.

In FIG 4.4, the formula is compared with four experimentally-derived curves of mobility vs. drop size, each for a different electrolyte. The free parameters mentioned above were used to fit the data. The values of physical parameters chosen and resulting mobilities are converted to dimensionless form using the scale factors that appear in TABLE 1. Note that in curves 1 and 2, the ζ-potentials required to fit the data are of moderate value, slightly out of range of ζ-potentials that give accurately-computed

TABLE 4.1. Fitting Parameters for comparison of mobility formula with experimental data of Mooney (1924) (See FIG 4.4)

$$\frac{\omega_S^k}{\omega^k} = 0.51$$

	Electrolyte	$\Gamma_G^{\pm}$ (mol/cm^2)	ρ_S (C/cm^2)	ζ^* (mV)
1:	1×10^{-3} M NaOH	1×10^{-10}	-7.20×10^{-7}	-97.1
2:	1×10^{-4} M NaOH	2×10^{-11}	-1.55×10^{-7}	-66.1
3:	1×10^{-4} M HCl	8×10^{-12}	-0.90×10^{-7}	-38.4
4:	8×10^{-4} M $CuSO_4$	1×10^{-11}	-2.30×10^{-7}	-18.0

* Surface potential ζ varies with the drop size, according to (4.56). The value given here is the limit in large $a\kappa$.

mobility. This likely explains why the fit is not quite as good as in the other two graphs, although qualitatively, one still sees the variability of mobility with drop size, and tendency to an upper limit for increased size.

It is also noted that to match the analytic result with experimental data involved setting the surface charge density ρ_S higher for the solution of higher salt concentration. It has been suggested [33] that the surface charge density of an oil drop is due to adsorption of hydroxyl (OH) ions from the water. Thus it is plausible that a hydroxyl-based salt would lend more such ions to the drop surface for a higher concentration. This would lead to a larger-sized (negative) zeta potential and thus a higher (negative) mobility.

One striking result is the effect of the surface excesses of solutes, which increases the dependence of mobility on size. Setting the parameters Γ_G^k to zero, for example, results in no size dependence, except for extremely small drops. This is the case even for a highly viscous oil, such as nujol. It is noted that in order to fit the mobility data for 1×10^3 M NaOH in FIG 4.4, a surface excess Γ_G^k value of 1×10^{-1} mol/cm^2 was used. This is high for a salt [1]. This, in addition to the fact that a moderately

TABLE 4.2. Fitting Parameters for comparison of numerically-derived electrophoretic mobility with experimental data of Mooney (1924) (See FIG 4.5)

		$\frac{\omega_S^k}{\omega^k} = 0.51$		
	Electrolyte	$\Gamma_G^{\pm}$ (mol/cm^2)	ρ_S (C/cm^2)	ζ_∞ (mV)
1:	1×10^{-3} M NaOH	7×10^{-11}	-7.20×10^{-7}	-99.8
2:	1×10^{-4} M NaOH	1.4×10^{-11}	-1.50×10^{-7}	-63.4
3:	1×10^{-4} M HCl	6×10^{-12}	-0.92×10^{-7}	-39.2
4:	8×10^{-4} M $CuSO_4$	1×10^{-11}	-2.36×10^{-7}	-17.8

* Surface potential ζ varies with the drop size. The value given here determined from (4.56) in the limit of large $a\kappa$.

high value of interfacial potential $\tilde{\zeta}_E$ was used suggests that this data is out of the range of applicability of the small-$\tilde{\zeta}_E$ mobility (4.55), leaving the desire for a large-$a\kappa$ analysis or numerically-derived mobility to compare such data.

In FIG 4.5, a similar comparison is made, but with the drop mobility computed numerically. The electrokinetics, or mobility problem was again computed via orthogonal collocation on finite elements, and the results are taken to be an exact solution to the problem as stated. FIG 4.5 shows similar to slightly better fits to the experimentally-measured mobilities than shown in FIG 4.2. The physical parameters that went into the computations are somewhat different than those used in FIG 4.4, with the most telling difference being that the surface excesses are smaller (compare TABLES 4.1 and 4.2). This is encouraging, as it lends even more credence to the model. An adjustment that needs to be made is to have the potential $\tilde{\zeta}_E$ computed from the numerically-derived charge regulation based on (3.17) as opposed to the linear approximation as opposed to the linear approximation (4.56). It is supposed that such a more exact calculation of the $\tilde{\zeta}_E$-potential based on the surface charge densities would lead to a better fit of the data with even lower — and more realistic

— values of the surface excesses.

Comparison with Experimental Observations: Aqueous Two-phase Systems

The experiments described in [8, 43] have shown that electrophoretic mobility increases linearly with drop size, through drop sizes of 15 microns in diameter. This is in contrast to the experiments and analysis on oil drops discussed in the preceding section, where the increase with size was linear only up to drops of less than 5 microns in diameter before the mobility began leveling off (see FIG 4.4).

In addition to the linear size dependence of mobility, it was also seen that the direction of drop migration is reversed by inverting the two phases. In particular, PEG-rich drops migrated in the direction of the applied field, while the dextran-rich drops moved in the opposite direction. An electric dipole across the interface — the orientation of which reverses upon reversing the phases of the dispersion — is believed to be the cause of the opposite mobilities. This is reflected in the approximation to the mobility (4.48), (4.49), (4.51), (4.54), which are linear in $\tilde{\zeta}_{\mathrm{E}}$ and $\tilde{\zeta}_{\mathrm{I}}$. Suppose for example, that with all else being equal for the interior and exterior properties, that the exterior and interior potentials $\tilde{\zeta}_{\mathrm{E}}$ and $\tilde{\zeta}_{\mathrm{I}}$ are equal in magnitude but have opposite signs. Inverting the drop/continuous phase system would result is accomplished in theory by interchanging the values of $\tilde{\zeta}_{\mathrm{E}}$ and $\tilde{\zeta}_{\mathrm{I}}$, which results in the same mobility but with opposite sign. Another observation, which perhaps is much more surprising, was that although the two phases are of very different viscosities, the order of magnitude of the mobilities stayed the same even with phase reversal.

The experimental conditions and measurements of Brooks *et al.* [8] have been used in the formula (4.48) in order to test the small-$\tilde{\zeta}$ results derived here. In the experiments, an aqueous two-phase system was prepared, one phase being dextran-rich and the other polyethylene glycol (PEG) rich. 0.2M Potassium sulfate was added to the system and partitioned unequally in the two phases. An interphase potential difference between the two phases and the viscosity of each phase was measured.

Drops of each phase were dispersed in the other, and electrophoretic mobility of those drops was measured and plotted as a function of drop size.

The data behind the published figure of Brooks *et al.* [8] was provided, and these data have been used for to make a comparison. The two phases being aqueous, their permittivities were taken to be equal. The viscosity of the dextran phase was roughly 10 times that of the PEG phase. The ionic strength and of the solutes were each different from 0.2 M due to the partitioning between the phases. From those values, as well as the published range of drop sizes, values of the scaled radii $a\kappa$ were computed, with a range of roughly 4000 to 20000. The ratio $\bar{\mu}/\mu$ was roughly 10, depending on whether the drop phase was the dextran phase or the PEG phase. The ratios of mobilities of the phases, $\bar{\omega}^k/\omega^k$, were taken to be the inverse of the viscosity ratio. The ratios ω_S/ω^k were taken to be the average of the ratios of ion mobilities of the phases. The scaled interphase potential difference, $\Delta\Psi$ has a value of -0.093 when the drop phase is the dextran-rich phase, and 0.093 otherwise.

In addition to the parameters based on measured quantities, some important quantities were treated as free parameters, those being surface charge density, ρ_S, surface excesses of solutes, Γ_G, and jump in the interfacial potential, denoted as χ. From ρ_S, χ, and $\Delta\Psi$, the interfacial potentials $\tilde{\zeta}_E$ and $\tilde{\zeta}_I$ is determined from

$$\chi = \Phi_0(1) - \bar{\Phi}_0(1) = \tilde{\zeta}_E - \tilde{\zeta}_I + \Delta\Psi \tag{4.57}$$

and the small-$\tilde{\zeta}$ charge regulation condition

$$\tilde{\zeta}_E\,(a\kappa + 1) + \frac{\bar{\epsilon}}{\epsilon}\tilde{\zeta}_I\,(a\bar{\kappa}\coth a\bar{\kappa} - 1) = a\kappa\rho_s. \tag{4.58}$$

To derive (4.58), the right-hand-side of (2.6) was replaced by ρ_S and the electric field expressions were from the Debye-Hückel potentials.

To simulate variation of the drop size, the surface charge density was held constant, while $a\kappa$ and $a\bar{\kappa}$ were varied concurrently. From (4.58), it is seen that for large values of $a\kappa$, the interfacial potential values level off. Since the mobility formula is linear

in these potentials, one would expect the mobility itself to level off to certain values as the drop increases in size, as is seen in the experimental data for oil drops 4.4. The question remains as to whether drops in aqueous two-phase systems have the same property. The data of [8] would suggest otherwise, but it is argued here that if the experiment were carried out for larger drops, one would see the the mobilities eventually level off with increasingly larger drops. Now, recall that the values of $a\kappa$ and $a\bar{\kappa}$ for the experimental conditions range of [8] range from roughly 4000 to 20000. These are considerably higher values than those for the oil drops. Recalling that the mobility formula is linear with the potentials $\tilde{\zeta}_{\mathrm{E}}$ and $\tilde{\zeta}_{\mathrm{I}}$, and once again noting that the $\tilde{\zeta}$ potentials are determined from (4.58), this would indicate that mobility should, for drops in aqueous two-phase systems, level off with drop size (dictated by $a\kappa$ and $a\bar{\kappa}$) as it does for non-conducting drops. Recall again that it was the inclusion of surface excesses of solutes that gave greater dependence of mobility on drop size. For these values of double-layer thickness, however, the values of surface excesses that would give a linear dependence are outrageously high. Moreover, the $\tilde{\zeta}_{\mathrm{E}}$ and $\tilde{\zeta}_{\mathrm{I}}$-potentials, as dictated by interfacial dipole and surface charge density, must be so high as to be well out of the range of applicability of the mobility formula.

It must also be noted that according to experiments [8, 43], that when the drop and continuous phases are reversed, that the mobilities remain at the same order of magnitude. This is quite counterintuitive, as one might expect that for a system in which the continuous phase is more viscous, the mobility should be lower. The small potential mobility does not account for this observation. The derived mobility expression supports the more intuitive notion that the mobility should be lower when the exterior phase is more viscous than the drop phase.

To be able to account for larger potentials and also to consider the very thin double-layers (large $a\kappa$), it is natural to want an approximation to the mobility based on thin double-layers, or have a robust numerical code that can account for such large values of $a\kappa$. Given the success of the model for describing the electrophoretic

behaviour of oil drops, it is reasonable to suppose that a solution that works for thin double-layers would come closer to accounting for the drop mobility in an aqueous two-phase system.

4.4. Conclusions

A formula has been derived for the electrophoretic mobility of a spherical fluid drop. It is a general formula in that it accounts for more physical situations than have been considered in the past. The formula reduces to many well-known formulas in limiting cases. It is derived in the limited range of small interfacial potentials $\tilde{\zeta}_{\mathrm{E}}$, and $\tilde{\zeta}_{\mathrm{I}}$, and compares well with exact (numerical) results for moderate potentials. For drops with nontrivial interior electrostatics, the formula accounts nicely for a reversal in mobility with an inversion of the drop and continuous phases, but does not account for the mobilities being of equal order of magnitude upon phase reversal even when the viscosities differ by an order of magnitude. The formula shows drop-size dependence on electrophoretic mobility for limited sizes, which is in accordance with past mobility measurements on oil drops [34]. This size dependence is largely due to the inclusion in the model of surface excesses of solutes. Size dependence in the formula can be extended to larger drops but only for larger potentials, which is outside its applicability range. To account for observations of the mobility increasing with size for larger drops [8], one must look to a numerical solution that can accommodate large $a\kappa$ and $a\bar{\kappa}$ values or perhaps a formula based on thin double-layer analysis. It is suggested here that mobility measurements of drops in aqueous two-phase systems be made but with lower ionic strengths.

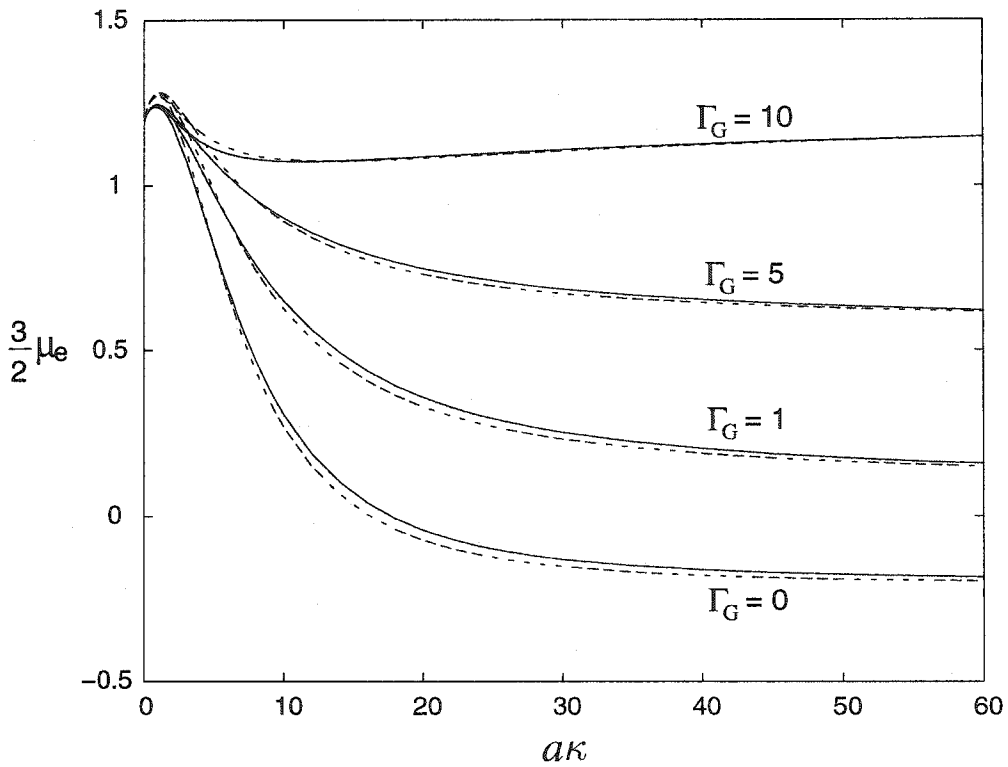

FIGURE 4.1. Comparison of linear analytic approximations of electrophoretic mobility of a fluid drop to a numerically-derived mobility, for several values of surface excesses Γ_G. Electrolyte is aqueous KCl inside and out. Potential is continuous across the interface, with $\zeta = \bar{\zeta} = 1$. $\bar{\mu}/\mu = 1$, and $a\bar{\kappa} = 10$. ——, Numerical solution; ---, linear approximation.

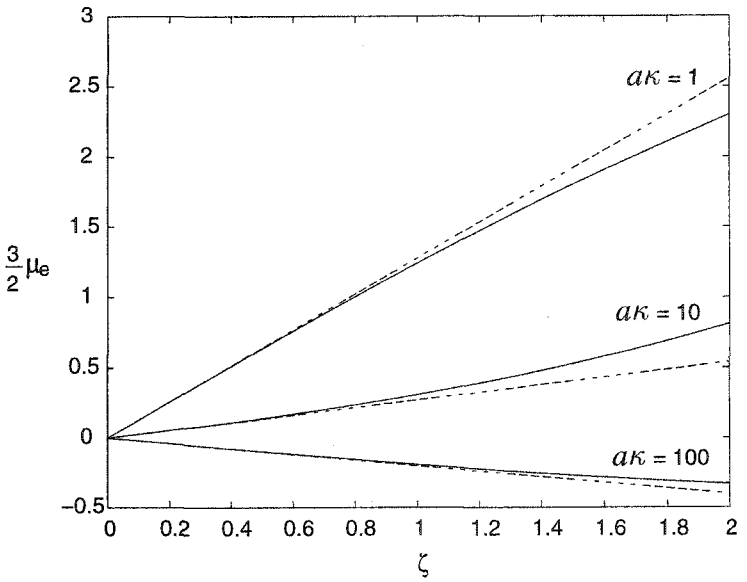

FIGURE 4.2. Comparison of linear analytic approximations of dimensionless electrophoretic mobility of a fluid drop with numerically-derived values, interior scaled radius $a\bar{\kappa} = 10$. Electrolyte is aqueous KCl inside and out. Potential is continuous across the interface, $\bar{\mu}/\mu = 1$, and $a\bar{\kappa} = 10$. ——, Numerical solution; ---, linear approximation.

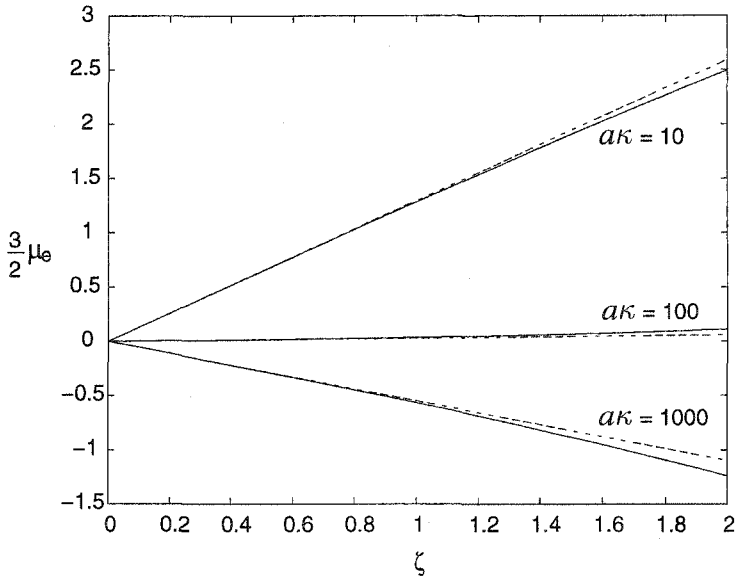

FIGURE 4.3. Comparison of linear analytic approximations of dimensionless electrophoretic mobility of a fluid drop with numerically-derived values, interior scaled radius $a\bar{\kappa} = 100$. Electrolyte is aqueous KCl inside and out. Potential is continuous across the interface, $\bar{\mu}/\mu = 1$. ——, Numerical solution; ---, linear approximation.

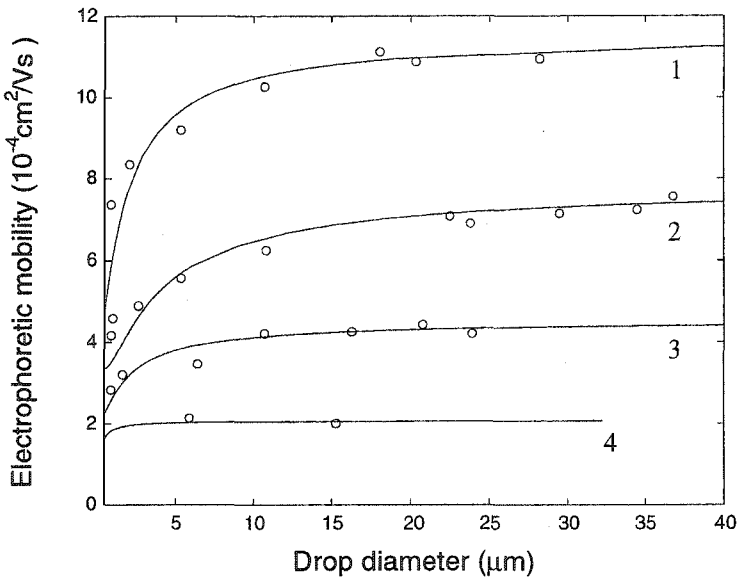

FIGURE 4.4. Comparison of mobility formula with experimental data of Mooney (1924), for Stanolind oil drops. Fitting parameters are given in TABLE 4.1.

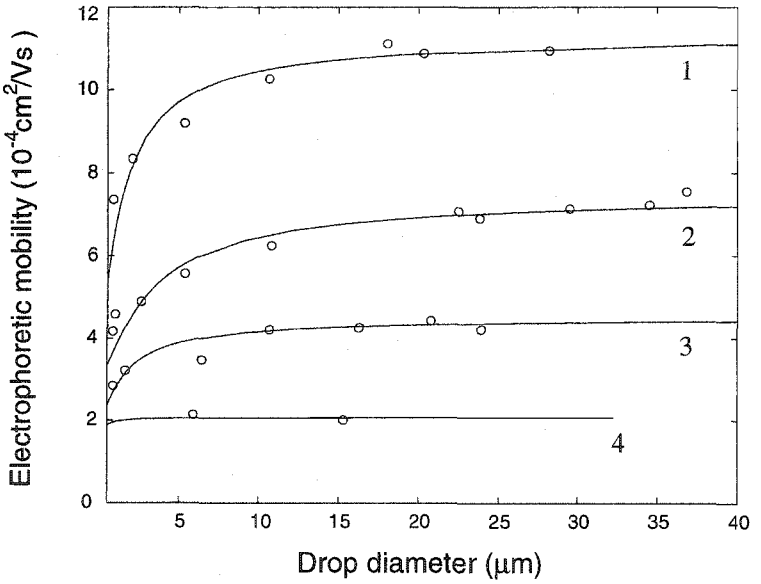

FIGURE 4.5. Comparison of numerically-derived electrophoretic mobility with experimental data of Mooney (1924), for Stanolind oil drops. Fitting parameters are given in TABLE 4.2.

5. Radial Temperature Variations in Cylindrical Electrophoresis Columns

5.1. Background

The electrolyte buffers used in electrophoretic separations are ionic conductors, so imposition of an electric field along the axis of an electrophoresis column, or capillary, gives rise to Joule heating [21, 22]. The vast majority of the generated heat must exit the system through the column walls. Thus, the temperature varies radially over the column cross-section, or lumen, and the centerline temperature is elevated relative to that at the column periphery.

Because temperature gradients associated with Joule heating typically have a deleterious effect on electrically-driven separations [19, 21, 22, 26], the temperature field within electrophoresis columns has been the subject of numerous studies [4, 9, 13, 15, 18, 24]. With one exception [15], these studies have been restricted to cases in which the temperature variations over the cross-section of the capillary are in some sense small. The reasons for this, at least in part, involve the practical need to control temperatures within the capillary to prevent such effects as the denaturing of analyte proteins [21] or the loss of resolution due to analyte dispersion [19]. It should be noted, however, that in lab-on-a-chip technology substantial Joule heating in capillaries can be desirable. For example, Joule heating can incubate polymerase chain reactions (PCR) for the replication of DNA [27].

Our focus here is on a cylindrical geometry, though there are various other geometries of channels used in electrically-driven separations. Tsuda et. al. [53] point out the virtues of rectangular capillaries, and Brown and Hinckley [10] compute the temperature profile due to Joule heating for such a geometry assuming no temperature dependence on the electric and thermal conductivities, which they also did for

a cylindrical geometry. With the proliferation of on-chip capillary electrophoresis devices [16, 32, 44], channels of various geometries are used, including but not limited to cylindrical, rectangular, and half-cylindrical [50].

Coxon and Binder [13] established that, for columns of circular cross-section, the temperature profile $T(r)$ is nearly parabolic in the radial coordinate r when $S \equiv G_{\mathrm{w}}R^2/k_{\mathrm{w}}T_{\mathrm{w}} \ll 1$, i.e.

$$T(r) = T_{\mathrm{w}}\left\{1 + \frac{S}{4}\left[1 - \left(\frac{r}{R}\right)^2\right] + O(S^2)\right\}, \qquad r \leq R, \tag{5.1}$$

where r is measured from the centerline, and R is the inner radius, of the column; k_{w} and G_{w} are, respectively, the thermal conductivity and the (Joule) heat generation rate at T_{w}, the temperature of the capillary interior wall[1] ($r = R$). Jones and Grushka [24] illustrated that (5.1) is often adequate for the narrow-bore (ca. 50 μm i.d.) columns used in capillary electrophoresis, but more generally, (5.1) underestimates the radial temperature variations, as a number of studies have shown [4, 9, 13, 15, 18, 24]. Certainly, for larger-bore columns (ca. 1 cm i.d.), such as those used in preparative-scale electrochromatography [12], better approximate solutions are required.

The difficulty encountered in the analysis of $T(r)$ is that the relevant transport coefficients, viz. the electrical and thermal conductivities of the material that fills the column, vary locally with the temperature and so the governing differential equation is nonlinear. In a numerical study, Davis [15] has shown that it is important to properly account for the temperature dependence of the electrical and thermal conductivity—particularly when S exceeds 0.01.

Here is revisited the problem for the temperature field and approximate $T(r)$ by regular perturbation methods. The strategy briefly explored by Coxon and Binder (cf. the appendix of [13]) is generalized and extended to obtain formulae that can

[1] The subscript w is used throughout to indicate that the quantity to which it is affixed is evaluated at the wall temperature T_{w}.

accommodate virtually any temperature dependence of the transport coefficients. The result of our analysis is a set of analytical expressions that are accurate through $O(S^5)$. When tested with property correlations tailored for aqueous electrolytes, the resultant expressions prove to be in excellent agreement with a numerically-derived numerical solution.

Previous investigators [4, 9, 13, 15, 18] have developed various $O(S^2)$ approximations, with [4] considering the analogous phenomenon of the heating of an electrical wire. By extending the analysis to fifth order, one can explicitly examine the accuracy of lower-order approximations, and to assess the convergence of the resultant asymptotic expansion. For example, the approximation to $O(S^2)$ is remarkably concise and accurate. It is within 0.1 Kelvin of the higher-order and numerical results for operating conditions common to capillary electrophoresis, where $S < 0.1$. It is also shown that beginning at $O(S^2)$, the temperature dependence of both the thermal and electrical conductivity can be readily and properly accounted for, though some $O(S^2)$-approximations unnecessarily omit consideration of the temperature dependence of the thermal conductivity [9, 13, 15]. For values of S beyond 0.1, the autothermal effect [18] becomes increasingly significant, making it necessary to use the higher order approximations.

The asymptotic series converges slowly with S, so the somewhat higher accuracy of the fourth and fifth order approximations must be weighed against their cumbersome length. Fortunately, by using classical Shanks transformations, one can accelerate the convergence of the series, such that transformations in the first two and three terms of the series yield accuracy comparable to that given by the fourth and fifth-order series, respectively. This enables one to get highly accurate estimates without the algebraic complexity.

5.2. Problem Formulation

Joule heating, generated by the imposition of an electric field down the axis of the column, is balanced by radial thermal conduction. The steady-state temperature profile is thus governed by

$$\nabla \cdot (k \nabla T) = -G, \tag{5.2}$$

which due to cylindrical symmetry reduces to the ordinary differential equation

$$\frac{1}{r}\frac{d}{dr}\left[r\left(k\frac{dT}{dr}\right)\right] = -G. \tag{5.3}$$

Where k is the local thermal conductivity and G is the heat generation rate due to ohmic conduction processes. If σ is the local electrical conductivity and E is the electric field strength,

$$G = \sigma E^2. \tag{5.4}$$

Because the buffer in the column is an ionic conductor, the heat generation rate varies radially owing primarily to the temperature dependence of the viscosity. For example, in the absence of any column packing,

$$\sigma = e^2 \sum_{i=1}^{N} (z^i)^2 \omega^i c^i, \tag{5.5}$$

where e is the fundamental charge on a proton, and z^i, ω^i, and c^i are, respectively, the valence, mobility and concentration of the ith-type ionic buffer constituent. The mobility ω^i follows from the Stokes-Einstein relationship, viz.

$$\omega^i = \frac{1}{6\pi\mu a^i}, \qquad i = 1, 2, ..., N, \tag{5.6}$$

where N is the number of ionic species in the buffer, a^i is the Stokes-Einstein radius of species i, and μ is the buffer viscosity.

Substituting (5.4)–(5.6) into (5.3) gives

$$\frac{k_w}{r}\frac{d}{dr}\left[r\left(\kappa(T)\frac{dT}{dr}\right)\right] = -G_w \lambda(T), \tag{5.7}$$

with

$$\kappa(T) = \frac{k(T)}{k_{\rm w}}, \qquad \lambda(T) \equiv \frac{\sigma(T)}{\sigma_{\rm w}} = \frac{\mu_{\rm w}}{\mu(T)},$$

and

$$G_{\rm w} \equiv \sigma_{\rm w} E^2 = \frac{e^2}{6\pi\mu_{\rm w}} \left[\Sigma_{i=1}^{N} (z^i)^2 c^i / a^i\right] E^2.$$

As is evident from the RHS of (5.7), the local generation rate varies with the viscosity. For circumstances where the lumen includes chromatographic or other packing materials, it is appropriate to regard λ and $G_{\rm w}$ in terms of their primary definitions, and to regard (5.7) as an effective-medium representation of the column contents.

Note that $\kappa(T)$ and $\lambda(T)$ are typically nonlinear functions of temperature, so exact solutions to (5.7) are generally not possible. Nevertheless, one can construct analytic approximations for $T(r)$, given correlations for $\kappa(T)$ and $\lambda(T)$.

Here is considered the circumstance where

$$T = T_{\rm w} \text{ at } r = R \tag{5.8}$$

and, due to the cylindrical symmetry,

$$\frac{dT}{dr} = 0 \text{ at } r = 0. \tag{5.9}$$

We begin by placing the governing equations in dimensionless form. Let $\Theta = (T - T_{\rm w})/T_{\rm w}$ and $\rho = r/R$. Then (5.7) becomes

$$\frac{1}{\rho}\frac{d}{d\rho}\left[\rho\left(\kappa(\Theta)\frac{d\Theta}{d\rho}\right)\right] = -S\lambda(\Theta), \tag{5.10a}$$

with

$$\Theta = 0 \text{ at } \rho = 1 \quad \text{and} \quad \frac{d\Theta}{d\rho} = 0 \text{ at } \rho = 0. \tag{5.10b}$$

It is apparent that Θ will depend parametrically on S, i.e. $\Theta = \Theta(\rho; S)$.[2] A natural temperature scale for the radial variations is $ST_{\rm w}$, or $G_{\rm w}R^2/k_{\rm w}$, which for reasonable

[2]The dimensionless temperature Θ will also depend on those parameters that appear in the correlations $\lambda(\Theta)$ and $\kappa(\Theta)$. Correlations suitable for aqueous buffers are given in Appendix B.

values of the electrical conductivity, the electric field strength, etc., is on the order of 10 Kelvin or less. It seems appropriate, therefore, to postulate asymptotic behavior of the form

$$\Theta(\rho; S) = S\Theta_1(\rho) + S^2\Theta_2(\rho) + S^3\Theta_3(\rho) + S^4\Theta_4(\rho) + \dots , \qquad S \ll 1. \tag{5.11}$$

This is done in Section 3 where, in addition, analytical expressions for $\Theta_1(\rho)$, $\Theta_2(\rho)$, ... are developed. A method of accelerating the convergence of (5.11), namely the Shanks transformation, is then discussed in Section 4. To validate the perturbation scheme, in Section 5 the approximate solutions for $\Theta(\rho; S)$ are compared with the numerical results obtained by Davis [15], who employed the property correlations shown in Appendix B for $\lambda(\Theta)$ and $\kappa(\Theta)$. It will be pointed out in Section 7 that the perturbation series (5.11) yields a non-linear algebraic relationship between T_w and the electrical power dissipated in the column. In principle, this permits one to eliminate T_w from the problem, without having to rely on assumptions about the heat transfer conditions external to the column.

5.3. Perturbation Scheme

Approximations for the temperature field are readily derived once one recognizes that:

$$\lim_{S \to 0} \Theta(\rho; S) = 0 \tag{5.12}$$

$$\lim_{S \to 0} \lambda(\Theta) = 1 \qquad \lim_{S \to 0} \kappa(\Theta) = 1. \tag{5.13}$$

Note these limits apply irrespective of the specific correlations chosen to represent the temperature dependence of the electrical and thermal conductivities.

Postulating a regular perturbation expansion of the form given in (5.11), the following asymptotic expansions are obtained from the Taylor series for $\kappa(\Theta)$ and $\lambda(\Theta)$:

$$\kappa = 1 + S\kappa_1(\rho) + S^2\kappa_2(\rho) + S^3\kappa_3(\rho) + S^4\kappa_4(\rho) + \dots , \qquad S \ll 1, \tag{5.14}$$

and

$$\lambda = 1 + S\lambda_1(\rho) + S^2\lambda_2(\rho) + S^3\lambda_3(\rho) + S^4\lambda_4(\rho) + \dots\ , \qquad S \ll 1, \tag{5.15}$$

where

$$\lambda_1 = \lambda_0'\Theta_1, \tag{5.16a}$$

$$\lambda_2 = \lambda_0'\Theta_2 + \frac{1}{2}\lambda_0''\Theta_1^2, \tag{5.16b}$$

$$\lambda_3 = \lambda_0'\Theta_3 + \lambda_0''\Theta_1\Theta_2 + \frac{1}{6}\lambda_0'''\Theta_1^3, \tag{5.16c}$$

$$\lambda_4 = \lambda_0'\Theta_4 + \frac{1}{2}\lambda_0''\left(\Theta_2^2 + 2\Theta_1\Theta_3\right) + \frac{1}{2}\lambda_0'''\Theta_1^2\Theta_2 + \frac{1}{24}\lambda_0''''\Theta_1^4. \tag{5.16d}$$

and

$$\begin{aligned}\lambda_5 = \ & \lambda_0'\Theta_5 + \lambda_0''(\Theta_1\Theta_4 + \Theta_2\Theta_3) + \frac{1}{2}\lambda_0'''(\Theta_1^2\Theta_2 + \Theta_1^2\Theta_2) \\ & + \frac{1}{6}\lambda_0''''\Theta_1^3\Theta_2 + \frac{1}{120}\Theta_1^5\end{aligned} \tag{5.16e}$$

In (5.16a–d), the primes indicate differentiation with respect to Θ and the subscript 0 indicates that the derivative is evaluated at $\Theta = 0$; e.g.

$$\lambda_0' = \left(\frac{d\lambda}{d\Theta}\right)_{\Theta=0}, \qquad \lambda_0'' = \left(\frac{d^2\lambda}{d\Theta^2}\right)_{\Theta=0}, \qquad \dots$$

Expressions completely analogous to (5.16a–d) apply for the terms $\kappa_1, \kappa_2, \dots$, in (5.14). In a similar manner, one can compute the derivative, λ',

$$\begin{aligned}\lambda' &= (\lambda')_0 + S(\lambda')_1 + S^2(\lambda')_2 + S^3(\lambda')_3 \\ &= \lambda_0' + S\lambda_0''\Theta_1 + S^2\left(\lambda_0''\Theta_2 + \frac{\lambda_0'''}{2}\Theta_1^2\right) \\ &\quad + S^3\left(\lambda_0''\Theta_3 + \lambda_0'''\Theta_1\Theta_2 + \frac{\lambda_0''''}{6}\Theta_3^3\right)\end{aligned} \tag{5.17}$$

Upon substituting (5.11), (5.14) and (5.15) into (5.10a) and collecting like powers in S, thus is obtained a hierarchy of linear, ordinary differential equations that govern the functions $\Theta_1(\rho)$, $\Theta_2(\rho)$, ... From (5.16a) and the solution for $\Theta_1(\rho)$, is obtained

$\lambda_1(\rho)$; an expression for $\kappa_1(\rho)$ is obtained from the analog to (5.16a). Having thus established the leading behavior of the perturbation expansions, we subsequently move on to higher orders in the hierarchy. Below is illustrated the procedure through $O(S^3)$; for the sake of brevity, the results at $O(S^4)$ and $O(S^5)$ are simply quoted in Appendix A.

At $O(S)$, Eqn (5.10a) reads

$$\frac{1}{\rho}\frac{d}{d\rho}\left(\rho\frac{d\Theta_1}{d\rho}\right) = -1, \tag{5.18}$$

which has the solution

$$\Theta_1 = \frac{1}{4}\left(1-\rho^2\right). \tag{5.19}$$

This is the dimensionless form of (5.1). To leading order, the temperature field is unaffected by the temperature dependence of the electrical and thermal conductivities. Thus combining (5.19) and (5.16a) yields the leading order variation of the electrical conductivity over the lumen, viz.

$$\lambda_1 = \frac{1}{4}\lambda_0'\left(1-\rho^2\right) \tag{5.20}$$

and, by analogy, the variation in the thermal conductivity, i.e.

$$\kappa_1 = \frac{1}{4}\kappa_0'\left(1-\rho^2\right). \tag{5.21}$$

The $O(S^2)$-analysis proceeds along the lines of the $O(S)$-problem. For $\Theta_2(\rho)$,

$$\frac{1}{\rho}\frac{d}{d\rho}\left(\rho\frac{d\Theta_2}{d\rho}\right) = \frac{1}{4}\kappa_0'\left(1-2\rho^2\right) - \frac{1}{4}\lambda_0'\left(1-\rho^2\right), \tag{5.22}$$

which has the solution

$$\Theta_2 = \frac{1}{64}\lambda_0'(3-\rho^2)(1-\rho^2) - \frac{1}{32}\kappa_0'\left(1-\rho^2\right)^2. \tag{5.23}$$

The radial dependence of λ_2 can now be extracted from (5.16b), viz.

$$\lambda_2 = \frac{1}{64}\lambda_0'^{\,2}(3-\rho^2)(1-\rho^2) + \frac{1}{32}\left(\lambda_0'' - \lambda_0'\kappa_0'\right)\left(1-\rho^2\right)^2, \tag{5.24}$$

and, similarly,

$$\kappa_2 = \frac{1}{64}\kappa_0'\lambda_0'(3-\rho^2)(1-\rho^2) + \frac{1}{32}\left(\kappa_0'' - \kappa_0'^2\right)\left(1-\rho^2\right)^2. \tag{5.25}$$

Coxon and Binder [13] derived an expression equivalent to (5.23) for the circumstance where κ and λ vary linearly with Θ. While some investigators have neglected variation of κ (e.g. [18] and references therein), it is clear from (5.23) that, generally, the temperature dependence of λ *and* κ affect the temperature field at $O(S^2)$.

At $O(S^3)$, the governing equation for $\Theta_3(\rho)$ reads

$$\begin{aligned}\frac{1}{\rho}\frac{d}{d\rho}\left(\rho\frac{d\Theta_3}{d\rho}\right) = \frac{1}{64}\Big[\; & 2\left(\kappa_0'' - 3\,\kappa_0'^2\right)\left(1-\rho^2\right)\left(1-3\,\rho^2\right) \\ & +\kappa_0'\lambda_0'\left(9-24\,\rho^2+11\,\rho^4\right) \\ & -\lambda_0'^2\left(1-\rho^2\right)\left(3-\rho^2\right) - 2\lambda_0''\left(1-\rho\right)^2\left(1+\rho\right)^2\Big].\end{aligned}$$

The solution to Eqn (5.26) is

$$\begin{aligned}\Theta_3(\rho) \;=\; & \frac{1}{384}\left(3\kappa_0'^2 - \kappa_0''\right)\left(1-\rho^2\right)^3 + \frac{1}{2304}\Big[\left(\rho^4 - 8\,\rho^2 + 19\right)\lambda_0'^2 \\ & + \left(2\,\rho^4 - 7\,\rho^2 + 11\right)\lambda_0'' - \left(11\,\rho^4 - 43\,\rho^2 + 38\right)\lambda_0'\kappa_0'\Big]\left(1-\rho^2\right)\end{aligned} \tag{5.26}$$

The solution for $\lambda_3(\rho)$ follows from Eqn (5.16c), viz.

$$\begin{aligned}\lambda_3(\rho) \;=\; & \frac{1}{384}\left(3\lambda_0'\kappa_0'^2 - \lambda_0'\kappa_0'' + \lambda_0''' - 3\lambda_0''\kappa_0'\right)\left(1-\rho^2\right)^3 \\ & +\frac{\lambda_0''\lambda_0'}{256}\left(1-\rho^2\right)^2\left(3-\rho^2\right) - \frac{1}{2304}\Big[\left(11\,\rho^4 - 43\,\rho^2 + 38\right)\lambda_0'^2\kappa_0' \\ & - \left(\rho^4 - 8\,\rho^2 + 19\right)\lambda_0'^3 - \left(2\,\rho^4 - 7\,\rho^2 + 11\right)\lambda_0'\lambda_0''\Big]\left(1-\rho^2\right).\end{aligned} \tag{5.27}$$

An analogous result obtains for $\kappa_3(\rho)$, viz.

$$\begin{aligned}\kappa_3(\rho) \;=\; & \frac{1}{384}\left(3\kappa_0'^3 - 4\kappa_0''\kappa_0' + \kappa_0'''\right)\left(1-\rho^2\right)^3 \\ & +\frac{\kappa_0''\lambda_0'}{256}\left(1-\rho^2\right)^2\left(3-\rho^2\right) - \frac{1}{2304}\Big[\left(11\,\rho^4 - 43\,\rho^2 + 38\right)\lambda_0'\kappa_0'^2 \\ & - \left(\rho^4 - 8\,\rho^2 + 19\right)\lambda_0'^2\kappa_0' - \left(2\,\rho^4 - 7\,\rho^2 + 11\right)\lambda_0''\kappa_0'\Big]\left(1-\rho^2\right).\end{aligned} \tag{5.28}$$

As is evident from (5.26)–(5.28), the forms of the solutions are algebraically straightforward, though increasingly lengthy. The algebra for the $O(S^4)$ and $O(S^5)$ problems is unwieldy and those results are quoted in Appendix A.

Comparison to Solution of Linearized Problem

For the case that thermal conductivity is constant and electrical conductivity is linear in temperature, the governing equation becomes a Bessel equation, with solution

$$\Theta = \frac{J_0(\sqrt{S\alpha_1}\rho) - J_0(\sqrt{S\alpha_1})}{\alpha_1 J_0(\sqrt{S\alpha_1})}, \tag{5.29}$$

where J_0 is a Bessel function of the first kind, and α_1 is the linear coefficient in the electrical conductivity. A similar solution but for different boundary conditions has been shown by Jones and Grushka [24]. Note that expanding 5.29 in a power series in S gives the series solution when one applies the constant (thermal) and linear (electrical) conductivities. Since the expansion in S of the Bessel functions are slowly convergent, it is no surprise that the same is true of the more general series solution derived here.

5.4. Acceleration of Convergence

A well-known non-linear transformation described by Shanks [47] has been applied to the asymptotic series (2.9). Letting $\Theta^{(n)}$ denote the nth partial sum $\Sigma_{k=1}^{n} S^k \Theta_k$, the transformation is denoted recursively as

$$e_1^1(\Theta^{(n)}) = \frac{\Theta^{(n-1)}\Theta^{(n+1)} - \Theta^{(n)^2}}{\Theta^{(n+1)} + \Theta^{(n-1)} - 2\Theta^{(n)}}, \tag{5.30}$$

$$e_1^{m+1}(\Theta^{(n)}) = \frac{e_1^m(\Theta^{(n-1)})e_1^m(\Theta^{(n+1)}) - e_1^m(\Theta^{(n)})^2}{e_1^m(\Theta^{(n+1)}) + e_1^m(\Theta^{(n-1)}) - 2e_1^m(\Theta^{(n)})}. \tag{5.31}$$

Expressions (5.30) and (5.31) shall henceforth be referred to as the Shanks transformation. Here, $\Theta^{(0)} = 0$ is taken to be zero in the computation of $e_1^1(\Theta^{(1)})$. In addition, $e_1^m(\Theta^{(0)}) = 0$ will also be taken as zero for $m \geq 2$, which will facilitate computation of $e_1^m(\Theta^{(1)})$.

Fortunately, as will be seen, low-order Shanks transformations on the partial sums provide substantial improvements over the simple asymptotic series (2.9), obviating computation of the fourth and fifth order terms Θ_4 and Θ_5 to gain an accurate formula for the temperature.

The transformation gives partial sums that closely resemble those in (2.9) but for a factor in the highest order term. As examples of the modified partial sums,

$$e_1^1(\Theta^{(1)}) = S\Theta_1 + S^2\Theta_2 \frac{1}{1 - S\Theta_2/\Theta_1}, \tag{5.32}$$

and

$$e_1^1(\Theta^{(2)}) = S\Theta_1 + S^2\Theta_2 + S^3\Theta_3 \frac{1}{1 - S\Theta_3/\Theta_2}. \tag{5.33}$$

While these forms show the resemblance to the partial sums $\Theta^{(2)}$ and $\Theta^{(3)}$, respectively, it should be noted that they can be simplified to

$$e_1^1(\Theta^{(1)}) = \frac{S\Theta_1}{1 - S\Theta_2/\Theta_1}, \tag{5.34}$$

and

$$e_1^1(\Theta^{(2)}) = S\Theta_1 + \frac{S^2\Theta_2}{1 - S\Theta_3/\Theta_2}. \tag{5.35}$$

It will be seen that the Shanks transformation on the first three terms of the asymptotic expansion gives a temperature profile that is as accurate as the series of all five terms. As will be seen in the results section, we thus have a highly accurate approximation to the solution using only three terms of the series, even for S as high as 0.4.

5.5. Comparison with Numerical Solution

FIG 5.1 shows a comparison of the asymptotic and numerical solutions for the radial profile of dimensionless temperature Θ, at selected values of the dimensionless source strength S. The calculations were carried out for $T_w = 298$ K and with the $\lambda(\Theta)$ and $\kappa(\Theta)$ correlations described in Appendix B. To our knowledge, this is the first comparison of numerical and asymptotic solutions that account for the temperature dependence of the thermal conductivity, though Davis [15] has examined numerical and $O(S^2)$-results for the circumstance where $\kappa(\Theta) \equiv 1$.

Accuracy of the approximate analytic solutions to (5.10) is measured here against a numerically-computed solution to that boundary-value problem, taken to be exact. The numerical scheme was simply a shooting method in conjunction with a 7th/8th order Runge-Kutta method. In all cases, $\Theta^{(5)}(0)$ was used as the initial guess for the centerline temperature $\Theta_{\text{℄}}$ in order to keep the number of iterations low. Of course, one could use one of the lower order estimates or one of the Shanks transformations on the lower order solutions for a good initial guess. The numerical solution to (5.10) is denoted as Θ^N.

For the cases shown, the temperature dependence on the parameter S is significantly nonlinear and the asymptotic approximations are in agreement with the numerical results. The $O(S^4)$-solution is within roughly 10% (relative error) of the numerical result at $S = 0.4$, the largest source strength for which Davis reports numerical results. The $O(S^5)$ solution is within 7% of the exact solution for $S = 0.4$. Discrepancies between the numerical and the asymptotic results are greatest at the centerline and grow with S, as one would expect. This point is made clearer in FIGS 5.2 and 5.3, where $\Theta_{\text{℄}}$ is shown as a function of S. FIGS 5.2 and 5.3 also illustrates that, for the property correlations of Appendix B, extending the approximations to $O(S^3)$ or $O(S^4)$ may offer little benefit. The $O(S^2)$-solution is certainly reliable for $S < 0.1$, while the $O(S^3)$ and $O(S^4)$-solutions begin to deviate from Θ^N

at S equal to 0.2 and 0.3, respectively. The highly nonlinear dependence on S is known as the autothermal effect: local increases in the temperature increase the local electrical conductivity, which increases the local heat generation. The autothermal effect is mitigated, to some extent, by increases in the thermal conductivity, as thermal conductivity increases with temperature. For the situation depicted in FIGS 5.1 and 5.2, the electrical conductivity is roughly a factor of 8 more sensitive to temperature variations. The perturbation scheme consequently departs from the numerical solution when S moves from 0.2 toward 0.4, as λ is an exponential function of Θ.

The convergence of the asymptotic expansion to the exact solution is evident in TABLE 5.1, where the Shanks transformations have been employed. The highest order of the transform shown here, $e_1^4(\Theta^{(1)})/S$, operates on all five terms that are derived herein and yield a 0.2% relative error at the centerline for our maximum S value of 0.4. The inclusion of this higher-order result, however, is primarily pedagogical. One of the main reasons for constructing such an expansion is to obtain a reliable formula that is simple compared to implementation of a numerical algorithm. From that standpoint, the desirability of computing anything beyond the third-order term is questioned. The derivation of the higher-order terms and their transformations, more than anything, are included in order to verify that the approximate solutions indeed converge to the correct results, which is not apparent from the series through $O(S^3)$ for the higher values of S. Note that the Shanks transformation on the first two terms is more accurate than the series at fourth-order, and the two transformations on the first three terms are more accurate than the series at fifth-order. The Shanks transformations thus render formulae that offer significant improvement over the well-established quadratic results at very little cost in algebraic complexity.

The Shanks transformations on the first three terms, namely $e_1^1(\Theta^{(2)})/S$ and $e_1^2(\Theta^{(1)})/S$, each yield less than 4% relative error at the centerline for $S = 0.4$. This translates into less than 1% relative error in actual temperature for a wall temperature of 298 K. This is quite high accuracy for the relative simplicity of terms involved.

For this reason, in all figures, the transformations on no terms higher than $O(S^3)$ are included. The approximate solutions through order 3 and their transformations from the higher-order approximations are separated within TABLE 5.1, for clarity. The six such results are those that appear in the figures describing the temperature profile.

The temperature gradient at the inner wall of the column is shown in FIG 5.4. Here again the comparison between the perturbation and numerical schemes indicates that the $O(S^2)$-solution works well for $S < 0.1$, and the $O(S^3)$, $O(S^4)$ and $O(S^5)$-solutions are within 15%, 9%, and 6% (relative error) of the numerical result at $S = 0.4$, respectively. The temperature gradient at the inner wall of the column has been investigated for 288 K $\leq T_w \leq$ 318 K and was found to have behaviour consistent with that depicted in FIG 5.4.

The temperature gradient is of interest because it, as will be seen, relates to the conductivity, resulting in a nonlinear algebraic relationship for T_w.

TABLE 5.2 compares the analytic results for the temperature gradient at the wall with the numerically-computed values. The partitioning, as in TABLE 5.1, separates the expansion with terms up to $O(S^3)$ and their Shanks transformations, from higher-order terms and transformations. Once again, convergence of the series to the correct value is noticed, with the order 5 expansion yielding less than 6% relative error and the highest-order Shanks transformation yielding a 0.2% relative error, for $S = 0.4$. The smallest error from the lower order terms comes from the $e_1^2(\partial_\rho \Theta^{(1)})/S$ transformation, with a 2.5% relative error. Relative errors from the lower-order terms are depicted in FIG 5.5.

A radial profile of dimensionless electrical conductivity is depicted in FIG 5.6, for the first three terms in the series for λ as well as the Shanks transformation $e_1^2(\lambda^{(2)})/S$, with results equally satisfactory to those previously described.

5.6. Discussion

The temperature field in electrophoresis columns has been of interest for several decades. The analysis presented here contributes to the understanding of the problem in several ways. First, because S is invariably less than unity, it establishes a reasonably general framework for describing radial temperature variations in cylindrical columns, including cases with power densities as high as 1 kW/cm^3 [18]. In most circumstances, power densities are at least an order of magnitude lower and the $O(S^2)$-solution will provide an accurate and simple representation of the temperature profile; to use the formulas at this order, one need only know the rate of change, with respect to temperature, of the electrical and thermal conductivity of the column contents. Here correlations appropriate for aqueous buffers have been used, but other correlations can be accommodated. Alternatively, one can directly measure the temperature dependence of the transport coefficients (see, for example, [18]) and use interpolations of those data in conjunction with the formulas rendered here.

Because the approximate solutions have such a simple form, they can be readily incorporated into the analysis of thermal effects on analyte dispersion. A number of authors have considered the effect of radial temperature variations on analyte dispersion [15, 18, 19]. However, these analyses have either neglected the temperature dependence of the thermal conductivity, or have relied on numerical solutions. One can readily show that the dispersivity of the analyte can be expressed as a regular perturbation expansion in S, where the resultant terms involve the expansions for Θ, κ and λ that have been derived here.

Finally, the approximate solutions allow one to unambiguously relate the temperature field to the electrical power dissipated in the column, without having to make assumptions about the wall temperature T_w or the heat transfer conditions of the column exterior. This is particularly important since, depending on the experimental set-up, the capillary may or may not be thermostatted, and the column may have

various polymer coatings. The current-voltage relationship for a given column is an experimentally-accessible quantity that can be used to establish the steady temperature distribution within the lumen. See Section 5.8 for details.

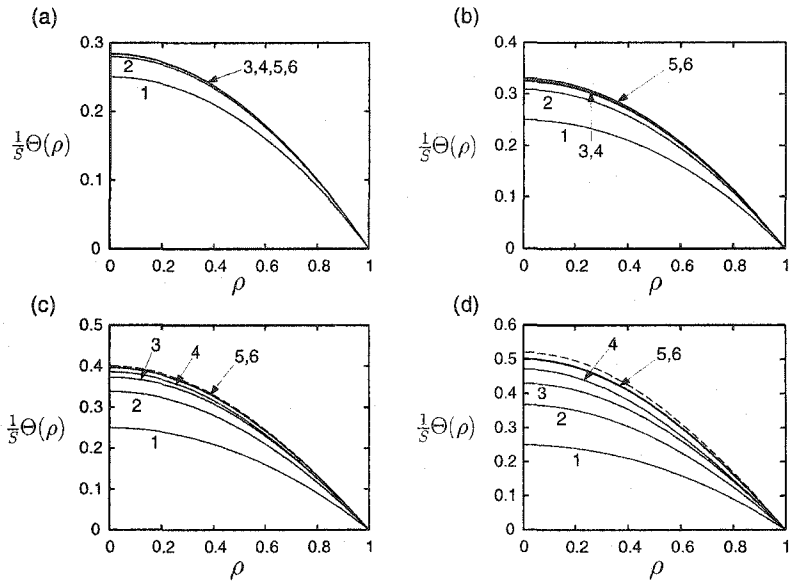

FIGURE 5.1. Dimensionless temperature profiles, $\Theta(\rho)/S$, for $T_w = 298$ K, as given by analytic approximations and the numerical solution. (a) $S = 0.1$, (b) $S = 0.2$, (c) $S = 0.3$, (d) $S = 0.4$. Legend: 1, $\Theta^{(1)}$; 2, $\Theta^{(2)}$; 3, $\Theta^{(3)}$; 4, $e_1^1(\Theta^{(1)})$; 5, $e_1^1(\Theta^{(2)})$; 6, $e_1^2(\Theta^{(1)})$; – – –, Θ^N.

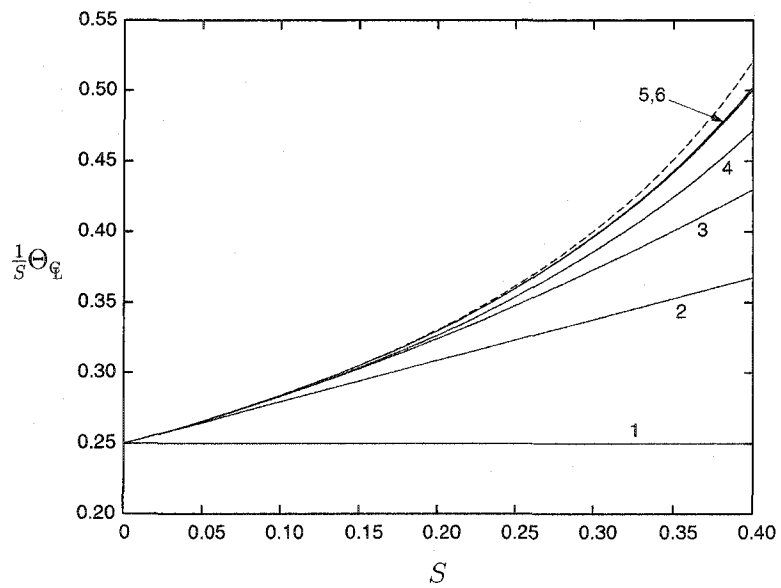

FIGURE 5.2. Variation of dimensionless centerline temperature $\Theta_{\mathfrak{L}}/S$ with S, as given by analytic approximations and the numerical solution, for $T_w = 298$ K. Legend: 1, $\Theta^{(1)}$; 2: $\Theta^{(2)}$; 3, $\Theta^{(3)}$; 4, $e_1^1(\Theta^{(1)})$; 5, $e_1^1(\Theta^{(2)})$; 6, $e_1^2(\Theta^{(1)})$; – – –, Θ^N.

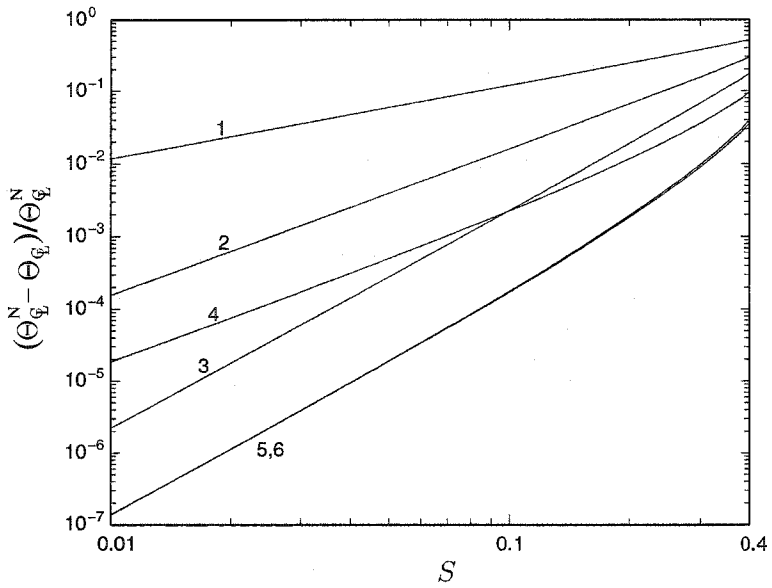

FIGURE 5.3. Relative error in analytic approximations of the centerline temperature $\Theta_{\mathfrak{L}}$, as a function of S, in log-log form. $T_w = 298$ K. The error is relative to $\Theta^N_{\mathfrak{L}}$ and is equivalent to the error in dimensional temperature calculations scaled on $T^N_{\mathfrak{L}} - T_w$. Legend: 1, $\Theta^{(1)}$; 2, $\Theta^{(2)}$; 3, $\Theta^{(3)}$; 4, $e^1_1(\Theta^{(1)})$; 5, $e^1_1(\Theta^{(2)})$; 6, $e^2_1(\Theta^{(1)})$.

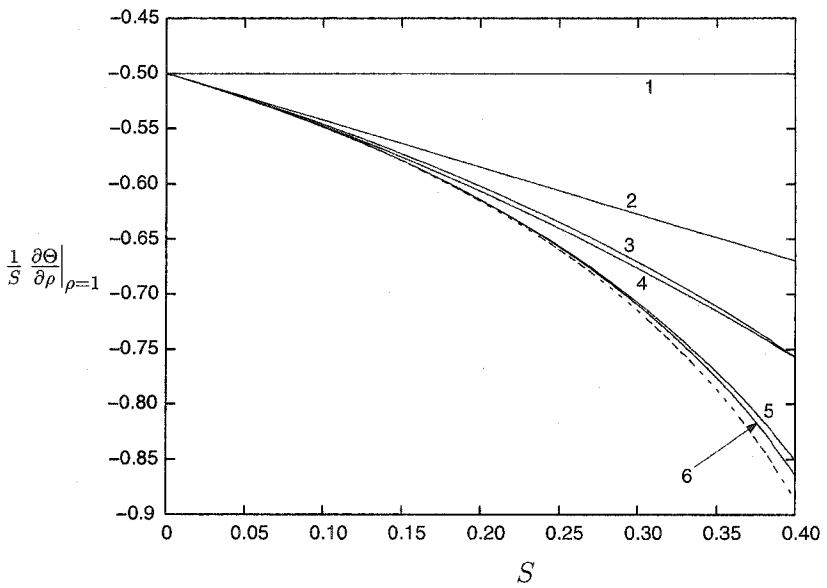

FIGURE 5.4. Variation of the dimensionless gradient at the inner capillary wall, $S^{-1}(\partial_\rho\Theta)_w$, with S, as given by analytic approximations and the numerical solution for $T_w = 298$ K. Legend: 1, $\partial_\rho\Theta^{(1)}$; 2, $\partial_\rho\Theta^{(2)}$; 3, $\partial_\rho\Theta^{(3)}$; 4, $e^1_1(\partial_\rho\Theta^{(1)})$; 5, $e^1_1(\partial_\rho\Theta^{(2)})$; 6, $e^2_1(\partial_\rho\Theta^{(1)})$; ---, $\partial_\rho\Theta^N$.

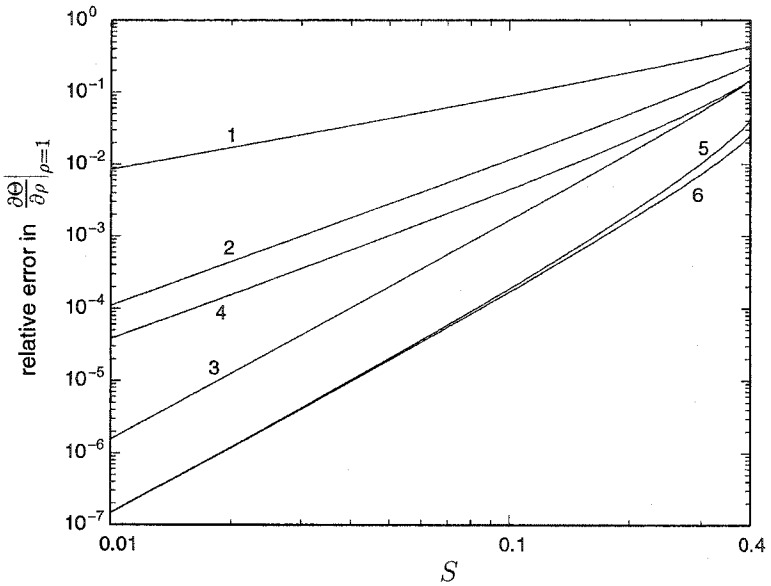

FIGURE 5.5. Relative error in analytic approximations of dimensionless temperature gradient at the inner capillary wall, $(\partial_\rho\Theta)_{\rm w}$, as a function of S, in log-log form. The error is relative to $(\partial_\rho\Theta^{\rm N})_{\rm w}$, and is equivalent to the error in the dimensional tempertature gradient relative to $(\partial_r T^{\rm N})_{\rm w}$. $T_{\rm w} = 298$ K. Legend: 1, $\partial_\rho\Theta^{(1)}$; 2, $\partial_\rho\Theta^{(2)}$; 3, $\partial_\rho\Theta^{(3)}$; 4, $e_1^1(\partial_\rho\Theta^{(1)})$; 5, $e_1^1(\partial_\rho\Theta^{(2)})$; 6, $e_1^2(\partial_\rho\Theta^{(1)})$.

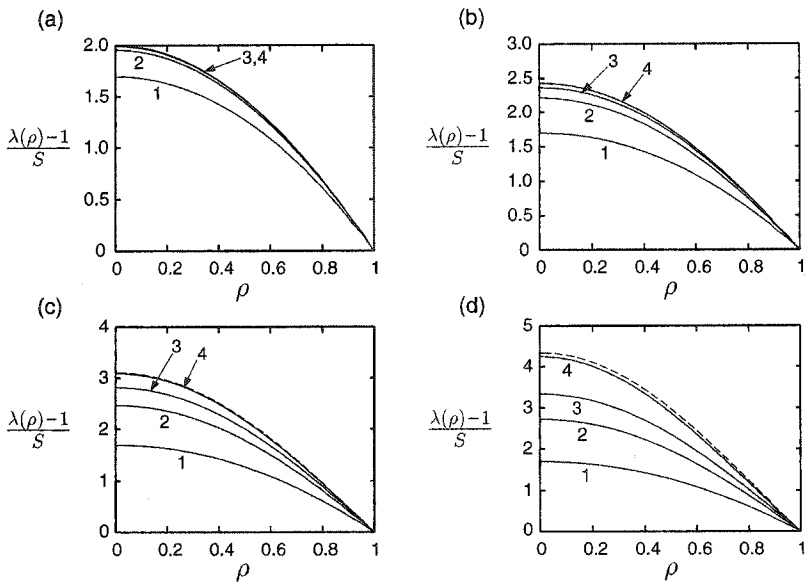

FIGURE 5.6. Radial variations of dimensionless electrical conductivity, $[\lambda(\rho) - 1]/S$, for $T_w = 298$ K, as given by analytic approximations and the numerical solution. (a) $S = 0.1$, (b) $S = 0.2$, (c) $S = 0.3$, (d) $S = 0.4$. Legend: 1, $\lambda^{(1)}$; 2, $\lambda^{(2)}$; 3, $\lambda^{(3)}$; 4, $e_1^1(\lambda^{(2)})$; ---, λ^N.

TABLE 5.1. Comparison of asymptotic expansions, $\Theta_{\mathfrak{L}}^{(n)}/S$, of the dimensionless centerline temperature and Shanks transformations, $e_1^m(\Theta_{\mathfrak{L}}^{(n)})/S$, with numerically-computed values, $\Theta_{\mathfrak{L}}^{\mathrm{N}}/S$, for select values of S, and $T_{\mathrm{w}} = 298$ K.

		$S = 0.1$;	$\Theta_{\mathfrak{L}}^{\mathrm{N}}/S = 0.283916$		
n	$\Theta^{(n)}/S$	$e_1^1(\Theta^{(n)})/S$	$e_1^2(\Theta^{(n)})/S$	$e_1^3(\Theta^{(n)})/S$	$e_1^4(\Theta^{(n)})/S$
1	0.250000	0.283277	0.283867	0.283915	0.283916
2	0.279368	0.283866	0.283915	0.283916	
3	0.283269	0.283911	0.283916		
4	0.283820	0.283916			
5	0.283902				
		$S = 0.2$;	$\Theta_{\mathfrak{L}}^{\mathrm{N}}/S = 0.330628$		
n	$\Theta^{(n)}/S$	$e_1^1(\Theta^{(n)})/S$	$e_1^2(\Theta^{(n)})/S$	$e_1^3(\Theta^{(n)})/S$	$e_1^4(\Theta^{(n)})/S$
1	0.250000	0.326772	0.330017	0.330591	0.330624
2	0.308735	0.329985	0.330590	0.330624	
3	0.324339	0.330494	0.330622		
4	0.328753	0.330597			
5	0.330054				
		$S = 0.3$;	$\Theta_{\mathfrak{L}}^{\mathrm{N}}/S = 0.400383$		
n	$\Theta^{(n)}/S$	$e_1^1(\Theta^{(n)})/S$	$e_1^2(\Theta^{(n)})/S$	$e_1^3(\Theta^{(n)})/S$	$e_1^4(\Theta^{(n)})/S$
1	0.250000	0.386047	0.396762	0.399991	0.400305
2	0.338103	0.396473	0.399965	0.400305	
3	0.373212	0.399089	0.400272		
4	0.388109	0.399904			
5	0.394692				
		$S = 0.4$;	$\Theta_{\mathfrak{L}}^{\mathrm{N}}/S = 0.521063$		
n	$\Theta^{(n)}/S$	$e_1^1(\Theta^{(n)})/S$	$e_1^2(\Theta^{(n)})/S$	$e_1^3(\Theta^{(n)})/S$	$e_1^4(\Theta^{(n)})/S$
1	0.250000	0.471592	0.502560	0.517657	0.519901
2	0.367470	0.500651	0.517217	0.519891	
3	0.429887	0.511202	0.519479		
4	0.465199	0.515840			
5	0.486004				

TABLE 5.2. Comparison of asymptotic expansions of dimensionless temperature gradient at the capillary wall, and Shanks transformations of the series, with numerically-computed values of wall derivative, $S^{-1}(\partial_\rho \Theta^{\mathrm{N}})_{\mathrm{w}}$, for select values of S, and $T_{\mathrm{w}} = 298$ K.

		$S = 0.1$;	$S^{-1}(\partial_\rho \Theta^{\mathrm{N}})_{\mathrm{w}} = -0.548832$		
n	$\partial_\rho \Theta^{(n)}/S$	$e_1^1(\partial_\rho \Theta^{(n)})/S$	$e_1^2(\partial_\rho \Theta^{(n)})/S$	$e_1^3(\partial_\rho \Theta^{(n)})/S$	$e_1^4(\partial_\rho \Theta^{(n)})/S$
1	-0.500000	-0.546376	-0.548738	-0.548828	-0.548831
2	-0.542440	-0.548728	-0.548828	-0.548831	
3	-0.547917	-0.548824	-0.548831		
4	-0.548695	-0.548831			
5	-0.548811				
		$S = 0.2$;	$S^{-1}(\partial_\rho \Theta^{\mathrm{N}})_{\mathrm{w}} = -0.615684$		
n	$\partial_\rho \Theta^{(n)}/S$	$e_1^1(\partial_\rho \Theta^{(n)})/S$	$e_1^2(\partial_\rho \Theta^{(n)})/S$	$e_1^3(\partial_\rho \Theta^{(n)})/S$	$e_1^4(\partial_\rho \Theta^{(n)})/S$
1	-0.500000	-0.602235	-0.614660	-0.615595	-0.615677
2	-0.584879	-0.614409	-0.615594	-0.615677	
3	-0.606787	-0.615489	-0.615670		
4	-0.613015	-0.615644			
5	-0.614864				
		$S = 0.3$;	$S^{-1}(\partial_\rho \Theta^{\mathrm{N}})_{\mathrm{w}} = -0.715099$		
n	$\partial_\rho \Theta^{(n)}/S$	$e_1^1(\partial_\rho \Theta^{(n)})/S$	$e_1^2(\partial_\rho \Theta^{(n)})/S$	$e_1^3(\partial_\rho \Theta^{(n)})/S$	$e_1^4(\partial_\rho \Theta^{(n)})/S$
1	-0.500000	-0.670815	-0.709905	-0.714247	-0.714974
2	-0.627319	-0.707752	-0.714220	-0.714974	
3	-0.676612	-0.713256	-0.714862		
4	-0.697631	-0.714499			
5	-0.706989				
		$S = 0.4$;	$S^{-1}(\partial_\rho \Theta^{\mathrm{N}})_{\mathrm{w}} = -0.886504$		
n	$\partial_\rho \Theta^{(n)}/S$	$e_1^1(\partial_\rho \Theta^{(n)})/S$	$e_1^2(\partial_\rho \Theta^{(n)})/S$	$e_1^3(\partial_\rho \Theta^{(n)})/S$	$e_1^4(\partial_\rho \Theta^{(n)})/S$
1	-0.500000	-0.757022	-0.864183	-0.879861	-0.884720
2	-0.669759	-0.850895	-0.879582	-0.884693	
3	-0.757390	-0.872867	-0.883420		
4	-0.807213	-0.879996			
5	-0.836789				

5.7. Determining the Wall Temperature in Capillary Electrophoresis

It is very important to know the extent of heat generated in capillary electrophoresis. Accordingly, it is desirable to devise ways of directly or indirectly measure the temperature in a capillary electrophoresis column. While there are ways of measuring, it is easier if the temperature can be determined from relationships with experimentally controllable or more easily-measured quantities. The latter approach is pursued here, through the relationship of the temperature to the quantities of applied voltage, the electrical and thermal conductivities of the buffer at room temperature, and correlations of the conductivities determined from measurements at various temperatures.

In the preceding chapter, there was given an approximate formula for the temperature in a cylindrical capillary electrophoresis column as a series expansion in the dimensionless power input, S (see below). For $S \ll 1$, the power input is small enough so that the temperature from the center of the capillary to the inner wall is nearly uniform. For moderate values of this parameter, the temperature profile is decidedly non-uniform, leading to band-broadening in separations that can be controlled by reverse pressure-driven flow [14, 18]. It was shown, however, that even for S as high as 0.4, only the first three terms of the series are needed for accurate results.

The problem with the analysis of the preceding paper is that it depends on knowing the wall temperature *a priori*. In this paper, the formula for the temperature profile is inverted in order to determine the temperature at the inner wall of the capillary. This is done by supposing knowledge of the applied voltage and buffer conductivities, and also the average electrical conductivity across the cylinder. This is determined experimentally by measuring the current across the cylinder during electrophoresis. The average conductivity relates to the applied voltage in an Ohm's law relationship, which it is noted is generally nonlinear due to the non-linear dependence of electrical conductivity on temperature, and the Joule heating.

This chapter is meant to be as self-contained as possible, that is, for the preceding

chapter to be unnecessary for understanding the present work. The results from that chapter will be presented as needed. To begin, the divergence theorem to the governing equation is applied, as in steady-state, the heat generated in the capillary is equivalent to that which escapes outward through the inner capillary wall. Doing this gives a somewhat simple relationship between the temperature gradient at the wall to the average buffer conductivity in the cylinder, which is taken to be measurable. The expression for the temperature gradient is simply derived from our series expansion for the temperature, and is an implicit function of the temperature at the wall. The relationship is then inverted numerically to determine the temperature. Measured data [36] is then used to determine buffer conductivities from voltage/current relationships. Computations are made based on plausible experimental parameters to show the extent to which Joule heating can occur.

5.7.1. Heat Flux at the Inner Wall

We begin with the governing equation for the temperature field, T,

$$\nabla \cdot (k \nabla T) = -\sigma E^2, \tag{5.36}$$

where k and σ are the local thermal and electrical conductivities, respectively, of the buffer, and E is the applied field strength. The right-hand side of (5.36) is the heat generation rate due to ohmic conduction processes.

Because the interest here is in the steady temperature profile, application of the divergence theorem to Eqn (5.36) gives

$$\int\int_{A_i} k\mathbf{n} \cdot \nabla T dA = -\int\int\int_{V_i} \sigma E^2 dV, \tag{5.37}$$

where $\mathbf{n}$ is the unit vector normal to A_i, the surface that bounds V_i, the volume of fluid contained within the capillary, which has an inner radius of R_i and length L. The aspect ratio $R_i/L \ll 1$, so contributions from the ends of the capillary to the integral on the LHS of Eqn (5.37) are negligible. Given the conditions stipulated at

the inception of the problem, i.e., that the temperature profile is steady and that axial variations are negligible, Eqn (5.37) becomes

$$k_{\mathrm{w}}\left(\frac{dT}{dr}\right)_{r=R_{\mathrm{i}}} = \frac{1}{2}R_{\mathrm{i}}\bar{\sigma}, \tag{5.38}$$

where

$$\bar{\sigma} = \frac{2}{R_{\mathrm{i}}^2}\int_0^{R_{\mathrm{i}}} r\,\sigma\,dr \tag{5.39}$$

is the cross-sectionally averaged electrical conductivity, and r is the radial variable in cylindrical coordinates. The subscript w with any denotes that the parameter's value is that at the inner radius, R_{i} In dimensionless form, Eqn (5.38) reads,

$$\left(\frac{d\Theta}{d\rho}\right)_{\rho=1} = \frac{1}{2}S\bar{\lambda}. \tag{5.40}$$

The governing equations are made dimensionless by

$$\kappa(T) = \frac{k(T)}{k_{\mathrm{w}}}, \qquad \lambda(T) = \frac{\sigma(T)}{\sigma_{\mathrm{w}}} = \frac{\mu_{\mathrm{w}}}{\mu(T)}, \qquad G_{\mathrm{w}} = \sigma_{\mathrm{w}}E^2, \tag{5.41}$$

and

$$\Theta(\rho) = \frac{T - T_{\mathrm{w}}}{T_{\mathrm{w}}}, \qquad \rho = \frac{r}{R_{\mathrm{i}}}, \tag{5.42}$$

where R_{i} is the inner radius of the capillary.

$\bar{\lambda}$ is now given by

$$\bar{\lambda} = 2\int_0^1 \rho\lambda(\rho)d\rho. \tag{5.43}$$

The Temperature Profile

In the preceding paper, an approximate solution for the radial temperature profile was derived in the form of a power series in the dimensionless parameter S,

$$S = \frac{\sigma_{\mathrm{w}}E^2R_{\mathrm{i}}^2}{k_{\mathrm{w}}T_{\mathrm{w}}}, \tag{5.44}$$

that is valid through $O(S^5)$. To balance algebraic simplicity with numerical accuracy, first three terms only will be used, viz.

$$\begin{aligned}\Theta(\rho) =& S\Theta_1(\rho) + S^2\Theta_2(\rho) + S^3\Theta_3(\rho)\\ =& \frac{S}{4}\left(1-\rho^2\right) + \frac{S^2}{64}(1-\rho^2)\left[\lambda_0'(3-\rho^2) - 2\kappa_0'\left(1-\rho^2\right)\right]\\ &+ \frac{S^3}{2304}\left(1-\rho^2\right)\left\{6\left(3{\kappa_0'}^2 - \kappa_0''\right)\left(1-\rho^2\right)^2 + \left[\left(\rho^4 - 8\,\rho^2 + 19\right){\lambda_0'}^2\right.\right.\\ &\left.\left.+ \left(2\,\rho^4 - 7\,\rho^2 + 11\right)\lambda_0'' - \left(11\,\rho^4 - 43\,\rho^2 + 38\right)\lambda_0'\kappa_0'\right]\right\}\end{aligned} \tag{5.45}$$

This solution is applied to (5.40), *viz.*

$$\bar{\lambda} = 1 + \frac{S}{8}\lambda_0' + \frac{S^2}{96}\left[\lambda_0'' - \lambda_0'\kappa_0' + 2(\lambda_0')^2\right] \tag{5.46}$$

5.7.2. Evaluating the Wall Temperature

Equation (5.46) is seen to be an implicit equation for the wall temperature, T_w. The values of λ_0', λ_0'', and κ_0' are obtained from correlations of experimental data for the thermal and electrical conductivities. The full expressions are given in the preceding paper [15], but here are given the terms that appear in equation (5.46),

$$\begin{aligned}\lambda_0' =& M^2 B_1 \ln 10,\\ \lambda_0'' =& 2M^2\left(B_2 - MB_1\right)\ln 10 + \left(M^2 B_1 \ln 10\right)^2,\end{aligned} \tag{5.47}$$

where

$$\begin{aligned}B_1 &= \left[165.9 + 1.053\times 10^{-3}\left(293 - T_\mathrm{w}\right)\left(43 - T_\mathrm{w}\right)\right]/T_\mathrm{w},\\ B_2 &= 1.053\times 10^{-3}\left(T_\mathrm{w} - 168\right),\\ M &= T_\mathrm{w}/\left(T_\mathrm{w} - 168\right),\end{aligned} \tag{5.48}$$

and

$$\kappa_0' = \frac{6.229\times 10^{-3} T_\mathrm{w} - 15.530\times 10^{-6} T_\mathrm{w}^2}{-0.5612 + 6.229\times 10^{-3} T_\mathrm{w} - 7.765\times 10^{-6} {T_\mathrm{w}}^2} \tag{5.49}$$

Moreover, it is noted that the electrical conductivity is measured at some reference temperature T_{ref}, and thus

$$\sigma_{\text{w}} = \sigma(T_{\text{w}}) = \sigma_{\text{ref}}\lambda_{\text{ref}}, \tag{5.50}$$

$\bar{\sigma}$ and σ_{ref} will be treated as independent parameters of the system. λ_{ref} is determined from the correlation for electrical conductivity, and is given by

$$\lambda_{\text{ref}} = 10^{-\delta(T)}, \tag{5.51}$$

where

$$\delta(T) = 1.3272(293 - T) - 1.053 \times 10^{-3}\frac{(293 - T)^2}{T - 168}. \tag{5.52}$$

Equation (5.46) now reads

$$\frac{\bar{\sigma}}{\sigma_{\text{ref}}} = \lambda_{\text{ref}}\left\{1 + \frac{S\lambda_0'}{8} + \frac{S^2}{96}\left[\lambda_0'' - \lambda_0'\kappa_0' + 2(\lambda_0')^2\right]\right\}. \tag{5.53}$$

Substituting (5.47), (5.49), (5.51), and (5.44) into (5.53), an equation for the wall temperature, T_{w}, is obtained, and can be easily solved with any of a number of root-finding algorithms. Given the functional form, it is best to use a method that does not employ derivatives [6].

In addition, a Shanks transformation was used to accelerate convergence of the series in S to get an even more reliable approximation. In this case, the first-order transformation on the first three of the partial sums was employed, obtaining

$$\frac{\bar{\sigma}}{\sigma_{\text{ref}}} = \lambda_{\text{ref}}\left\{1 + \frac{3}{2}\frac{S(\lambda_0')^2}{12\lambda_0' - S\left[\lambda_0'' - \lambda_0'\kappa_0' + 2(\lambda_0')^2\right]}\right\} \tag{5.54}$$

Thus here are two implicit equations for the wall temperature, T_{w}.

5.7.3. Results

Ohm's law relationships between applied voltage and measured current [36] have been used to estimate conductivities $\bar{\sigma}$ across capillary tubes with different radii.

The experimental data used are for different thermostating devices, where it was shown that for, a Peltier thermostat and a capillary radius of 25 microns, the buffer temperature can be held to a temperature of 293 K, up to a large applied voltage. The corresponding Ohm's law plot is very nearly linear. That data and that reference temperature were used to estimate the reference conductivity σ_{ref} to be 0.082 S/m.

Electrical current measurements were made for inner capillary radii of 25, 50, and 100 microns, with natural air and forced convection in addition to Peltier thermostating. For these types of cooling, the buffer certainly runs hotter, but as will be seen, the temperature is nearly uniform. The wall temperature as a function of voltage with a Peltier thermostat is plotted in FIG 5.7(a). The wall temperature was computed using Equation (5.54). The near-uniformity of the temperature in the buffer is reflected mathematically by the smallness of the parameter S, shown in FIG 5.7(b). Indeed, the abbreviated form of (5.53) with the just first two terms in the bracketed expression gives roughly the same result. One can see that the buffer runs hotter for the wider capillary. It is noted that in the calculations behind FIG 1, the capillary widths were adjusted from their stated values in [36] so that the observed values of the average conductivity $\bar{\sigma}$ are consistent with the experimental procedure that the temperature is at 293 K when no voltage is applied. The adjusted capillary radii are within ten percent of the stated values, a plausible discrepancy [3].

In FIG 5.8(a), there is another plot of wall temperature as a function of applied voltage, with the widths of capillaries as per FIG 5.7, but now with forced air cooling. With a less effective cooling than by the Peltier thermostat, the buffers run even hotter, with temperatures as high as 340 K, for large enough voltages. It is noticed, in FIG 5.8(b) that although these temperatures are quite high compared to the reference temperature, the dimensionless power S is quite small, in all cases less than 0.03. Thus, the temperature is expected to be nearly uniform in these laboratory conditions.

Now is considered the case whereby the heating is less uniform. A comparitively large capillary width of 100 microns and applied field of 1200 V/cm can lead to a

vlaue of S of almost 0.1. In FIG 5.9(a), the wall temperature T_w for these conditions is plotted agains the electric field, E. It can be seen that the implicit expression (5.53) with the first two terms used gives a wall temperature accurate to within half a degree K. The higher order expressions (5.53) and (5.54) are for these conditions close to what the exact temperature should be for this model. Finally, it is noted that the parameter S must also be computed implicitly, as it is dependent on the wall temperature, T_w. For the same conditions as in FIG 5.9(a), a plot is made of this dimensionless heat generation, in FIG 5.9(b).

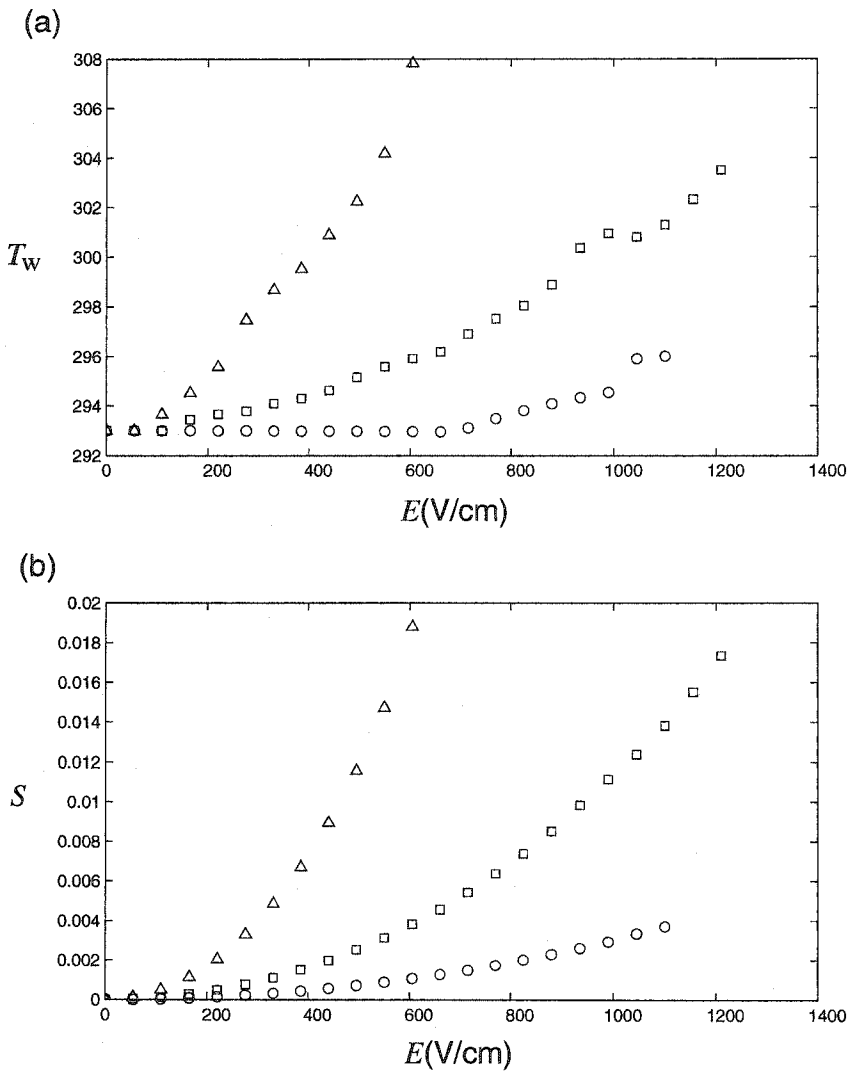

FIGURE 5.7. (a) Wall temperature T_w, plotted against applied electric field E, based on laboratory measurements of electric current and applied field [36], with Peltier thermostating, and capillary radii of 25 μm, 50 μm, and 100 μm. (b) Dimensionless power input S, plotted against applied electric field E.

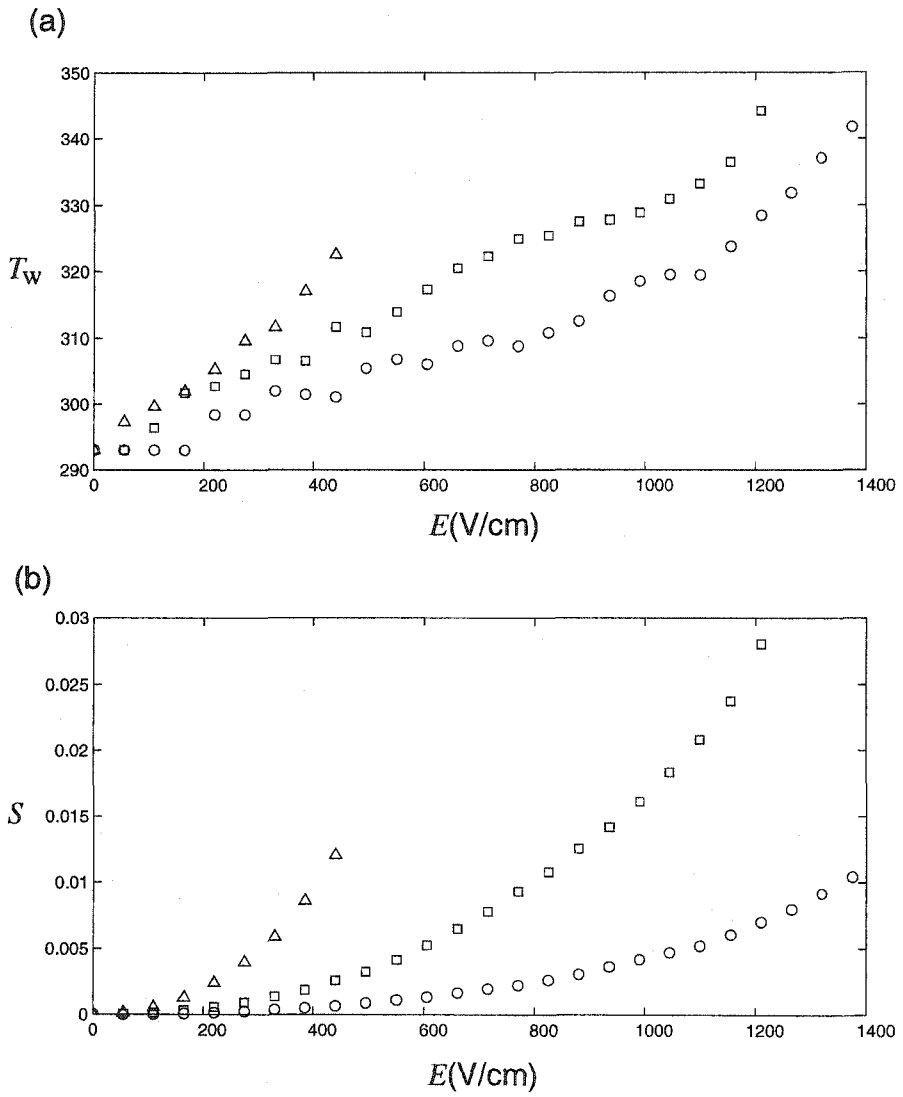

FIGURE 5.8. (a) Wall temperature T_w plotted against applied electric field E, based on laboratory measurements of electric current and applied field [36], with forced air cooling and capillary radii of 25 μm, 50 μm, and 100 μm. (b) Dimensionless power input S, plotted against applied electric field E.

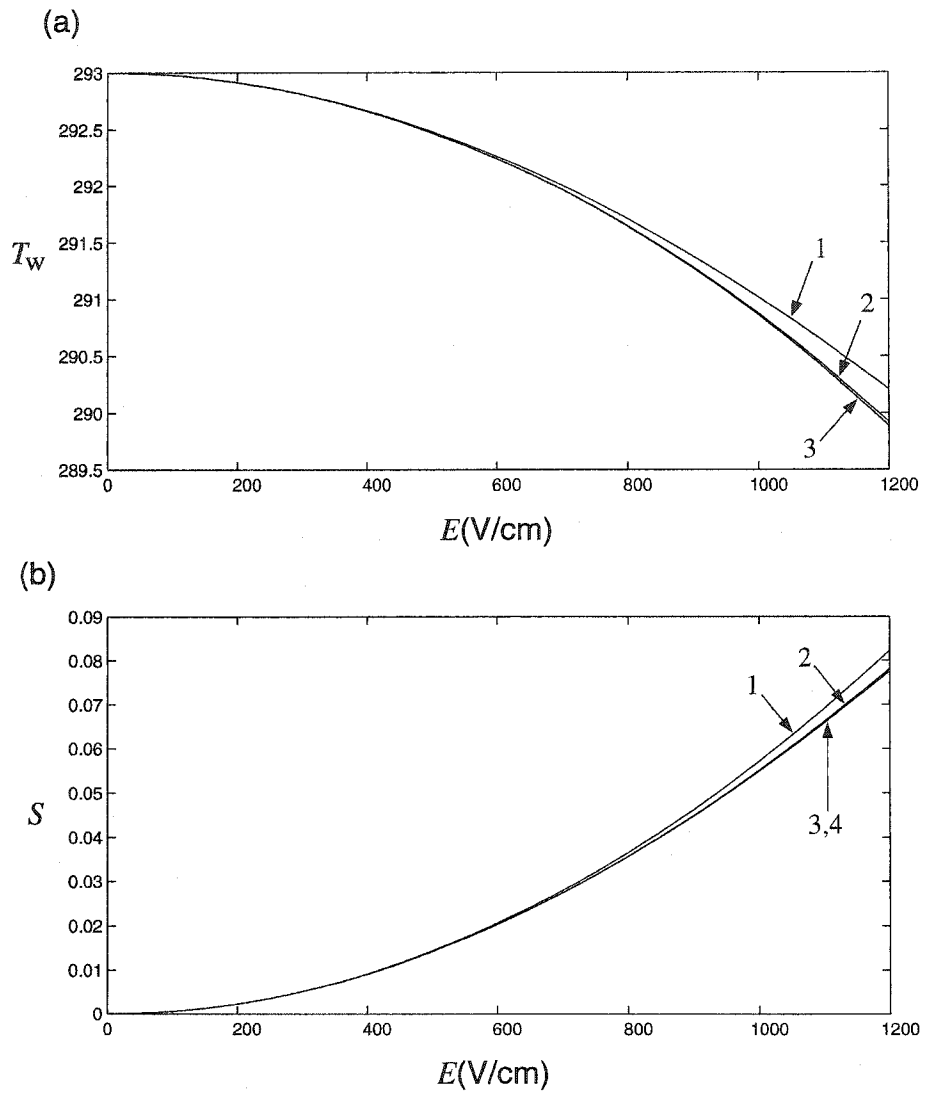

FIGURE 5.9. (a) Wall temperature, T_w, plotted against applied electric field, with the reference and wall conductivies, σ_{ref} and σ_w fixed at 0.1 S/m. Legend: 1, T_w computed from (5.53) to $O(S)$; 2, Eqn. (5.53) to $O(S^2)$; 3, Eqn. (5.54). (b) Dimensionless power generation S, plotted against applied electric field. Legend: 1, S computed from (5.44) (5.53) to leading order; 2, Eqn. (5.53) to $O(S)$; 3, Eqn. (5.53) to $O(S^2)$; 4, Eqn. (5.54).

6. Future Study

As most research should, this work has led to many questions as well as answers. Moreover, the work here can stand to be improved and refined, and used to further some studies of electrophoresis.

6.1. Drop Electrophoresis

In Chapter 3, a thin double-layer analysis was used to approximate the potential profile inside and outside a fluid drop. The results are quite satisfactory, meaning highly accurate, as compared with the (exact) numerical solution to the Poisson-Boltzmann equation. Applying this approximation to the electrokinetic problem would be quite challenging, but perhaps rewarding. Thin double-layer analysis has been employed by Ohshima, Healy, and White to approximate the electrophoretic mobility of non-conducting spheres [41] and mercury drops [42]. Those analyses were done with the consideration that current does not pass through the interface of the drop. In the model presented here, the exterior and interior electrokinetics are coupled due to the allowance of interfacial current, rendering the mathematics much more complicated. All hope is not lost, however. It is entirely realistic to have a fluid drop with extraordinarily thin double-layers, corresponding to values of $a\kappa$ of 1000 and greater [8]. In this case, even just one correction to the flat-plate electrostatics might provide for a useful mobility formula, as in [41] and [42]. Indeed, the coupling of exterior and interior electrokinetics will complicate matters, but perhaps not prohibitively.

In addition, the formulation of the electrokinetic, or mobility problem as a set of integral equations needs to be utilised more than has been done here. It is true that the integral equations greatly simplified the derivation of a mobility formula for small interfacial potentials. However, they can also be used for generating approximations

to the mobility for thin double-layers, as has been suggested in the previous paragraph. It is also believed that this formulation would lend itself well to a numerical solution of the electrokinetics.

Toward the end of the preparation of this thesis, it was thought to combine analytic and numerical techniques for the electrokinetic problem. In particular, it is seen (FIGS 3.2 and 3.3) that the double-layer approximation to the electrostatics has a very small absolute error when compared to the numerical one, even outside the double-layers. For values of $a\kappa$ of 100 and beyond, the error reaches a peak of roughly 5×10^{-8}. So it is stated that the third-order approximation to the equilibrium potential is for all intents and purposes exact. The smallness of the absolute error can be taken advantage of in the integral formulation. It would be worthwhile to generate a numerical solution to the integral formulation of the electrokinetic problem, using the third-order approximation is the equilibrium potential.

A thin-double layer analysis for the general drop problem would likely help to answer the question of to what extent the drop mobility is a function of the drop size. When comparing the mobility formula for small interfacial potential to experimental results (see FIG 4.4), we used zeta potentials of -66.1 and -97.1, which in the dimensionless system are -2.64 and -3.88 respectively, and thus out of the range of applicability for the formula. Calculations of the small potential results with such moderate and larger values of $\tilde{\zeta}_{\mathrm{E}}$ indicate more dependence of mobility on drop size. A thin-double layer analysis would impose no restrictions on the size of the potentials, and so would be well-suited to investigate such a dependence on size.

Finally, while the mathematical model is based on sound principles should be generalized in some way to account for a deficit of ionic species, or a negative excess.

6.2. Heating in Capillary Electrophoresis

A natural extension to the present study of heating in capillary electrophoresis would be to use the analysis of temperature variations and apply them to the fluid dynamic model and determine expressions for the fluid velocity. Just as the results presented have extended previously-derived expressions of the temperature variations in a capillary buffer, one can with the aid of these expressions do the same for the velocity profile.

Furthermore, as previously stated, when using the implicit formula for the temperature at the inner capillary wall, it was surprising to see that conditions whereby little temperature variation occurs within the capillary give rise to significant Joule heating in the buffer. Thus the temperature in the buffer may rise significantly from room temperature in the capillary but with little radial variation. An experiment to verify this phenomenon would be worthwhile.

A. Temperature Variations: The $O(S^4)$ and $O(S^5)$-Solutions

The implicit form of the equation for the temperature field $\Theta_4(\rho)$ is

$$\begin{aligned}\frac{1}{\rho}\frac{d}{d\rho}\left(\rho\frac{d\Theta_4}{d\rho}\right) = -\Big[&\lambda_3 + \kappa_2\Theta_2'' + 2(\kappa')_0\Theta_1'\Theta_3' + (\kappa')_2(\Theta_1')^2 \\ &+ \frac{\kappa_3\Theta_1'}{\rho} + \kappa_1\Theta_3'' + \frac{\kappa_1\Theta_3'}{\rho} + \frac{\kappa_2\Theta_2'}{\rho} \\ &+ (\kappa_0'(\Theta_1')^2 + \kappa_3\Theta_1'' + 2(\kappa')_1\Theta_1'\Theta_2'\Big]\end{aligned} \tag{A.1}$$

The right hand side is made explicit through substitution of equations (5.16), (5.17), and the terms Θ_i from the series solution.

The solution to Eqn (A.1) is

$$\begin{aligned}\Theta_4 = &-\frac{1}{6144}\left(15\,\kappa_0'^3 - 10\,\kappa_0''\kappa_0' + \kappa_0'''\right)\left(1-\rho^2\right)^4 \\ &-\frac{1}{147456}\Big[\left(\rho^6 - 15\rho^4 + 93\rho^2 - 211\right)\lambda_0'^3 \\ &\quad - \left(45\rho^6 - 355\rho^4 + 941\rho^2 - 835\right)\lambda_0'^2\kappa_0' \\ &\quad - \left(50\rho^6 - 222\rho^4 + 426\rho^2 - 326\right)\lambda_0''\kappa_0' \\ &\quad + \left(11\rho^6 - 85\rho^4 + 239\rho^2 - 369\right)\lambda_0'\lambda_0'' \\ &\quad + 2\left(133\,\rho^6 - 651\,\rho^4 + 969\,\rho^2 - 487\right)\lambda_0'\kappa_0'^2 \\ &\quad - 2\left(39\rho^6 - 193\rho^4 + 275\rho^2 - 133\right)\lambda_0'\kappa_0'' \\ &\quad + 2\left(3\rho^6 - 13\rho^4 + 23\rho^2 - 25\right)\lambda_0'''\Big]\left(1-\rho^2\right)\end{aligned} \tag{A.2}$$

And, at the 5th order,

$$\frac{1}{\rho}\frac{d}{d\rho}\left(\rho\frac{d\Theta_5}{d\rho}\right) = -\Bigg[\lambda_4 + (\kappa')_3(\Theta_1')^2 + \kappa_2\Theta_3'' + 2(\kappa')_0\Theta_1'\Theta_4' + \frac{\kappa_1\Theta_4'}{\rho} + \frac{\kappa_3\Theta_2'}{\rho} + 2\kappa_0\Theta_2'\Theta_3' + (\kappa')_1(\Theta_2')^2 + \frac{\kappa_2\Theta_3'}{\rho} + \kappa_1\Theta_4'' + \frac{\kappa_4\Theta_1'}{\rho} + \kappa_3\Theta_2'' + 2(\kappa')_1\Theta_1'\Theta_3' + \kappa_4\Theta_1'' + 2(\kappa')_2\Theta_1'\Theta_2'\Bigg], \tag{A.3}$$

and

$$
\begin{aligned}
\Theta_5 =& \frac{1}{122880}\left(10\kappa_0''^2 - 105\kappa_0'^2\kappa_0'' - \kappa_0'''' + 105\kappa_0'^4 + 15\kappa_0'''\kappa_0'\right)(1-\rho^2)^5 \\
&+ \frac{(1-\rho^2)}{14745600}\Big\{\left(78\rho^8 - 647\rho^6 + 1953\rho^4 - 3148\rho^2 + 3503\right)\kappa_0'\lambda_0''' \\
&\quad - \left(294\rho^8 - 1556\rho^6 + 3444\rho^4 - 4356\rho^2 + 2894\right)\lambda_0'\lambda_0''' \\
&\quad - 2\left(312\rho^8 - 1863\rho^6 + 3737\rho^4 - 3163\rho^2 + 1037\right)\lambda_0'\kappa_0''' \\
&\quad + \left(6790\rho^8 - 40260\rho^6 + 81940\rho^4 - 71460\rho^2 + 24190\right)\kappa_0'\lambda_0'\kappa_0'' \\
&\quad - \left(728\rho^8 - 6427\rho^6 + 19053\rho^4 - 23147\rho^2 + 11353\right)\lambda_0'^2\kappa_0'' \\
&\quad + \left(32\rho^8 - 243\rho^6 + 957\rho^4 - 1943\rho^2 + 2457\right)\lambda_0''^2 \\
&\quad - \left(773\rho^8 - 20373\rho^6 + 6327\rho^4 - 35027\rho^2 + 27948\right)\kappa_0'\lambda_0'\lambda_0'' \\
&\quad - \left(496\rho^8 - 2704\rho^6 + 6496\rho^4 - 7104\rho^2 + 3296\right)\kappa_0''\lambda_0'' \\
&\quad + \left(2010\rho^8 - 10890\rho^6 + 25710\rho^4 - 29490\rho^2 + 14460\right)\kappa_0'^2\lambda_0'' \\
&\quad + \left(45\rho^8 - 580\rho^6 + 3020\rho^4 - 8080\rho^2 + 12795\right)\lambda_0'^2\lambda_0'' \\
&\quad + \left(\rho^8 - 24\rho^6 + 276\rho^4 - 1624\rho^2 + 3651\right)\lambda_0'^4 \\
&\quad - 10\left(17\rho^8 - 218\rho^6 + 1112\rho^4 - 2568\rho^2 + 2377\right)\lambda_0'^3\kappa_0' \\
&\quad + 3\left(897\rho^8 - 7628\rho^6 + 23572\rho^4 - 31028\rho^2 + 16347\right)\lambda_0'^2\kappa_0'^2 \\
&\quad + 2\left(12\rho^8 - 63\rho^6 + 137\rho^4 - 163\rho^2 + 137\right)\lambda_0'''' \\
&\quad - 3\left(367\rho^8 - 2163\rho^6 + 4457\rho^4 - 3983\rho^2 + 1382\right)\lambda_0'\kappa_0'^3\Big\}
\end{aligned}
\tag{A.4}
$$

B. Correlations for Thermal and Electrical Conductivity

To illustrate the application of the perturbation scheme, we employ correlations used by Davis [15] for the temperature dependence of the thermal and electrical conductivity of an aqueous buffer. The correlation for the temperature dependence of the electrical conductivity is

$$\lambda(\Theta) = \exp\left[\frac{M^2}{1+M\Theta}\left(B_1\Theta + B_2\Theta^2\right)\ln 10\right] \tag{B.1a}$$

where

$$B_1 = \left[165.9 + 1.053\times 10^{-3}\left(293 - T_w\right)\left(43 - T_w\right)\right]/T_w, \tag{B.1b}$$

$$B_2 = 1.053\times 10^{-3}\left(T_w - 168\right), \tag{B.1c}$$

$$M = T_w/\left(T_w - 168\right), \tag{B.1d}$$

and thus

$$\lambda_0' = M^2 B_1 \ln 10, \tag{B.1e}$$

$$\lambda_0'' = 2M^2\left(B_2 - MB_1\right)\ln 10 + \left(M^2 B_1 \ln 10\right)^2, \tag{B.1f}$$

$$\lambda_0''' = -6M^3\left(1 - MB_1\ln 10\right)\left(B_2 - MB_1\right)\ln 10 + \left(M^2 B_1 \ln 10\right)^3, \tag{B.1g}$$

$$\lambda_0'''' = 12M^4\left[\left(2 - MB_1\ln 10\right)\left(1 - MB_1\ln 10\right) + B_2\ln 10\right] \times \left(B_2 - MB_1\right)\ln 10 + \left(M^2 B_1\ln 10\right)^4. \tag{B.1h}$$

Davis [15] remarks that (B.1a–d) is accurate to four significant digits.

The temperature dependence of the thermal conductivity was expressed as a quadratic polynomial, using a least-squares fitting of tabulated data [55]. Our coefficients are similar to those used by Davis [15], and are accurate to one part in one thousand. The correlation reads

$$\kappa(\Theta) = 1 + \alpha_1\Theta + \alpha_2\Theta^2, \tag{B.2a}$$

where

$$\alpha_1 = \left(6.229 \times 10^{-3} T_\mathrm{w} - 1.553 \times 10^{-5} {T_\mathrm{w}}^2\right)/\Delta, \tag{B.2b}$$

$$\alpha_2 = -7.765 \times 10^{-6} {T_\mathrm{w}}^2/\Delta, \tag{B.2c}$$

$$\Delta = -0.5612 + 6.229 \times 10^{-3} T_\mathrm{w} - 7.765 \times 10^{-6} {T_\mathrm{w}}^2, \tag{B.2d}$$

and

$$\kappa_0' = \alpha_1, \tag{B.2e}$$

$$\kappa_0'' = 2\alpha_2. \tag{B.2f}$$

We note that Δ is the thermal conductivity at wall temperature T_w.

C. Nomenclature

Drop Electrophoresis — Chapters 2–4

a	radius of spherical drop, m
b	radial value used as far-field boundary, dimensionless
c_∞^k	bulk number density for kth ion species, m^{-3}
$\bar{c}_\infty^k$	initerior bulk number density for kth ion species, m^{-3}
Ca	Capillary number, dimensionless.
e	the elementary charge, 1.602×10^{-19} C
E_∞	Applied electric field, $\mathrm{V\ m}^{-1}$
H	radial derivative of stream function at drop interfacem, dimensionless
h_1, $\bar{h}_1$	radial dependence of stream function, dimensionless
k_B	Boltzmann constant, 1.381×10^{-23} J K^{-1}
K^k	linear adsorption coefficient of the kth ion species, dimensionless
$\mathbf{n}$	unit outward normal to the interface
$n_0^k, \bar{n}_0^k$	equilibrium variation in number density of kth ion species, dimensionless
n_1^k, $\bar{n}_1^k$	perturbation in number density of kth ion species, dimensionless
n_∞^k $\bar{n}_\infty^k$	exterior bulk number density of kth ion species, dimensionless
N	number of ionic species in solution
$p, \bar{p}$	exterior and interior pressure, $\mathrm{N\ m}^{-2}$
p_0, $\bar{p}_0$	exterior and interior pressure variation at equilibrium, dimensionless
p_1, $\bar{p}_1$	exterior and interior perturbation in pressure induced by applied field, dimensionless
Pe	Peclet number
r	radial coordinate, dimensionless

s	strained coordinate, dimensionless
$\mathbf{T}_{\mathrm{M}}, \bar{\mathbf{T}}_{\mathrm{M}}$	Maxwell stress tensors, N m^{-2}
$\mathbf{T}_{\mathrm{N}}, \bar{\mathbf{T}}_{\mathrm{N}}$	stress tensors for a Newtonian fluid, N m^{-2}
T	room temperature, K
$\mathbf{u}$	fluid velocity, m s^{-1}
$\mathbf{u}_{\mathrm{S}}$	fluid velocity, m s^{-1}
U_{e}	electrophoretic velocity in laboratory reference frame, m s^{-1}
$\bar{x}$	scaled radial variable, dimensionless
z^k	valence of kth ion species, dimensionless
$\bar{\alpha}_i$	straining functions, dimensionless
$\bar{\beta}_i$	inverse straining functions, dimensionless
β	applied electric field strength, dimensionless
$\Delta\Psi$	interphase potential difference, dimensionless
γ	interfacial tension, J m^{-2}
γ_0	equilibrium interfacial tension, J m^{-2}
Γ_{G}^k	Gibbs surface excess of kth ion species, dimensionless
Γ_{S}^k	interfacial density of kth ion species, m^{-2}
Γ_0^k	equilibrium interfacial density of kth ion species, dimensionless
Γ_1^k	perturbation in interfacial density of kth ion species induced by applied field, dimensionless
$\epsilon, \bar{\epsilon}$	relative permittivity of exterior and interior phases, dimensionless
ζ, $\bar{\zeta}$	exterior and interior interfacial potentials, V
$\tilde{\zeta}_{\mathrm{E}}$, $\tilde{\zeta}_{\mathrm{I}}$	scaled interfacial potentials for the exterior and interior, dimensionless
κ, $\bar{\kappa}$	exterior and interior Debye screening lengths, m^{-1}
μ	electrochemical potential of kth ion species, J
μ_{e}	electrophoretic mobility, dimensionless
ρ_{e}	charge density, C m^{-3}
Φ_0, $\bar{\Phi}_0$	exterior and interior equilibrium potential, dimensionless

Φ_1, $\bar{\Phi}_1$	perturbation in exterior and interior potentials induced by applied field, dimensionless
Φ_1^k, $\bar{\Phi}_1^k$,	exterior and interior ionic potentials, dimensionless
ϕ_1^k, $\bar{\phi}_1^k$,	radial dependence of ionic potentials, dimensionless
χ	jump in potential at the interface, dimensionless
$\omega^k, \bar{\omega}^k, \omega_S^k$	mobility of kth ion type, dimensionless

Superscripts

k	pertaining to the kth ionic species in solution

Subscripts

0	indicates that the quantity is it's value at equilibrium
1	indicates that the quantity is it's perturbed value from equilibrium
e	stands for 'electric'
E	denotes exterior for interfacial potential
G	stands for Gibbs; pertains to surface excesses of solutes
I	denotes interior for interfacial potential
S	indicates that the value of a variable is that at the drop interface

Electrophoresis Column Temperature Variations — Chapter 5

a^i	molecular radius of the ith ion species in the buffer, m
B_1, B_2	coefficients in the correlation for electrical conductivity
c^i	number density of ith ion species in the buffer, m^{-3}
E	electric field strength, V m^{-1}
e	the elementary charge, 1.602×10^{-19} C
G	heat generation rate, J m^{-3} s^{-1}

k	thermal conductivity, J s^{-1} m^{-1} K^{-1}
L	length of the capillary
M	coefficient in the correlation for electrical conductivity
$\mathbf{n}$	unit outward normal to the capillary wall
R	radius of the capillary inner wall, m
r	radial coordinate, m
S	heat generation rate, dimensionless
T	temperature, K
z^k	valence of ith ion species in the buffer, dimensionless
α_1, α_2	coefficients in the correlation for thermal conductivity
Δ	coefficient in the correlation for thermal conductivity
κ	thermal conductivity of the buffer, dimensionless
λ	electrical conductivity of the buffer, dimensionless
μ	viscosity of the buffer
ρ	radial coordinate, dimensionless
σ	electrical conductivity of the buffer, C V^{-1} s^{-1} m^{-1}
Θ	scaled temperature, dimensionless
ω^i	mobility of the ith ion species in the buffer, m^2 J^{-1} s^{-1}

Superscripts

i	pertaining to the ith ionic species in solution

Subscripts

$\mathrm{C\!L}$	indicates that the value of a variable is that at the centerline of the capillary
ref	indicates that the value of a variable is that of a reference value
W	indicates that the value of a variable is that at the inner capillary wall

D. The Equilibrium Electric Potential and Surface Charge Density of Spherical Emulsion Drops with Thin Double Layers

Statement of Permission

JOURNAL OF COLLOID AND INTERFACE SCIENCE 179, 76–88 (1996)
ARTICLE NO. 0190

The Equilibrium Electric Potential and Surface Charge Density of Spherical Emulsion Drops with Thin Double Layers

J. A. ERKER* AND J. C. BAYGENTS*,†,[1]

*Program in Applied Mathematics and †Department of Chemical and Environmental Engineering, University of Arizona, Tucson, Arizona 85721

Received April 10, 1995; accepted October 25, 1995

Analytic approximations are derived for the solution to the Poisson–Boltzmann equation as applied to a spherical emulsion drop containing a binary electrolyte. Particular attention is given to the drop interior and the formulas that result are easily evaluated. The approximations are obtained by two separate asymptotic methods, which are analogous to those used previously by others to describe the electric potential profile on the exterior of a spherical colloidal particle. The analyses apply to emulsion drops with thin double layers, meaning the drop radius a is large compared to κ^{-1} and $\bar{\kappa}^{-1}$, the respective Debye screening lengths for the exterior and interior of the drop. Using $\delta = (a\bar{\kappa})^{-1}$ as a perturbation parameter, we obtain a matched-asymptotic solution that adds corrections through $O(\delta^3)$ to the flat-plate and Debye–Hückel solutions of the Poisson–Boltzmann equation. In the process, we recover expressions for the drop *exterior* that constitute an $O(\delta)$ improvement over the previously published results. Through a nonlinear transformation of the independent variable, we also derive a uniformly valid approximation that iteratively adds a correction to the flat-plate problem. Each technique yields accurate solutions. For example, the maximum relative error over the drop interior is on the order of 1% for $a\kappa$ as low as 5 with surface potentials as high as 250 mV. Accuracy improves for larger values of $a\bar{\kappa}$, with a maximum relative error below 0.1% for $a\bar{\kappa} > 15$. The asymptotic techniques are also used to obtain expressions for the surface charge density, with equally satisfactory results.

Key Words: **electrical double layer; Poisson–Boltzmann equation; aqueous two-phase systems; colloidal dispersions; perturbation methods.**

INTRODUCTION

Electrostatic interactions significantly influence the behavior of an emulsion. As with rigid particles in suspension, the surface charge density and the electric potential distribution on the exterior of the emulsified body affect the stability of the dispersion (1), as well as rate processes such as the scavenging of fine particles and contaminants by rising bubbles in froth flotation (2–4).

While the interior electrostatics of particles are typically of little effect, the interior electrostatics of emulsion drops do not, in general, play a subordinate role. For example, in aqueous two-phase partitioning (5), the distribution of proteins and other solutes depends on the electrostatics of both the dispersed and the continuous phases.

Similarly, the electrokinetic response of emulsion drops to externally applied electric fields depends on the electric potential distribution of their interior (6–8). An interesting demonstration of this has been reported by Brooks *et al.* (9), who found that, for aqueous two-phase dispersions formed from dextran and polyethylene glycol, the direction of drop electrophoresis could not be inferred directly from the electrostatic potential difference between the phases that are separated by the drop surface. To explain their results, Brooks *et al.* (9) postulated the existence of electric dipoles adsorbed to the drop surface, which cause an apparent discontinuity in the electric potential at the interface.

Technical interest in the imposition of electric fields on emulsion drops involves such applications as the use of the drop response to characterize the surface charge density by electrophoretic measurements (10); to electrokinetically demix, or break, emulsions due to relative motion between neighboring drops (11–14); and to enhance heat and mass transfer throughout space-filling dispersions by driving circulations in and about the individual drops (15).

While numerical descriptions of the electrokinetic behavior of drops are available (8, 16), analytic theories are not nearly as prevalent as they are for the well-studied case of colloidal particles. Booth (6) provides an analysis along the lines of that originally done by Henry for rigid bodies (17), examining drop electrophoresis in the absence of relaxation effects or charge rearrangement on the drop surface. The Booth theory applies to drops with uniformly distributed interior charge, as well as to drops with a conventional Gouy–Chapman diffuse layer on their interior. Nevertheless, in cases where the ζ-potential of the drop is not in some sense small, the Booth analysis does not strictly apply.

We have set out here to lay the groundwork for an analytic theory of electrokinetic effects with emulsion drops, which will apply when polarization and relaxation effects are im-

[1] To whom correspondence should be addressed.

0021-9797/96 $18.00

portant and which will account for the ionic transport processes that can obtain on the drop interior. Accordingly, the focus of this work is to develop analytic descriptions of the electrical double layer on the *inside* of a sphere whose surface is at a prescribed potential ζ. Working from this representation of the double layer structure, one can, in principle, go on to develop descriptions of the electrokinetics, as Ohshima *et al.* (18) have done for charged mercury drops in electrolyte solutions.

Considering that the interface of an emulsion drop is molecularly thin, we will in our treatment of the electrostatics problem assume that the interface has negligible thickness compared to the Debye screening length. We can then treat the electrostatics of the interior separate from that of the well-studied exterior. Additionally, this allows us to specify different surface (or zeta) potentials for the interior and exterior sides of the interface and thereby accommodate the possibility of surface dipoles, as suggested by Brooks *et al.* (9). It should be noted, though, that the thickness of the interface in aqueous two-phase dispersions is on the order of the polymer size and, thus, may be comparable to, or even exceed, the Debye length. To account for the effects of interfacial thickness on the structure of the equilibrium double layer, one would presumably need to prescribe additional constraints on the variation of the electric potential across the phase boundary, which, as noted, we will not do.

In this paper, we examine the electrostatics of an emulsion drop in a system for which the immiscible phases are z–z electrolytes that are neutral in the bulk. Accordingly, diffuse layers of charge exist on both sides of the interface, though the ionic strength of the interior will not generally be the same as that of the exterior. In particular, we analyze the case wherein the diffuse layers are thin compared to the drop radius a. Thus, to leading order, the problem reduces to finding the potential that sandwiches a flat plate of charge.

Corrections to the flat-plate solution are obtained by perturbation methods, where use is made of a small parameter $\delta \equiv 1/(a\kappa)$, the ratio of the Debye screening length κ^{-1} to the drop radius a. Here, κ refers to the Debye–Hückel parameter for the drop *interior*. Analytic expressions for the electrostatic potential in the drop exterior have been derived by Ohshima *et al.* (19) and Natarajan and Schechter (20), among others. Owing to the surface tension, the problem for the exterior is the same as that for a charged, rigidly spherical colloidal particle, to which their analyses pertained. The bulk of this paper applies their respective techniques to the complementary problem for the interior.

Neither technique proves to be as robust as when applied to the case of the unbounded exterior region. Insofar as the drop interior is a bounded domain, a value of $\delta \geq 1/3$ precludes the existence of a region wherein the electrostatic potential has decayed so much as to warrant the classical Debye–Hückel linearization. Such a region exists in the exterior, irrespective of whether δ is small. Consequently, accuracy of the asymptotic solutions for the interior begins to erode for $\delta \geq 1/3$.

To begin, we use the method of Natarajan and Schechter (NS) to construct a strained coordinate expansion around the Gouy–Chapman solution for a flat plate of charge. We find that the NS method gives a solution that is remarkably accurate within a Debye length or two of the surface, and as might be expected, the solution exhibits some degree of symmetry (or antisymmetry) of algebraic form with respect to the corrections to the flat-plate solution for the exterior problem. The strained coordinate solution is accurate to $O(\delta^3)$, which represents an $O(\delta)$ improvement on the NS work (20).

We then resolve the problem by the method of Ohshima, Healy, and White (OHW). This involves a change of variables that removes the singular nature of the perturbation, followed by an iteration procedure which provides a correction to the flat-plate approximation. The OHW method turns out to be slightly better suited for the exterior problem than for the interior, due to the nature of the boundary conditions distal to the interface. Nonetheless, for thin double layers, results for the interior problem are still quite good, and the relative error is less than 0.5% for values of $\delta < 0.1$. A virtue of the OHW technique is that the resulting expression is uniformly valid, whereas the NS approach yields one expression that is appropriate within several Debye layers of the drop surface, and another that is tailored to the balance of the drop interior.

Following the derivation of electrostatic potential expressions and a discussion of their accuracy, we convert the solutions for the electrostatic potential from the strained coordinate approach into expressions for the surface charge density, using the relationship between the charge density and the potential gradients. The expression generated by the iteration procedure can also be applied to obtain an expression for the surface charge density, but in this case, a more straightforward iteration procedure—one which does not employ the aforementioned change of variables—yields better results. Following a discussion of the accuracy of the results for surface charge density, the paper concludes with a few summary remarks.

THE SPHERICAL POISSON–BOLTZMANN EQUATION ON THE INTERIOR OF A SPHERE

Picture a charged spherical emulsion drop which contains a z–z electrolyte, and which has a uniform charge distribution on its surface. Suppose, with no loss in generality, that the excess charge on the surface is positive. At equilibrium, this surface charge creates an excess of negative ions and a shortage of positive ions local to the surface, with their respective number densities decaying and growing radially toward the drop center. The electrostatic potential ψ will accordingly tend toward the interphase potential difference

$\Delta\psi$, in a manner obeying the spherical Poisson–Boltzmann equation, viz.

$$\nabla_r^2\psi = -\frac{1}{\epsilon\epsilon_0}\left\{ze n_\infty^+ \exp\left[-\frac{ze}{k_BT}(\psi - \Delta\psi)\right] - ze n_\infty^- \exp\left[\frac{ze}{k_BT}(\psi - \Delta\psi)\right]\right\}. \quad [1]$$

The symbol ∇_r^2 denotes the spherically symmetric Laplacian operator, ϵ is the relative electric permittivity of the electrolyte, ϵ_0 is the permittivity of free space, e is the charge of a proton, k_BT is the Boltzmann temperature, and n_∞^+ and n_∞^- are the number densities of the positive and negative ions, respectively, when $\psi = \Delta\psi$. Consequently, $n_\infty^+ = n_\infty^- = n_\infty$. Equation [1] thus simplifies to

$$\partial_r^2\psi + \frac{2}{r}\partial_r\psi = \frac{2zen_\infty}{\epsilon\epsilon_0}\sinh\left[\frac{ze}{k_BT}(\psi - \Delta\psi)\right]. \quad [2]$$

The boundary condition for the drop surface is that $\psi(a)$ is the zeta potential, ζ. By spherical symmetry, $\partial_r\psi = 0$ at the center of the drop, where $r = 0$.

To put the equation is dimensionless form, we write

$$\phi = \frac{ze}{k_BT}(\psi - \Delta\psi), \quad \tilde{r} = \frac{r}{a}. \quad [3]$$

We then have

$$\partial_{\tilde{r}}^2\phi + \frac{2}{\tilde{r}}\partial_{\tilde{r}}\phi = A^2\sinh\phi, \quad [4]$$

where $A = a\kappa$ and $\kappa^{-1} = (2z^2e^2n_\infty/\epsilon\epsilon_0k_BT)^{-1/2}$ is the well-known Debye length. Then $1/A = \delta$ is the dimensionless Debye length scaled on the particle radius a. The boundary conditions now read

$$\phi(1) = \tilde{\zeta} = \frac{ze}{k_BT}(\zeta - \Delta\psi), \quad \partial_{\tilde{r}}\phi(0) = 0. \quad [5]$$

This form of the boundary value problem, Eqs. [4] and [5], will be referred to frequently, although the tilde on r will be suppressed with the understanding that the radial coordinate is henceforth dimensionless.

SINGULAR BEHAVIOR FOR THIN DOUBLE LAYERS

For large values of $a\kappa$, Eq. [4] is tractable to boundary-layer techniques. One can see this by noticing that near the drop surface, the particle radius is not in fact the length scale on which $O(\phi)$ variations in ϕ occur. If we consider the limit of large A in Eq. [4], we see that the trivial solution for ϕ, i.e., $\phi \equiv 0$, satisfies the boundary condition at the drop center and is not a bad approximation to the actual solution outside of the first several Debye lengths from the surface (for a thin double layer, i.e., large A, the potential is very small throughout most of the drop). Unfortunately, the trivial solution does not satisfy the boundary condition on the drop surface. Moreover, any correction terms, derived in a regular perturbation scheme that satisfies the surface boundary value, cannot make the improved solution converge uniformly to the leading order solution $\phi \equiv 0$ in the limit of large A. This singular behavior suggests that, to construct a solution for ϕ near the drop surface, one must choose a length scale other than a to characterize variations in ϕ within a layer near the surface boundary. Due to the ions' interactions with the surface charge, the radial derivative of the electrostatic potential is much larger within one Debye length κ^{-1} of the drop surface than in the remainder of the drop interior. Accordingly, the appropriate length scale for this boundary layer is the Debye screening length, as is well known. Indeed, if we scale the distance from the drop surface on κ^{-1}, the term containing the highest derivative on the left-hand side of Eq. [4] will balance with the right-hand side. Thus, a perturbation solution of the rescaled equation will be valid throughout the boundary layer, and perhaps within several Debye lengths of the drop surface.

The method of matched asymptotics was employed by NS to solve Eq. [4] for the exterior of a colloidal sphere; the specific method used was that of strained coordinates. In an alternative treatment of the exterior problem, it was shown by OHW that a judicious change of variables in Eq. [4] can facilitate an asymptotic expansion which is uniformly valid over the entire radial domain. Their (nonlinear) change of variables provided for the appropriate rescaling of radial distance local to the drop surface without significantly altering the balance of the equation far from the surface. Here, after first developing a strained coordinate solution to Eq. [4], we will rework the problem using the strategy of OHW, though we will invoke a change of variables that is more appropriate for the drop interior.

MATCHED ASYMPTOTICS

As mentioned, the electrostatic potential decays rapidly within one Debye length of the drop surface. The electrostatic potential in the region $|r - 1| \gg \delta$ is therefore small enough that $\sinh\phi \approx \phi$. Thus, to get a solution valid in this "outer" region, we use the following approximation to Eq. [4]:

$$\partial_r^2\phi_{out} + \frac{2}{r}\partial_r\phi_{out} - \frac{1}{\delta^2}\phi_{out} = 0, \quad \partial_r\phi(0) = 0. \quad [6]$$

Equation [6] is a spherical Bessel equation, whose solution is readily available (21), viz.

$$\phi_{out} = C\frac{\sinh(r/\delta)}{r}. \quad [7]$$

The coefficient C is not yet determined, since we cannot apply the boundary condition for $r = 1$ to the outer solution. Instead, C must be established by asymptotically matching ϕ_{out} with a solution ϕ_{in}, which is valid within the boundary layer $|r - 1| = O(\delta)$.

Inner Solution

To find a boundary layer, or inner solution, we must first suitably rescale the spatial variable. This will be done by considering the distance away from the drop surface and scaling it on δ, i.e.,

$$x = \frac{1 - r}{\delta}. \quad [8]$$

This change of variables is suggested by the fact that, in the double layer, κ^{-1} is the suitable reference length as opposed to the drop radius a and is equivalent to rescaling the distance from the drop surface on κ^{-1} in the original (dimensional) coordinate.

Thus $r = 1 - \delta x$ and $\partial_r\phi = -\delta^{-1}\partial_x\phi$. Substituting these into [4], we get

$$\partial_x^2\phi_{in} - \frac{2\delta}{1 - \delta x}\partial_x\phi_{in} = \sinh\phi_{in}, \quad \phi_{in}(0) = \tilde{\zeta}. \quad [9]$$

After van Dyke (22) and NS, we seek an inner, or boundary layer, solution ϕ_{in} by expanding the dependent variable ϕ_{in} and independent variable x in powers of δ, i.e.,

$$\phi_{in} = \phi_0 + \delta\phi_1 + \delta^2\phi_2 + \delta^3\phi_3 + \cdots, \quad [10]$$

$$x = s + \delta\alpha_1(s) + \delta^2\alpha_2(s) + \delta^3\alpha_3(s) + \cdots, \quad [11]$$

and then substitute into [9]. The condition that $\alpha_i(0) = 0$ for each i will be imposed, so that s will vanish with x; i.e., there is no straining of the coordinate on the drop surface. Upon substituting Eqs. [10] and [11] into Eq. [9], a hierarchy of differential equations based on orders of δ results. As done by NS for the drop exterior, we choose the α_i's such that $\phi_i = 0$ for $i \geq 1$. This will allow corrections to the flat-plate solution ($\delta \equiv 0$) to be obtained from Eq. [12] (see below), according to the expansion of the new independent variable s in terms of x (compare Eqs. [11] and [25]).

The first, or leading order, equation in the hierarchy of differential equations is the flat-plate problem, but with s as the independent variable. Its solution is therefore

$$\phi = 4\tanh^{-1}(pe^{-s}), \quad p = \tanh(\tilde{\zeta}/4), \quad [12]$$

and it will be the expansion of s in terms of x that will provide the corrections to the flat-plate solution [12]. The remaining differential equations turn out to be of the form

$$\alpha_i''(s) - 2q(s)\alpha_i'(s) = r_i(s), \quad i = 1, 2, 3, \ldots, \quad [13]$$

where

$$q(s) = \frac{1 + p^2e^{-2s}}{1 - p^2e^{-2s}}, \quad [14]$$

and the right-hand side functions r_i include solutions of the previous equations in the hierarchy, viz.

$$r_1(s) = -2, \quad [15]$$

$$r_2(s) = \tfrac{3}{2}\alpha_1'\alpha_1'' - \alpha_1' - 2s, \quad [16]$$

and

$$r_3(s) = \alpha_1'^2(\tfrac{1}{2}\alpha_1'' - 1) - 2\alpha_1 - 4\alpha_1's - 2s^2 + \alpha_2'(3\alpha_1'' + 2). \quad [17]$$

Integration of Eq. [13] is straightforward, and the constants of integration all turn out to be zero. This is due to the requirement that $\alpha_i(0) = 0$ for each i and the need to discard exponentially growing terms, as these terms would render ϕ_{in} incompatible with the outer solution [7]. For $i = 2$, the right-hand sides turn out to be the same as for the exterior problem (20), and for $i = 1$ and 3, the right-hand sides are the negatives of those for the exterior problem. In the case of the flat-plate problem, the solutions for the interior and exterior are of identical form, as there is no definition of interior or exterior for a flat plate of charge. For $i = 1$, which provides the first-order correction due to the curvature of the surface, the opposite signs indicate that in the exterior, the decay of electrostatic potential radially away from the drop surface is faster than for a flat plate of charge, while in the interior, the decay is slower to leading order.

Carrying out the solution as described above, we find that

$$\alpha_1(s) = s - \frac{p^2}{2}(1 - e^{-2s}), \quad [18]$$

$$\alpha_2(s) = \frac{s^2}{2} + s - 2p^2(1 - e^{-2s}) + \frac{3p^4}{8}(1 - e^{-4s}) + \frac{p^2}{2}se^{-2s} - \frac{1}{2}I_2(s) - (1 - p^4)\frac{\ln(1 - p^2)}{4p^2} + \frac{e^{2s}}{4p^2}h(s) - \frac{p^2e^{-2s}}{4}h(s), \quad [19]$$

where

$$h(s) = \ln(1 - p^2e^{-2s}) \quad \text{and}$$

$$I_2(s) = \int_{p^2e^{-2s}}^{p^2} \frac{\ln(1-t)}{t}\,dt, \quad [20]$$

and

$$\alpha_3(s) = \frac{s^3}{3} + \frac{s^2}{2}[3 + p^2e^{-2s}] + s\left[-\frac{3}{4}p^4e^{-4s} + \frac{3}{2} - \frac{p^2}{2} + \frac{9}{2}p^2e^{-2s} - \frac{1}{2}p^2e^{-2s}h(s) + \frac{1}{2}\frac{e^{2s}}{p^2}h(s)\right] - \frac{63}{8}p^2(1 - e^{-2s}) + \frac{13}{8}[h(s) - h(0)] + \frac{3}{8}p^4[h(s)e^{-4s} - h(0)] + \frac{19}{8}p^4 - \frac{1}{4}p^4e^{-2s} + \frac{1}{2p^2}[h(s)e^{2s} - h(0)] - \frac{5}{2}p^2[h(s)e^{-2s} - h(0)] - \frac{5}{12}p^6[1 - e^{-6s}] - \frac{17}{8}p^4e^{-4s} - \left(\frac{9}{4} + \ln p\right)I_2(s) + \frac{1}{2}I_3(s), \quad [21]$$

where

$$I_3(s) = \int_{p^2e^{-2s}}^{p^2} \frac{\ln t \ln(1-t)}{t}\,dt. \quad [22]$$

To our knowledge, the function $\alpha_3(s)$ has not been previously derived.

Through change of variables and integration by parts, $I_2(s)$ and $I_3(s)$ can be rewritten as

$$I_2(s) = -4\int_0^s \frac{t}{1 - p^2e^{-2t}}\,dt + 2s^2 + 2h(s) \quad [23]$$

and

$$I_3(s) = 4\int_0^s \frac{t^2}{1 - p^2e^{-2t}}\,dt - \frac{4}{3}s^2 - 2s^2\ln(1 - p^2e^{-2s}) + 2\ln pI_2(s). \quad [24]$$

The integrals in Eqs. [23] and [24] are Debye functions, which are tabulated in (21). In addition, $I_2(s)$ and $I_3(s)$ can be easily calculated numerically.

To obtain corrections to Eq. [12], we express s as an expansion in terms of x

$$s = x + \delta\beta_1(x) + \delta^2\beta_2(x) + \delta^3\beta_3(x) + \cdots, \quad [25]$$

by inverting Eq. [11], which yields

$$\beta_1(x) = -\alpha_1(x), \quad [26]$$

$$\beta_2(x) = -\alpha_1'(x)\beta_1(x) - \alpha_2(x), \quad [27]$$

and

$$\beta_3(x) = -\alpha_1'(x)\beta_2(x) - \alpha_2'(x)\beta_1(x) - \tfrac{1}{2}\alpha_1''(x)\beta_1^2(x) - \alpha_3(x). \quad [28]$$

Note that $\beta_1(x)$ and $\beta_3(x)$ are simply the negatives of the corresponding functions in the NS solution to the exterior problem, and $\beta_2(x)$ is equivalent to its exterior counterpart.

We now have three terms of [25] to substitute into [12], resulting in the boundary-layer solution

$$\phi_{in} = 4\tanh^{-1}(p\exp\{-[x + \delta\beta_1(x) + \delta^2\beta_2(x) + \delta^3\beta_3(x) + O(\delta^4)]\}). \quad [29]$$

One can see from Eqs. [19], [21], [27], and [28] that *explicit* representations of β_2 and β_3 are extraordinarily complicated. It is considerably simpler in practice to calculate these functions as they are given in Eqs. [27] and [28]; β_3, like α_3, has not been previously reported in the literature.

Matching the Inner and Outer Solutions

The inner solution ϕ_{in} can now be used to determine the coefficient that appears in Eq. [7]. We do this by matching asymptotically the behavior of the outer solution as r approaches unity with the behavior of the inner solution for large x. So that we can match in the same coordinates, we will first rewrite Eq. [7] in the inner variable, according to Eq. [8], i.e.,

$$\phi_{out} = C\frac{\sinh(\delta^{-1} - x)}{1 - \delta x}. \quad [30]$$

Using an identity for hyperbolic functions, Eq. [30] can be expressed as

$$\phi_{out} = \frac{C}{1 - \delta x}\sinh\left(\frac{1}{\delta}\right)[e^{-x} + O(\delta)]. \quad [31]$$

Noting that $\delta x = 1$ at precisely one Debye length from the

surface, we see from Eq. [31] that as we approach the boundary layer from within the drop,

$$\phi_{out} \sim C \sinh\left(\frac{1}{\delta}\right) e^{-x}[1 + \delta x + \delta^2 x^2 + \delta^3 x^3 + O(\delta^4)]. \quad [32]$$

Equation [32] will be matched to the asymptotic behavior of ϕ_{in} for large x.

To determine the behavior of ϕ_{in}, we first notice that for large x, $\tanh^{-1}(pe^{-s(x)}) \approx pe^{-s(x)}$, and then make use of the respective asymptotic forms of the β_i's, e.g.,

$$\beta_3 \sim -\frac{x^3}{3} + \gamma_3, \quad x \to \infty, \quad [33]$$

where

$$\gamma_3 = \frac{1}{4} + \frac{47}{8}p^2 - 2p^4 + \frac{5}{12}p^6 + (2 + 13p^2 - 18p^4 + 3p^6)\frac{\ln(1-p^2)}{8p^2} + \left(\frac{7}{4} + \ln p\right)I_2(\infty) - \frac{1}{2}I_3(\infty). \quad [34]$$

This gives

$$\phi_{in} \sim 4p \exp\left[-\frac{\delta p^2}{2} - \delta^2\gamma_2 - \delta^3\gamma_3\right] e^{-x}[1 + \delta x + \delta^2 x^2 + \delta^3 x^3 + O(\delta^4)], \quad [35]$$

where

$$\gamma_2 = \frac{1}{4}\left[1 + 6p^2 - \frac{3}{2}p^4 + \frac{(1-p^4)}{p^2}\ln(1-p^2) + 2I_2(\infty)\right]. \quad [36]$$

The integrals in γ_2 and γ_3 can be evaluated numerically or recast as zeta functions, by using Eqs. [23] and [24] and the relationship

$$\int_0^\infty \frac{t^n}{e^t - 1}\,dt = n!\zeta(n+1). \quad [37]$$

The zeta function can be found in standard mathematical tables. It is also noted that $I_3(\infty)$ contains an integrable singularity which can be avoided through integration by parts. This would be helpful to numerical integration.

By matching [32] and [35], we see that the coefficient C for the outer solution is

$$C = \frac{4p}{\sinh(1/\delta)}\left[1 - \delta\frac{p^2}{2} + \delta^2\left(\frac{p^4}{8} - \gamma_2\right) - \delta^3\left(\frac{p^6}{48} - \frac{p^2}{2}\gamma_2 + \gamma_3\right) + O(\delta^4)\right], \quad [38]$$

where the exponential part of this coefficient has been expanded as a power series in δ.

The product of $4p$ and the bracketed terms in Eq. [38] form a power series estimate of what Loeb *et al.* (23) call the *reduced surface potential,* viz.

$$\bar{Y} = 4p\left[1 - \delta\frac{p^2}{2} + \delta^2\left(\frac{p^4}{8} - \gamma_2\right) - \delta^3\left(\frac{p^6}{48} - \frac{p^2}{2}\gamma_2 + \gamma_3\right) + O(\delta^4)\right],$$

$$\text{with } p = \tanh\left[\frac{ze}{4k_BT}(\bar{\zeta} - \Delta\psi)\right]. \quad [39]$$

We thus have as our desired representation of the outer solution

$$\phi_{out} = \frac{\bar{Y}}{\sinh(1/\delta)}\frac{\sinh(r/\delta)}{r}, \quad [40]$$

where $\bar{Y}$ is accurate through $O(\delta^3)$; the analogous expression for the drop exterior is

$$\phi_{out} = Y\frac{e^{-a\kappa(r-1)}}{r}, \quad [41]$$

where

$$Y = 4p\left[1 + \delta\frac{p^2}{2} + \delta^2\left(\frac{p^4}{8} - \gamma_2\right) + \delta^3\left(\frac{p^6}{48} - \frac{p^2}{2}\gamma_2 + \gamma_3\right) + O(\delta^4)\right],$$

$$\text{with } p = \tanh\left(\frac{ze}{4k_BT}\zeta\right), \quad [42]$$

which NS obtained through $O(\delta^2)$. Here, $\bar{\zeta}$ and ζ denote the zeta potential of the surface as viewed from the drop interior and exterior, respectively.

ITERATION PROCEDURE: NONLINEAR RESCALING

Now we will implement another method for improving the flat-plate approximation to the solution of the Poisson–Boltzmann equation, namely an iteration technique. Such a method was employed successfully by OHW to derive an expression for the equilibrium potential exterior to the drop. Following OHW, we will rescale the independent variable in Eq. [4] according to

$$R = Ar. \qquad [43]$$

This is equivalent to scaling the original dimensional radial coordinate on the Debye screening length κ^{-1}. The boundary value problem then reads

$$\partial_R^2\phi + \frac{2}{R}\partial_R\phi = \sinh\phi, \qquad [44]$$

$$\phi = \zeta \text{ at } R = A, \quad \partial_R\phi = 0 \text{ at } R = 0. \qquad [45]$$

Rewriting the outer solution [40] according to Eq. [43], we see that the solution in the region far from the particle surface behaves as

$$c\frac{A}{R}\frac{\sinh R}{\sinh A}, \qquad [46]$$

where c is the reduced surface potential and is order one. Thus, if we evaluate [46] at the drop surface ($R = A$), we should expect a value of order one.

Consider the change of independent variable

$$s = \frac{A}{R}\frac{\sinh R}{\sinh A}, \qquad [47]$$

where s is not to be confused with that in the previous section. Note that $\partial_R s \approx 1$ near the drop surface, i.e., for $R \approx A$. The rescaling in Eq. [43] is thus unaffected near the surface when we cast the system in the new variable s. This is desirable, since the rescaling reflects the fact that the Debye length is the characteristic length scale local to the surface. What the change of variable in Eq. [47] will do is allow us to rewrite Eq. [44] in a fashion suitable to a perturbation technique while preserving the balance of terms throughout the entire radial domain.

Substituting Eq. [47] into Eq. [44] yields upon rearrangement

$$s^2\partial_s^2\phi + s\partial_s\phi = \sinh\phi + \frac{2A-1}{(A-1)^2}F(R)(\sinh\phi - s\partial_s\phi), \qquad [48]$$

where

$$F(R) = \left(\frac{A-1}{R\coth R - 1}\right)^2\left(\frac{R^2 - (R\coth R - 1)^2}{2A-1}\right), \qquad [49]$$

with the boundary conditions

$$\phi = \zeta \text{ at } s = 1, \quad s\partial_s\phi = c\frac{A}{\sinh A} \text{ at } s = \frac{A}{\sinh A}. \qquad [50]$$

The constant c, which appears in Eq. [46] and the boundary condition at the drop center, is unknown, but based on our analysis to this point, it is $O(1)$. Prescribing $s\partial_s\phi$ at the drop center would require knowledge of both ϕ and its radial derivative there. In the exterior problem, the boundary analogous to the drop center is an infinite radial distance from the drop. For that problem, we have knowledge of both ϕ and its first derivative in the "far field." In particular, we know that they both tend to zero as $r \to \infty$, thereby making $s\partial_s\phi = 0$ the far-field boundary condition. For Eq. [48], we do not know the value of ϕ at the drop center, but we will use the fact that $s\partial_s\phi$ is very small there for large A.

Since $F(R)$ is $O(1)$ for $R \approx A$, i.e., in the region near the particle surface, the iteration procedure is to replace the right-hand side of Eq. [48] with its limit for $A \to \infty$, which involves ϕ_0, the flat-plate approximation of the solution. Because

$$s\partial_s\phi_0 = 2\sinh(\phi_0/2) \approx 2\sinh(\phi/2), \qquad [51]$$

Eq. [48] becomes

$$s^2\partial_s^2\phi + s\partial_s\phi = \sinh\phi + \frac{2A-1}{(A-1)^2}[\sinh\phi - 2\sinh(\phi/2)], \quad A \gg 1, \qquad [52]$$

which can be solved to obtain a correction to the flat-plate solution. Integrating Eq. [52] once gives

$$(s\partial_s\phi)^2 - (s\partial_s\phi)^2|_{\text{center}} = \frac{4A^2}{(A-1)^2}[f(\phi) - f(\phi_c)], \qquad [53]$$

where

$$f(\phi) = \sinh^2(\phi/2)\left[1 - \left(\frac{2A-1}{A^2}\right)\frac{1}{\cosh^2(\phi/4)}\right], \qquad [54]$$

and ϕ_c is the electrostatic potential at the drop center. While Eq. [53] is separable, an exact solution becomes all but unmanageable, due to the presence of the constant $f(\phi_c)$.[2]

At this stage, it is important to remember that the analysis done here is for the case of a thin double layer, and so the potential far from the surface is very small, even if nonzero. Using the second boundary condition in Eq. [50], and taking the leading-order approximations of the sinh and cosh functions in $f(\phi_c)$ (cf. Eq. [54]), causes the expression

$$(s\partial_s\phi)^2|_{\text{center}} - \frac{4A^2}{(A-1)^2} f(\phi_c) \qquad [55]$$

to vanish. Equation [53] thus can be integrated to obtain

$$\phi_{\text{nlr}} = 2 \ln\left[\frac{(1 + c_1 s)(1 + c_2 s)}{(1 - c_1 s)(1 - c_2 s)}\right], \qquad [56]$$

where

$$c_1 = \tanh(\tilde{\zeta}/4)\left(1 + \frac{A}{A-1}\right) \times \left[1 + \sqrt{1 + \frac{2A-1}{(A-1)^2}\tanh^2(\tilde{\zeta}/4)}\right]^{-1}, \qquad [57]$$

$$c_2 = -c_1/(2A-1), \qquad [58]$$

and the subscript nlr indicates that this solution results from the nonlinear rescaling. Equation [56] closely resembles the formula for the electrostatic potential obtained by OHW for the exterior of the drop.

ACCURACY OF SOLUTIONS

The formulas derived in the previous sections, namely Eqs. [29], [40], and [56], have been tested against numerical solutions of the Poisson–Boltzmann equation. The numerical solutions were obtained by using a shooting algorithm in conjunction with a standard fourth-/fifth-order Runge–Kutta integration package. Figure 1 shows a representative graph of the percentage of relative error of these three solutions as a function of dimensionless particle radius, for $a\kappa = 10$ and $\tilde{\zeta} = 5$. The percentage of relative error is given by the familiar formula

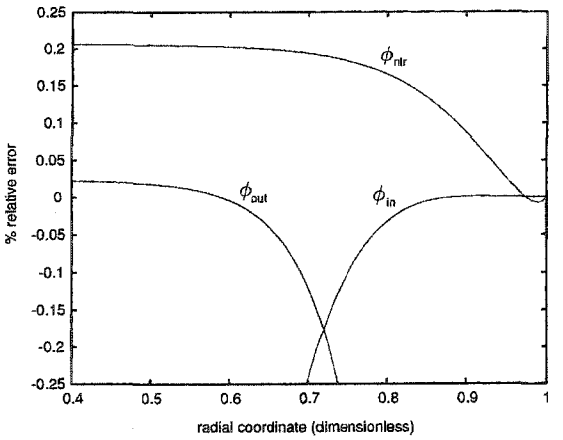

FIG. 1. Percentage of relative error of asymptotic solutions to the spherical Poisson–Boltzmann equation (Eq. [4]), which appear as Eqs. [29], [40], and [56], as functions of dimensionless radial distance r/a from the drop center, for $a\kappa = 10$ and $\tilde{\zeta} = 5$. The region from 0.9 to 1.0 in the radial coordinate represents the first Debye layer.

$$100 \times \left(\frac{\phi_{\text{num}} - \phi_{\text{approx}}}{\phi_{\text{num}}}\right), \qquad [59]$$

where ϕ_{num} is the numerical solution and ϕ_{approx} is the analytic solution being tested.

We can see in Fig. 1 that ϕ_{in} is optimally accurate within one Debye length of the drop surface ($0.9 \leq r \leq 1$), with a percentage of relative error of order 10^{-4} or lower throughout this boundary layer. Going radially inward, the accuracy begins to drop off considerably two Debye lengths from the surface. The third-order solution [29] agrees with the exact solution to one more decimal place than does the corresponding solution with two correction terms, maintaining 0.02% accuracy within two Debye lengths of the surface in this example. That $a\kappa$ is large ensures the accuracy of ϕ_{out} too, since for such values the potential will decay significantly within the drop. This justifies the approximation $\sinh\phi \approx \phi$ used in Eq. [6] and allows $\bar{Y}$ to be written as an expansion in δ. It is at roughly two Debye lengths that the outer solution begins to reach its optimal accuracy as one traverses radially inward.

A crude way of obtaining a uniformly valid solution from the inner and outer solutions would be to "change where the two curves cross" (22) if one looked at the corresponding graph of the absolute value of the relative error (or in case the two curves do not intersect, the point of minimal difference between the two). In Fig. 1, the intersection point occurs close to three Debye lengths from the surface. In the absence of a numerical solution, one could identify this point as that at which the graphs of ϕ_{in} and ϕ_{out} intersect.

In Fig. 2a, we have plotted the crossing point of the inner

[2] This case deviates from that of OHW, for the far-field boundary value of ϕ in the exterior problem is zero, and so in their treatment, the expression analogous to $f(\phi_c)$ is zero.

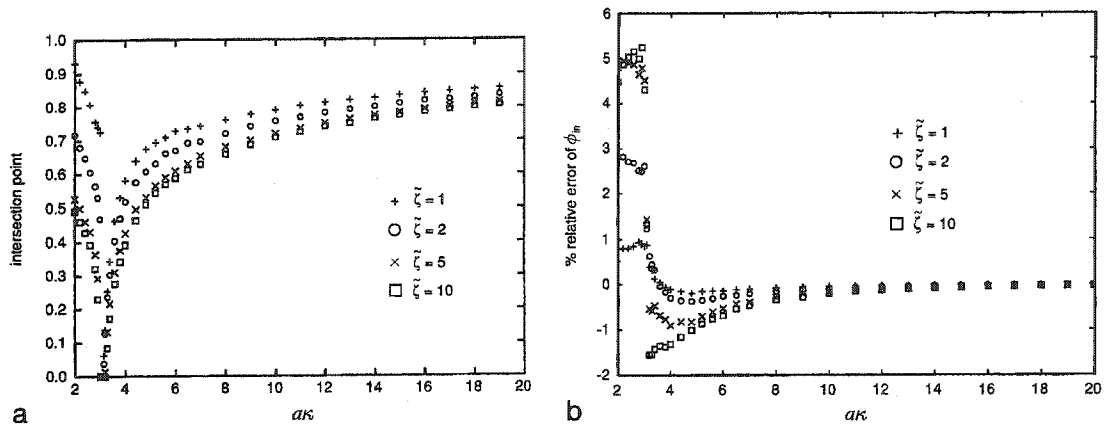

FIG. 2. (a) Radial coordinate at which the percentage of relative error for ϕ_{in} and ϕ_{out} are equal, expressed as a function of $a\kappa$ for several zeta potentials, $\tilde{\zeta}$. (b) Percentage of relative error at the intersection of the error curves.

and outer solutions as a function of $a\kappa$, for various potentials $\tilde{\zeta}$. Note that this point in most cases is two to four Debye lengths from the surface. We can infer from this that for values of $a\kappa \lesssim 3$, there is no matching region. Mathematically this implies that the method, and hence the solution, breaks down for these values, as the method depends on asymptotic matching. This is evident in Figs. 2 and 3.

Figure 2b gives the error of ϕ_{in} at the point where ϕ_{in} and ϕ_{out} differ least. When the solutions do cross, as is usually the case (cf. Fig. 2a), this error is the maximum error of the composite solution obtained by taking the inner solution for r greater than the crossing point and the outer solution for r less than this value. Neither function in Figs. 2a and 2b seems to vary smoothly with $a\kappa$, so we have plotted values at discrete points to give a sense of the behavior.

Figure 3 shows the relative percentage of error of ϕ_{out} at the drop center as a function of $a\kappa$. As shown in Fig. 1, the accuracy at the center persists throughout most of the drop for large values of $a\kappa$. One can see from Fig. 3 that the error is large for $a\kappa \lesssim 3$, since there is no region in which the Debye–Hückel linearization holds. When $a\kappa = 3$, the center of the drop is but three Debye lengths from the surface and the potential has not decayed to a value small enough to permit the linearization.

In Fig. 4, the maximum percentage of relative error of ϕ_{in} over the first Debye layer ($1 - \delta < r < 1$) is plotted against $a\kappa$ for several values of $\tilde{\zeta}$. Note the (expected) trend toward higher accuracy with increasing $a\kappa$. The solutions are least

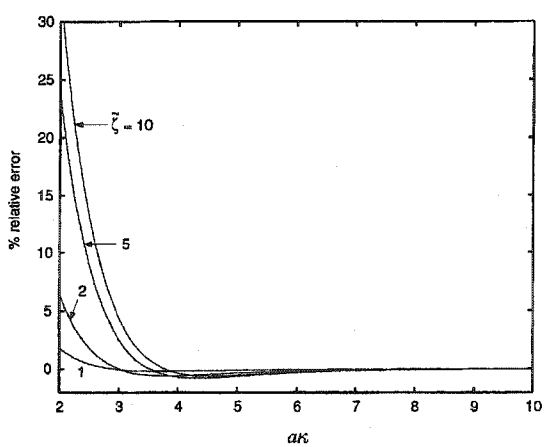

FIG. 3. Percentage of relative error of ϕ_{out} evaluated at the drop center, as a function of $a\kappa$, for various values of $\tilde{\zeta}$.

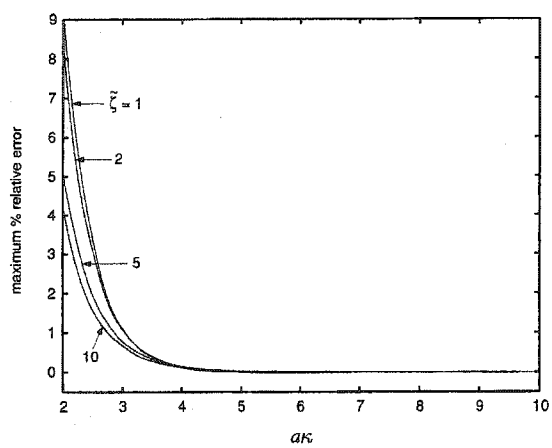

FIG. 4. Maximum percentage of relative error of ϕ_{in} as a function of $a\kappa$, for various values of $\tilde{\zeta}$. For each value of $a\kappa$, the maximum error is calculated over the first Debye layer only.

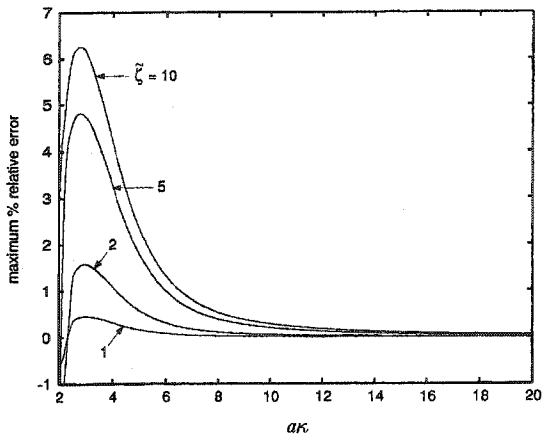

FIG. 5. Maximum percentage of relative error of ϕ_{nir} as a function of $a\kappa$, for various values $\bar{\zeta}$. The domain for calculating the error is the entire drop interior.

accurate several Debye lengths away from the surface, as illustrated in Fig. 1.

In classical matched asymptotics, the sum

$$\phi_{unif} = \phi_{out} + \phi_{in} - \phi_{match} \qquad [60]$$

would typically be used to obtain an estimate of ϕ that is useful over the entire drop interior. In this case,

$$\phi_{match} = \bar{Y}e^{-x}(1 + \delta x + \delta^2 x^2 + \delta^3 x^3) \qquad [61]$$

and unfortunately, ϕ_{unif} does not provide a uniformly valid solution. To see why, we note that the $O(\delta^4)$ error term in Eq. [35] really behaves as $(\delta x)^4$. Outside of the boundary layer, where $\delta x > 1$, this term will become quite large, causing a significant difference between ϕ_{in} and ϕ_{match} for large x. Success of Eq. [60] depends on ϕ_{match} accurately estimating the inner solution in the outer region and vice versa, which is not necessarily equivalent to matching the inner and outer solutions asymptotically.

On the other hand, the solution ϕ_{nir} obtained from the nonlinear rescaling and iteration is uniformly accurate (cf. Eq. [56]). For the case shown in Fig. 1, the maximum percentage of relative error of roughly 0.2%. This accuracy is comparable to that obtained by OHW for the exterior of the drop. The uniform validity is plainly an advantage of Eq. [56] over the solutions ϕ_{in} and ϕ_{out} obtained through matched asymptotics, though ϕ_{nir} is not as accurate as ϕ_{in} and ϕ_{out} in their respective regions. Equation [56] is also much simpler to implement and contains no analytically intractable integrals.

Figure 5 contains plots of the maximum percentage of relative error of ϕ_{nir} over the entire drop interior, as a function of $a\kappa$. As with the boundary layer analysis, ϕ_{nir} breaks down for $a\kappa \lesssim 3$. This is so because the approximations that caused the vanishing of expression [55] are not justified in the absence of an outer region. Moreover, the change of independent variable in Eq. [47] is based on the form of Eq. [46], which is not valid for small $a\kappa$.

SURFACE CHARGE DENSITY

The calculations made in the previous sections readily lend themselves to computation of the surface charge density of the drop. Classical electrostatics dictates that, for a spherical drop surface,

$$q/\epsilon_0 = -\epsilon\partial_r\psi|_{r=a} + \bar{\epsilon}\partial_r\bar{\psi}|_{r=a}, \qquad [62]$$

where q is the (dimensional) surface charge density. Note that whenever it is not clear from the context, overbars are used to indicate that the variables refer to the drop interior. In dimensionless form, Eq. [62] reads

$$(a\kappa)\sigma = -\partial_r\phi|_{r=1} + \frac{\bar{\epsilon}}{\epsilon}\partial_r\bar{\phi}\bigg|_{r=1}, \qquad [63]$$

where $a\kappa$ is for the exterior and

$$\sigma = q\left(\kappa\frac{\epsilon\epsilon_0 k_B T}{ze}\right)^{-1}. \qquad [64]$$

Matched Asymptotics: Strained Coordinate Method

To apply the strained coordinate approach for calculating σ, we make use of Eq. [11], as well as the NS results for the exterior. Rescaling the interior and exterior radial coordinates on δ and $\bar{\delta}$, respectively, recasts Eq. [63] as

$$\sigma = -\partial_x\phi|_{x=0} - \frac{\bar{\epsilon}}{\epsilon}\frac{\bar{\kappa}}{\kappa}\partial_{\bar{x}}\bar{\phi}\bigg|_{\bar{x}=0}. \qquad [65]$$

Finally, we express Eq. [65] in terms of the strained coordinates s and $\bar{s}$ by applying the chain rule. For the drop interior,

$$\partial_x\bar{\phi}|_{x=0} = f_0(\bar{p}) + \delta f_1(\bar{p}) + \delta^2 f_2(\bar{p}) + \delta^3 f_3(\bar{p}) + O(\delta^4),$$
$$\bar{p} = \tanh\left[\frac{ze}{4k_B T}(\bar{\zeta} - \Delta\psi)\right], \qquad [66]$$

where

$$f_0(\bar{p}) = \frac{4\bar{p}}{1 - \bar{p}^2}, \qquad [67]$$

$$f_1(\bar{p}) = -4\bar{p}, \qquad [68]$$

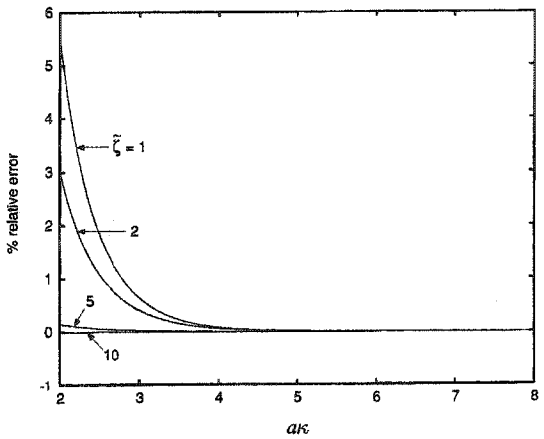

FIG. 6. Percentage of relative error of the analytic estimates of the interior surface potential gradient from the strained coordinate expansion, Eq. [66], as a function of $a\kappa$, for various values of $\tilde{\zeta}$.

$$f_2(\bar{p}) = -2\bar{p}(1-\bar{p}^2)\left[1 + \frac{\ln(1-\bar{p}^2)}{\bar{p}^2}\right], \quad [69]$$

and

$$f_3(\bar{p}) = (1-\bar{p}^2)f_2(\bar{p}). \quad [70]$$

The analytic approximation of the interior gradient is quite accurate for thin double layers, as can be seen in Fig. 6. As was the case for the potential functions, Eq. [66] becomes unreliable for $a\bar{\kappa} \lesssim 3$.

To obtain the derivative for the drop exterior, it suffices to recall that

$$\bar{\alpha}_i = (-1)^i\alpha_i, \quad i = 1, 2, 3, \quad [71]$$

and that the flat-plate solutions for the interior and exterior are identical. Therefore,

$$\partial_x\phi|_{x=0} = f_0(p) - \delta f_1(p) + \delta^2 f_2(p) - \delta^3 f_3(p) + O(\delta^4), \quad p = \tanh\left(\frac{ze}{4k_BT}\zeta\right). \quad [72]$$

The accuracy of Eq. [72] for the exterior potential gradient has been discussed by NS, and Eqs. [65], [66], and [72] yield a very accurate expression for the charge density.

Iteration Procedure

As suggested by OHW, Eq. [9] lends itself to an iteration procedure as well as a strained coordinate analysis. In particular, we write for the interior

$$\partial_x^2\phi = \sinh\phi + \frac{2}{A}F(\phi), \quad [73]$$

where

$$F(\phi) = \frac{A}{A-x}\partial_x\phi. \quad [74]$$

The procedure here is to successively substitute approximations to $F(\phi)$ in the limit of large A, starting with the expression we get from the flat-plate approximation to ϕ, and integrating the resulting differential equation.

Because the flat-plate approximation gives

$$\partial_x\phi_0 = -2\sinh(\phi_0/2), \quad [75]$$

$F(\phi_0)$ is also $-2\sinh(\phi_0/2)$ in the limit of large A. We look to obtain an improved approximation to $\partial_x\phi$ by substituting this limiting form into Eq. [73] and integrating via reduction of order, to get

$$\partial_x\phi = -2\sqrt{\sinh^2(\phi/2) - \frac{8}{A}\sinh^2(\phi/4) - \left(\sinh^2(\phi_c/2) - \frac{8}{A}\sinh^2(\phi_c/4)\right)}, \quad [76]$$

where again, ϕ_c is the (unknown) potential at the drop center.

Considering that for large A, ϕ_c is very small, especially compared to the potential at the drop surface, we will ignore those terms in Eq. [76] that contain ϕ_c and expand the square root on the RHS of Eq. [76]. To first order in $1/A$, we obtain

$$\partial_x\phi = -2\sinh(\phi/2)\left[1 - \frac{1}{\lambda A\cosh^2(\phi/4)}\right], \quad [77]$$

where λ is a fitting parameter. We set $\lambda = 2$ so as to obtain the correct limiting form of the first derivative of ϕ at $x = 0$, for small $\tilde{\zeta}$-potentials, while allowing Eq. [77] to be asymptotically equivalent to Eq. [76].

Recalling that the limiting form of Eq. [74] for large A is $\partial_x\phi$, we substitute [77] for $F(\phi)$ in Eq. [73] and integrate, obtaining

$$\partial_x\phi|_{x=0} = -2\sinh(\tilde{\zeta}/2) \times \sqrt{1 - \frac{2}{A\cosh^2(\tilde{\zeta}/4)} + \frac{8\ln[\cosh(\tilde{\zeta}/4)]}{A^2\sinh^2(\tilde{\zeta}/2)}} \quad [78]$$

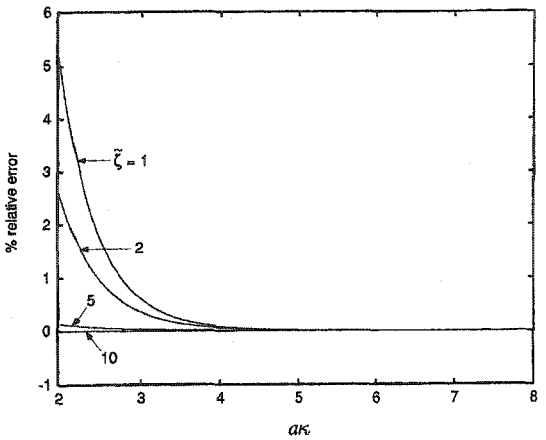

FIG. 7. Percentage of relative error of the analytic estimates of the interior surface potential gradient from the iteration technique, Eq. [78], as a function of $a\kappa$, for various values of $\tilde{\zeta}$.

if we again ignore the terms with ϕ_c. In Fig. 7, Eq. [78] is compared to the numerical calculations. Note the similarity to Fig. 6 for values of $a\kappa$ close to 3.

The surface charge density follows from substituting Eq. [78] and the OHW expression for the exterior surface gradient into Eq. [65], viz.

$$\sigma = 2\sinh(\zeta/2)\sqrt{1 + \frac{2}{A\cosh^2(\zeta/4)} + \frac{8\ln[\cosh(\zeta/4)]}{A^2\sinh^2(\zeta/2)}} + 2\frac{\bar{\epsilon}}{\epsilon}\frac{\bar{A}}{A}\sinh(\tilde{\zeta}/2) \times \sqrt{1 - \frac{2}{\bar{A}\cosh^2(\tilde{\zeta}/4)} + \frac{8\ln[\cosh(\tilde{\zeta}/4)]}{\bar{A}^2\sinh^2(\tilde{\zeta}/2)}},$$

where ζ is understood to be in scaled form.

ACCURACY OF CHARGE DENSITY RESULTS

The expressions for the interior surface potential gradient have also been tested against numerical solutions. The accuracy of Eq. [66] as a function of $a\kappa$ for several values of $\tilde{\zeta}$ is given in Fig. 6, and similarly for Eq. [78] in Fig. 7. As is the case for the approximations of ϕ, accuracy breaks down for $a\kappa \gtrsim 3$.

For small and large values of $a\kappa$, there is not much difference in accuracy between the expressions in Eqs. [66] and [78]. For $\tilde{\zeta} = 1$, the percentage of relative error of Eq. [66] varies from 7×10^{-5} to 2×10^{-5} as $a\kappa$ goes from 15 to 20. The corresponding errors for Eq. [78] in this range of $a\kappa$ are slightly smaller, viz. 2×10^{-5} to 0.5×10^{-5}. For $\tilde{\zeta} = 10$, the errors from Eqs. [66] and [78] are roughly 1×10^{-6} in this range of $a\kappa$.

Note also the increasing accuracy with increasing $\tilde{\zeta}$. This is perhaps unexpected, since the analyses are in part based on matching the behavior of ϕ in the region local to the surface with a far-field, linearized solution, which is less valid for larger potentials. One must consider, however, that a large surface potential is caused by a sizeable surface charge, and that we are measuring accuracy by *relative* error.

CONCLUDING REMARKS

Previous analyses of the equilibrium double layer of a charged spherical particle have been adapted to the interior of an emulsion drop, with comparable success for $a\kappa$ considerably greater than 3. The expression ϕ_{in} is an excellent boundary layer solution, and derivation of the third correction to the flat-plate solution improves the accuracy of the outer solutions for both the interior and the exterior of the drop. Other than the asymptotic series, we have made no attempt to empirically derive a formula for the reduced surface potential $\bar{Y}$ for the interior, as Loeb *et al.* (23) have done for the exterior. For the exterior, the solution to the linearized Poisson–Boltzmann equation can be arbitrarily accurate, given enough distance from the drop surface and the appropriate reduced surface potential constant. This is simply not so for the drop interior.

Computation of a fourth correction to the flat-plate solution would be conceptually straightforward, as indicated in Eq. [13]. However, the complexity of the second- and third-order corrections indicates that such a term would be rather unwieldy; at $O(\delta^4)$ the computational simplicity of the analytic solution is forfeited and it would seem easier to numerically integrate the Poisson–Boltzmann equation [4].

The expression ϕ_{nlr} obtained from nonlinear rescaling and iteration is clearly simpler to calculate than both ϕ_{in} and ϕ_{out}, at the expense of some accuracy. Also, it may be possible that better approximations of the constants in Eq. [53] may lead to an improved result.

Improvement of the surface charge density expressions by the strained coordinate method would require computation of $\alpha_4'(s)$, which although simpler than $\alpha_4(s)$, would be at best a tedious task. Equations [66] and [78], while highly accurate for large $a\kappa$, have the same limitation as do the expressions for ϕ, namely that accuracy breaks down for $a\kappa \gtrsim 3$. Equation [78] has the same limitation of ϕ_{nlr}, namely that it was derived without knowledge of the potential at the drop center, a term which appeared in the derivations of each. Nonetheless, for thin double layers, the results are quite useful.

ACKNOWLEDGMENTS

This work was supported by the NASA Office of Life and Microgravity Sciences and Applications, through Grants NAG8948 and NGT-51122.

REFERENCES

1. Russel, W. B., Saville, D. A., and Schowalter, W. R., "Colloidal Dispersions." Cambridge Univ. Press, New York, 1989.
2. Okada, K., Akagi, Y., and Yoshioka, N., *Can. J. Chem. Eng.* **66,** 276 (1988).
3. Okada, K., Akagi, Y., Kogure, M., and Yoshioka, N., *Can. J. Chem. Eng.* **68,** 393 (1990).
4. Fukui, Y., and Yuu, S., *Chem. Eng. Sci.* **35,** 1097 (1980).
5. Johansson, G., *in* "Partitioning in Aqueous Two-Phase Systems" (H. Walter, D. E. Brooks, and D. Fisher, Eds.), p. 161. Academic Press, Orlando, FL, 1985.
6. Booth, F., *J. Chem. Phys.* **19,** 1331 (1951).
7. Levine, S., *in* "Materials Processing in the Reduced Gravity Environment of Space" (G. E. Rindone, Ed.), p. 241. Elsevier, New York, 1982.
8. Baygents, J. C., and Saville, D. A., *J. Chem. Soc. Faraday Trans.* **87,** 12 (1991).
9. Brooks, D. E., Sharp, K. A., Bamberger, S., Tamblyn, C. H., Seaman, G. V. F., and Walter, H., *J. Colloid Interface Sci.* **102,** 1 (1984).
10. Dukhin, S. S., and Derjaguin, B. V., *in* "Surface and Colloid Science" (E. Matijevic, Ed.), Vol. 7, Chap. 2. Wiley–Interscience, New York, 1974.
11. Rao, K. S. M. S. R., Stewart, R. M., and Todd, P., *Sep. Sci. Technol.* **25,** 985 (1990).
12. Loewenberg, M., and Davis, R. H., *J. Fluid Mech.* **288,** 103 (1995).
13. Zhang, X., Basaran, O. A., and Wham, R. M., *AIChE J.* **41,** 1629 (1995).
14. Nichols, C. S., Loewenberg, M., and Davis, R. H., Submitted for publication (1995).
15. Scott, T. C., *Sep. Purif. Meth.* **18,** 65 (1989).
16. Baygents, J. C., and Saville, D. A., *PhysicoChem. Hydrodynam.* **10,** 543 (1988).
17. Henry, D. C., *Proc. R. Soc. London A* **133,** 106 (1931).
18. Ohshima, H., Healy, T. W., and White, L. R., *J. Chem. Soc. Faraday Trans. 2* **80,** 1643 (1984).
19. Ohshima, H., Healy, T. W., and White, L. R., *J. Colloid Interface Sci.* **90,** 17 (1982).
20. Natarajan, R., and Schechter, R. S., *J. Colloid Interface Sci.* **99,** 1 (1984).
21. "Handbook of Mathematical Functions" (M. Abramowitz and I. A. Stegun, Eds.). U.S. Department of Commerce, Washington, DC, 1964.
22. Van Dyke, M., "Perturbations Methods in Fluid Mechanics." Parabolic Press, Stanford, CA, 1975.
23. Loeb, A. L., Overbeek, J. Th. G., and Wiersema, P. H., "The Electrical Double Layer Around a Spherical Colloidal Particle." MIT Press, Cambridge, MA, 1961.

References

[1] Adamson, A. W., *Physical Chemistry of Surfaces* Wiley & Sons, New York (1976).

[2] Baygents, J. C., Saville, D. A., Electrophoresis of Drops and Bubbles, *J. Chem Soc. Faraday Trans.,* **87**, 1883 (1991).

[3] Belongia, B. M., and Baygents, J. C., Measurements on the Diffusion Coefficient of Colloidal Particles by Taylor-Aris Dispersion, *J. Colloid. Int. Sci.*, **195**, 19 (1997).

[4] Bird, R. B., Stewart, W. E., and Lightfoot, E. N., *Transport Phenomena*, p. 272, John Wiley & Sons (1960).

[5] Booth, F., The Cataphoresis of Spherical Fluid Droplets in Electrolytes, *J. Chem. Phys.,* **19**, 1331 (1951).

[6] R. P. Brent *Algorithms for Minimization without Derivatives*, Dover, New York (2001).

[7] Brooks, D. E., and Bamberger, S., Studies on Aqueous Two Phase Polymer Systems Useful for Partitioning of Biological Materials, in *Materials Processing in the Reduced Gravity Environment of Space* (G.E. Rindone ed.), p. 233. Elsevier Science, New York, (1982).

[8] Brooks, D. E., Sharp, K. A., Bamberger, S., Tamblyn, C. H., Seaman, G.V.F., and Walter, H., Electrostatic and Electrokinetic Potentials in Two Polymer Aqeuous Phase Systems, *J. Colloid Interface Sci.*, **102**, 1 (1984).

[9] Brown, J. F., and Hinckley, J. O. N., *J. Chromatogr.,* Electrophoretic Thermal Theory II. Steady-State Radial Temperature Gradients in Circular Section Columns, **109**, 218 (1975).

[10] Brown, J. F., and Hinckley, J. O. N., Electrophoretic Thermal Theory III. Steady-State Radial Temperature Gradients in Rectangular Section Columns, *J. Chromatogr.,* **109** 225 (1975).

[11] Carey, G. F., and Finlayson, B. A., Orthogonal Collocation on Finite Elements **Chem. Eng. Sci. 30**, 587 (1975).

[12] Cole, K. D., and Cabezas, Jr., H., *Applied Biochem. Biotechnol.,* **54**, 159 (1995).

[13] Coxon, M., and Binder, M. J., Radial Temperature Distribution in Isotachophoresis Columns of Circular Cross-Section, *J. Chromatogr.,* **101**, 1 (1974).

[14] Datta, R., and Kotamarthi, V. R., *A.I.Ch.E. J.*, **36**, 916 (1990).

[15] Davis, J. M., Influence of Thermal Variation of Diffusion Coefficient on Non-Equilibrium Plate Height in Capillary Zone Electrophoresis, *J. Chromatogr.*, **517**, 521 (1990).

[16] Dolnik, V., Liu, S., and Jovanovich, S., Capillary Electrophoresis on Microchip, *Electrophoresis,* **21**, 41 (2000).

[17] Erker, J.A., and Baygents, J.C., The Equilibrium Electric Potential and Surface Charge Density of Spherical Emulsion Drops with Thin Double Layers, *J. Colloid Interface Sci.*, **179**, 76 (1996).

[18] Gobie, W. A., and Ivory, C. F., Thermal Model of Capillary Electrophoresis and a Method for Counteracting Thermal Band Broadening, *J. Chromatogr.,* **516**, 191 (1990).

[19] Grushka, E., McCormick, R. M., and Kirkland, J. J., Effect of Temperature-Gradients on the Efficiency of Capillary Zone Electrophoresis Separations, *Anal. Chem.,* **61**, 241 (1989).

[20] Henry, D. C., The Cataphoresis of Suspended Particles. I. The Equation of Cataphoresis *Proc. R. Soc. London, Ser A,* **133**, 106 (1931).

[21] Hinckley, J. O. N., *J. Chromatogr.,* **109**, 206 (1975).

[22] Hjerten, S., *Chromatogr. Rev.,* **9**, 122 (1967).

[23] Hunter, R.J., *Zeta Potential in Colloid Science*, Academic Press, London (1981).

[24] Jones, A. E., and Grushka, E., Nature of Temperature Gradients in Capillary Zone Electrophoresis, *J. Chromatogr.,* **466**, 219 (1989).

[25] Keller, H. B., *Numerical Methods for Two-Point Boundary-Value Problems*, Dover, New York (1992).

[26] Knox, J. H., and McCormack, K. A., Temperature Effects in Capillary Electrophoresis. 1: Internal Capillary Temperature and Effect Upon Performance, *Chromatographia.,* **38**, 207 (1994).

[27] Kopf-Sill, A. R., Miick, C., Mehta, T. B., Brooks, C., and Gliech, L., Putting Joule Heating to Good Use it Abstr. Pap. Am. Chem. Soc., **219**, 398 (2000).

[28] Landers, J. P. ed., *Handbook of Capillary Electrophoresis*, CRC Press, Ann Arbor, MI, (1994).

[29] Levich, V. G., *Physicochemical Hydrodynamics,* Prentice Hall, Englewood Cliffs, New Jersey, (1962).

[30] Levine, S., A Theory of Electrophoresis of Emulsion Drops in Aqeuous Two-Phase Polymer Systems, in *Materials Processing in the Reduced Gravity Environment of Space* (G.E. Rindone ed.), p. 241. Elsevier Science, New York, (1982).

[31] Loeb, A. L., Overbeek, J. Th. G., and Wiersema, P. H., *The Electrical Double Layer Around a Spherical Colloidal Particle,* MIT Press, Cambridge, MA, (1961).

[32] Manz, A., Harrison, D. J., Verpoorte, E. M. J., Fettinger J. C., Paulus, A., Ludi, H., and Widmer, H., M., *J. Chromatogr.*, **593** 253 (1992).

[33] Marinova, K. G., Alargova, R. G., Denkov, N. D., Velev, O. D., Petsev, D. N., Ivanov, I. B., Borwankar, R. P., *Langmuir* **12**, 2045 (1996).

[34] Mooney, M., Electrophoresis and the Diffuse Ionic Layer, *Phys. Rev.* **23**, 396 (1924).

[35] Natarajan, R., and Schechter, R. S., The Solution of the Nonlinear Possoin-Boltzmann Equation for Thin, Spherical Double Layers, *J. Colloid Interface Sci.* **99**, 1 (1984).

[36] Nelson, R J., Paulus, A., Cohen, A. S., Guttman, A., and Karger, B. L., Use of Peltier Thermoelectric Devices to Control Column Temperature in High-Performance Capillary Electrophesis, *J. Chromotog.*, **480**, 111 (1989).

[37] Newman, J. S., *Electrochemical Systems* Prentice Hall, Englewood Cliffs, NJ (1991).

[38] O'Brien, R. W., and White, L. R., Electrophoretic Mobility if a Spherical Colloidal Particle, *J. Chem. Soc., Faraday Trans. 2,* **43**, 1607 (1978).

[39] Oda, R. P., and Landers, J. P., in *Handbook of Capillary Electrophoresis*, (J. P. Landers ed.), CRC Press, Ann Arbor, MI, (1994).

[40] Ohshima, H., Healy, T. W., and White, L. R., Accurate Analytic Expressions for the Surface Charge Density/Surface Potential Relationship and Double-Layer Potential Distribution for a Spherical Colloidal Particle, *J. Colloid Interface Sci.* **90**, 17 (1982).

[41] Ohshima, H., Healy, T. W., and White, L. R., Approximate Analytic Expressions for the Electrophoretic Mobility of Spherical Colloidal Particles and the Conductivity of their Dilute Suspensions, *J. Chem. Soc., Faraday Trans. 2,* **79**, 1613 (1983).

[42] Ohshima, H., Healy, T. W., and White, L. R., *J. Chem. Soc., Faraday Trans. 2,* **80**, 1643 (1984).

[43] Raghavarao, K. S. M. S., Stewart, R. M., Rudge, S. R., and Todd, P., Electrokinetic Demixing of Aqueous Two-Phase Systems. 3. Drop Electrophoretic Mobilities and Demixing Rates, *Biotechnol. Prog.* **14**, 922 (1998).

[44] Reyes, D. R., Iossifidis, D., Aroux, P. A., and Manz, A., *Anal. Chem.,* **74** 2623 (2002).

[45] Russell, W. B., Saville, D. A., and Schowalter, W. R., *Colloidal Dispersions,* Cambridge University Press, Cambridge (1991).

[46] Shampine, L. F., Kierzenka, J., and Reichelt, M. W., Solving Boundary Value Problems for Ordinary Differential Equations in MATLAB with bvp4c, The Mathworks (2000).

[47] Shanks, D., Non-Linear Transformations of Divergent and Slowly Convergent Sequences, *J. Math. and Phys.,* **34** 1 (1955).

[48] Smoluchowski, M. von, Contribution à la Théorie de L'endosmose Électric et de Quelque Phenoménes Corrélatifs, *Bull. Int. Acad. Sci. Cracovie,* **8**, 182 (1903).

[49] Stone, H. A., Philip Saffman and Viscous Flow Theory, *J. Fluid Mech.* **409**, 165 (2000).

[50] Swinney, K, and Bornhop, D. J., Quantification and Evaluation of Joule Heating in On-Chip Capillary Electrophoresis, *Electrophoresis,* **23**, 613 (2002).

[51] Taylor, G., Studies in Electrohydrodynamics I. The Circulation Produced in a Drop by an Electric Field, it Proc. Roy. Soc. A **291**, 159 (1966).

[52] Theos, C. W., and Clark, W. M., Electroextraction: Two-Phase Electrophoresis, *Appl. Biochem. Biotech.* **54** 143 (1995).

[53] Tsuda, T., Sweedler, J. V., and Zare, R. N., Rectangular Capillaries for Capillary Zone Electrophoresis, *Anal. Chem.,* **62** 2149 (1990).

[54] Van Dyke, M., *Perturbations Methods in Fluid Mechanics.* Parabolic Press, Stanford, CA (1975).

[55] Weast, R. C. ed., *CRC Handbook of Chemistry and Physics,* p. E-11, CRC Press, Boca Raton, FL (1988).

[56] Walter, H., Brooks, D.E., and Fisher, D. eds. *Partitioning in Aqueous Two-Phase Systems* Academic Press, Orlando, FL (1985).